2017-06-01

Formation of Rapakivi Feldspars in the Deer Isle Granite Complex, Coastal Maine: *In Situ* Lead Isotope and Trace Element Analysis

William Desmond OBrien
Brigham Young University

Formation of Rapakivi Feldspars in the Deer Isle Granite Complex, Coastal Maine: *In Situ* Lead Isotope and Trace Element Analysis

William Desmond O'Brien

A thesis submitted to the faculty of
Brigham Young University
in partial fulfillment of the requirements for the degree of

Master of Science

Michael J. Dorais, Chair
Eric H. Christiansen
Stephen T. Nelson
David Gibson

Department of Geological Sciences

Brigham Young University

ABSTRACT

Formation of Rapakivi Feldspars in the Deer Isle Granite Complex, Coastal Maine: *In Situ* Lead Isotope and Trace Element Analysis

William Desmond O'Brien
Department of Geological Sciences, BYU
Master of Science

Rapakivi and alkali feldspar phenocrysts from the Deer Isle Granite Complex were investigated using *in situ* trace element and Pb isotope geochemistry to see if magma mixing or isothermal decompression was responsible for their formation. Pb isotope and trace element profiles, along with CL imagery of quartz phenocrysts, indicate compositional changes in the magma chamber occurred during rapakivi and alkali feldspar growth. Repeated episodes of magma mixing/replenishment by relatively isotopically primitive and LREE enriched magmas (along with hybridized variations with the host magma) created localized disequilibration. Alkali feldspar phenocrysts proximal to these zones of thermal perturbation were first resorbed and then mantled by plagioclase. Entrainment back into this zone of mixing caused multiple mantles of plagioclase to form on some phenocrysts. For grains more distal to these zones of mixing, complete disequilibration of the grain did not occur and continued growth resulted in Ba-rich alkali feldspar mantles over Ba-poor alkali feldspar cores. As crystallization of the chamber continued along solidification fronts, batches of cooler crystal-rich magmas settled *en masse* to the floor. Disaggregation of these batches during settling, and subsequent accumulation on the chambers floor, brought grains with disparate crystallization histories together. Filter pressing of the cumulate pile flushed highly evolved fluids out from interstitial pores. Small amounts of evolved liquid, trapped interstitial to the cumulate, formed LREE depleted albitic rims on some grains. The crystallization, transportation and juxtaposition of rapakivi, mantled alkali feldspar and plagioclase phenocrysts suggests that a relatively large and active magma chamber, periodically recharged by batches of melt, must have existed.

Keywords: rapakivi, magma mixing, LA-ICP-MS, Deer Isle Granite Complex

ACKNOWLEDGMENTS

Where to begin…

First and foremost I want to say thank you to my advisor, and friend, Michael Dorais, for your shared love of New England geology, our shared love for the outdoors, and our mutual distain for “Massholes”. Just remember, Maine will always have pine cone bouquets and more coast line than New Hampshire.

To Eric Christiansen, I will always be greatly appreciative of your attention to detail and for keeping me (and the rest in the grad cubes) on task just by being there. Thank you again for sharing Thanksgiving with me and your family.

David Gibson, thank you for introducing me to rapakivi feldspars in the first place and for our conversations at the office. I can honestly say if it wasn’t for you, I don’t know if I would have enjoyed undergrad geology so much. I look forward to more fieldwork together.

A very special thank you to the staff and faculty of the Geological Sciences Department for all their help and friendship throughout the years. You each gave me encouragement in your own way.

A great big hug and thank you to Nan, Kris and Judy… the girls that kept me fed, employed, and laughing. I will miss not being able to stop by and talk to you whenever I get stressed or need a distraction. We have lots of blueberry pie (and lighthouses) in Maine and you are welcome whenever.

To all my friends in the Grad Cubes (those who have gone on before and those who still remain), thank you for the distractions, laughter, debates and tomfoolery. I thank Gabe for the kolache runs, and Alex for the Sodalicious runs (and the resulting heartburn).

To Richard Brandley, I say thank you for encouraging me to continue my education when I seemed to be unsure of where I was going.

To Pat and Joan, I say thank you for not giving up on me and for your continued love, support and encouragement throughout my academic career.

I thank Sue and Dave Cole for giving me a place to write and all the whoopie pies I didn't really need, but really did enjoy!

And last but not least, I have to say thank you to my parents. Thank you Mom for letting Dad and me bring home all those rocks throughout the years and thank you Dad for taking me camping so we could look for more!

TABLE OF CONTENTS

Formation of Rapakivi Feldspars in the Deer Isle Granite Complex, Coastal Maine: *In Situ* Lead Isotope and Trace Element Analysis i
ABSTRACT ii
ACKNOWLEDGMENTS iii
TABLE OF CONTENTS v
LIST OF FIGURES vii
LIST OF TABLES viii
INTRODUCTION 1
GEOLOGICAL BACKGROUND 3
METHODS 8
RESULTS 11
Petrography 11
Rapakivi Grains 11
Plagioclase Phenocrysts 17
Alkali Feldspar Phenocrysts 17
Quartz Phenocrysts 20
Geochemistry 22
Major elements 22
Trace Elements 24
Pb Isotopes 33
DISCUSSION 37
Formation of feldspars 38
Alkali feldspar and rapakivi cores 38
Rapakivi and alkali feldspar mantles 41
Quartz phenocrysts 43
Chamber dynamics 44
CONCLUSIONS 47
REFERENCES 48
APPENDIX 1 52
APPENDIX 2 53

APPENDIX 3 90
APPENDIX 4 99

LIST OF FIGURES

Figure 1. Map of Coastal Maine magmatic province 4
Figure 2. Geological map of the Deer Isle Granite Complex 6
Figure 3. Field photographs of the Flye Point facies 7
Figure 4. X-ray element maps of rapakivi grain FP-4-1R1 13
Figure 5. X-ray element maps of rapakivi grain FP-4-7R2 14
Figure 6. X-ray element maps of rapakivi grain FP-3-1R1 15
Figure 7. X-ray element maps of rapakivi grain FP-5-8R1 16
Figure 8. X-ray element maps of plagioclase phenocryst FP-6-1P1 18
Figure 9. X-ray element maps of unmantled alkali feldspar phenocryst FP-4-7R1 19
Figure 10. Cathodoluminescence image of quartz phenocryst 21
Figure 11. Feldspar ternary diagram 23
Figure 12. Trace element and Pb isotope profiles of rapakivi grain FP-4-1R1 28
Figure 13. Trace element and Pb isotope profiles of rapakivi grain FP-4-7R2 29
Figure 14. Trace element and Pb isotope profiles of rapakivi grain FP-3-1R1 30
Figure 15. Trace element and Pb isotope profiles of rapakivi grain FP-5-8R1 31
Figure 16. CL image showing oscillatory zoning in rapakivi grain FP-4-1R1 32
Figure 17. CL image showing coarse sieve texture of rapakivi grain FP-3-1R1 32
Figure 18. Pb isotope profiles of rapakivi grain FP-4-7R1 36
Figure 19. Crystal growth/resorption histories in Relative Ba / 207Pb/206Pb space 39
Figure 20. Theoretical Cross-section of the Deer Isle Granite Complex 46

LIST OF TABLES

Table 1. Element and associated dwell times 10

INTRODUCTION

The rapakivi texture (*sensu stricto)* of granites, first defined by Sederholm (1891), and later by Vorma (1976), is characterized by: 1) ovoidal alkali feldspar phenocrysts; 2) the majority of ovoids partially to completely mantled by plagioclase shells; and 3) the ubiquitous presence of two generations of alkali feldspar and quartz, with the first generation of quartz crystallizing as high (β) quartz and idiomorphic in nature. Granites exhibiting this texture are called rapakivi granites (Vorma, 1976). Vorma used the term rapakivi granite (*sensu stricto*) to describe only those granites with 1) rapakivi texture, 2) a Precambrian age (ca. 1700 Ma), and 3) found largely in the Baltic Shield. Haapala and Rämö (1992) modified the definition of rapakivi granites to be genetically A-type and not limited to being Precambrian in age. Within this paper, the term rapakivi feldspars (*sensu lato*) will be used to describe plagioclase-mantled alkali feldspars regardless of their age, relation to orogenesis, or tectonic setting.

The process by which rapakivi feldspars formed has been hypothesized by many authors (e.g. Sederholm, 1891; Whitney, 1975; Stull, 1979; Hibbard, 1981; Bussy, 1990; Nekvasil, 1991; Stimac and Wark, 1992; Dempster et al., 1994; Eklund and Shebanov, 1999) and summarized by Rämö and Haapala (1995). Of these, three are more widely accepted and are described below.

In 1991, Nekvasil, building on Whitney's work (1975), hypothesized that rapkakivi growth could occur if an ascending granitic magma (1) did not become saturated with respect to H_2O, (2) cooling rates are within ~5 - 10 °C/kbar, (3) both alkali feldspar and plagioclase are present in the magma prior to ascent, and (4) initial temperatures of the magma are low enough to prevent complete resorption of alkali feldspar. With these conditions met, alkali feldspar would destabilize while plagioclase remained stable. The resorbed ovoidal alkali feldspars would then provide nuclei for continued growth of plagioclase.

The second hypothesis holds that the formation of rapakivi feldspars occurs through magma-mixing (Hibbard, 1981; Wark and Stimac, 1992; Stimac and Wark, 1992). Here two contrasting magmas (mafic vs. granitic) mix and, either completely or partially, hybridize. A granitic magma mixing with a hotter mafic magma will cause resorption of alkali feldspar and quartz due to increases in the systems temperature. Disequilibrium in the system forces plagioclase to nucleate on the resorbed alkali feldspars (Hibbard, 1981), and allows for the additional growth of quartz over the resorbed quartz when equilibrium is again reached.

A third hypothesis has also been presented by Dempster et al. (1994). They propose that the rapakivi texture is formed by the subsolidus exsolution of plagioclase in the alkali feldspars. Here plagioclase migrates towards the rims and thus "mantles" the alkali feldspars. Although this third hypothesis is not widely accepted (*cf.* Rämö and Haapala, 2005), many studies support the first or second hypothesis (Eklund and Shebanov, 1999; Narayana et al., 2000; Wang et al., 2008; Müller et al., 2008; Heinonen et al., 2010, Vernon, 2016). However, no consensus has been reached as to which is responsible for the formation of rapakivi textures. This may be due to the fact that not just one process is involved in the development of the distinctive rapakivi texture; or there is a lack of means to determine what the process was.

Rämö and Haapala (2005), Müller et al. (2008), and Wang et al. (2008) all have urged further work in the field of rapakivi granites and textures and this project was designed to do just that by a study of the rapakivi granite of the Deer Isle Granite Complex of coastal Maine. This study includes 1) Trace element analyses by laser ablation inductively coupled plasma mass spectrometry (LA-ICP-MS) of plagioclase inclusions within alkali feldspar ovoids, plagioclase mantles, and phenocrystic plagioclase within the granite matrix, 2) *In situ* laser ablation multi-collector inductively coupled plasma mass spectrometry (LA-MC-ICP-MS) Pb isotopic analyses

of alkali feldspar ovoids and plagioclase inclusions within, plagioclase mantles and plagioclase phenocrysts, and 3) acquisition of cathodoluminescence images of zoning in quartz and rapakivi phenocrysts. We use this data to show that magma mixing is the best explanation for the production of mantled feldspars in the Deer Isle Granite Complex.

GEOLOGICAL BACKGROUND

The Deer Isle Granite Complex is located in East Penobscot Bay, 65 km south of Bangor, Maine, and forms the majority of the island for which it is named. The complex is part of the Coastal Maine magmatic province of eastern coastal Maine (Fig. 1) (Hogan and Sinha, 1989). The province contains over 100 post-tectonic, late Silurian to Mississippian (Hogan and Mataragio, 2006) plutons that intruded a collage of northeast-trending, fault-bounded, lithotectonic terranes of Proterozoic to Devonian metasedimentary and metavolcanic rocks (Hogan and Sinha, 1989). These terranes were sutured together during the Late Silurian to Early Devonian (Stewart *et* al., 1995) and later were accreted as a whole to the southeast edge of Laurentia during the Acadian Orogeny (Early Devonian) (Stewart and Tucker, 1998; Schulz et al., 2008).

Magmatism within the Coastal Maine Magmatic Province is thought to have occurred in an extensional environment within a transtensional regime of a transcurrent fault system. Underplating and intraplating of mafic magmas produced gabbros and diorites early on. After emplacement, a change to a transpressional regime caused these mafic magmas to be trapped within the crust. These trapped mafic magmas caused melting in the overlying crustal rocks and produced peralkaline and metaluminous granites (Hogan and Sinha, 1989). Some plutons and complexes indicate that these crustal melts variably interacted with the trapped mafic magmas

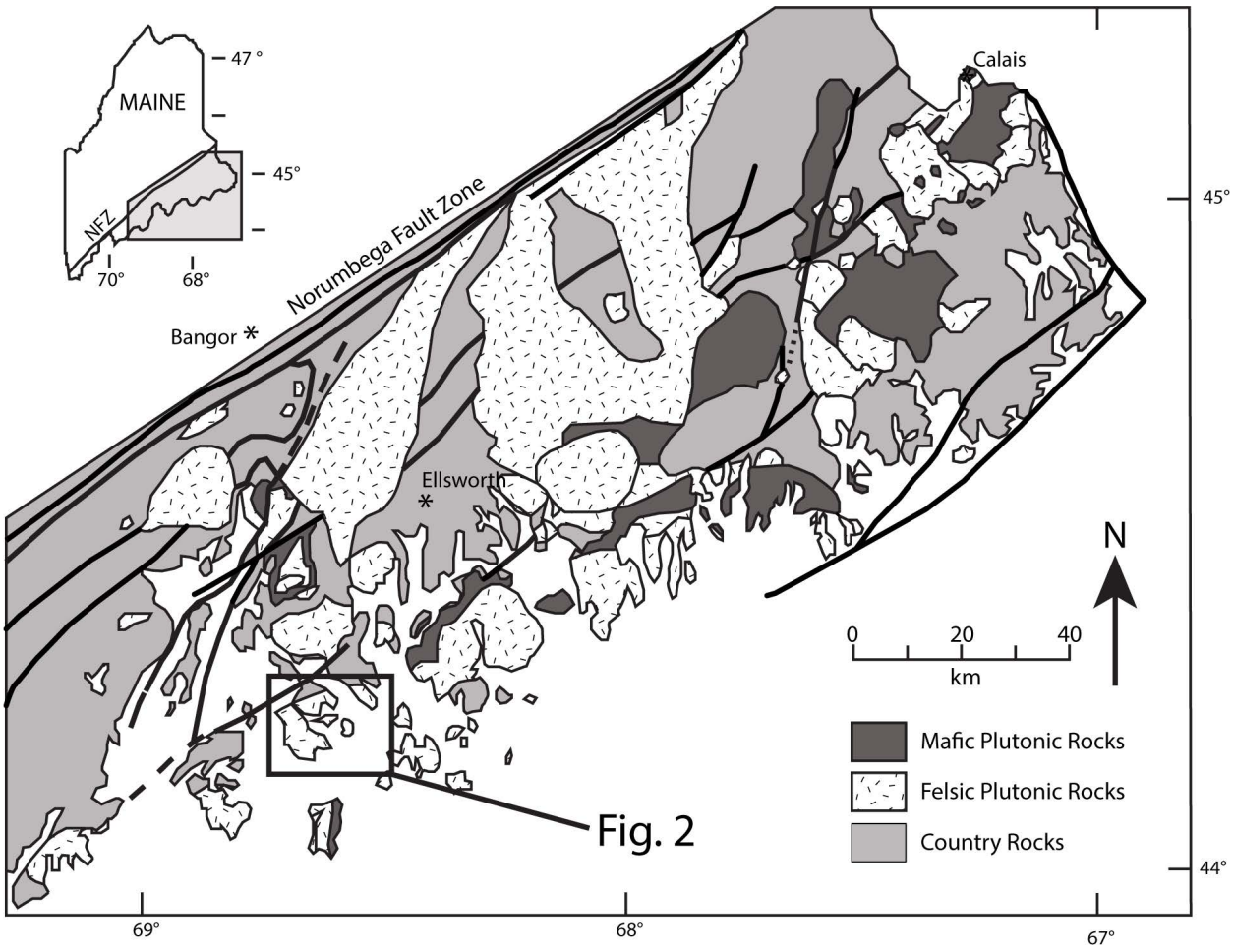

Figure 1. Map of Coastal Maine magmatic province (after Hogan and Sinha, 1989). Rectangle indicates study area (see Fig. 2)

and produced hybrid magmas (e.g. Gibson et al., 2004; Wiebe et al., 2004; Lux et al., 2007; Waight et al., 2007) (Hogan and Sinha, 1989).

The Deer Isle Granite Complex (Fig. 2) was first subdivided into two types by Stewart (1956): The Stonington and Oak Point granites. Hooks (2003) divided the complex further; the Flye Point and Oak Point facies of the Oak point granite, and the Settlement Quarry and Crotch Island facies of the Stonington granite. Lux *et al.* (2007) believed the complex as a whole represents a "fossil" magma chamber that has been tilted, allowing for a cross-sectional view,

with the Flye Point facies representing the bottom of the chamber and the Crotch Island facies representing the top (Fig. 2).

Due to the lack of internal contacts, the major distinguishing feature between each facies is the number of rapakivi feldspar grains (*sensu lato*), called plagioclase-mantled K-feldspar by Lux et al. (2007). The Flye Point facies has the most abundant rapakivi feldspars at 614 per m^2, and represents the northeastern extent of the pluton. To the southwest, and towards the top of the chamber, the Oak Point facies, has an average of 357 rapakivi feldspars per m^2. The Settlement Quarry and Crotch Island, representing the upper portions of the "fossil" magma chamber, have the least amount of rapakivi feldspars; 95 and 71 per m^2 respectively (Lux et al., 2007).

The Flye Point facies is a coarse-grained, hornblende-biotite monzogranite to quartz monzonite (Fig. 3). Alkali feldspar, plagioclase and quartz form a framework of touching phenocrysts with interstitial grains of plagioclase, alkali feldspar, quartz, and mafics. Phenocrysts of perthitic alkali feldspars range in size from 0.5 to 2.0 cm across, are concentrically zoned and subhedral to euhedral. Plagioclase inclusions are common within alkali feldspars and form concentric zones mimicking the growth of the alkali feldspar. Other less common inclusions found within alkali feldspar cores and phenocrysts include biotite, hornblende, and quartz. Forty percent of these alkali feldspars are ovoids rimmed with up to 4 mm thick plagioclase mantles (i.e. rapakivi) however their abundances are highly variable (Lux et al., 2007).

Plagioclase is also abundant and forms euhedral to subhedral phenocrysts with common inclusions of biotite and hornblende. Occasionally plagioclase phenocrysts (those that do not obviously mantle an alkali feldspar grain) exhibit disequilibrium textures and include coarse-sieve textured, oscillatory zoning, and reverse zoning (Hooks, 2003; Lux et al., 2007).

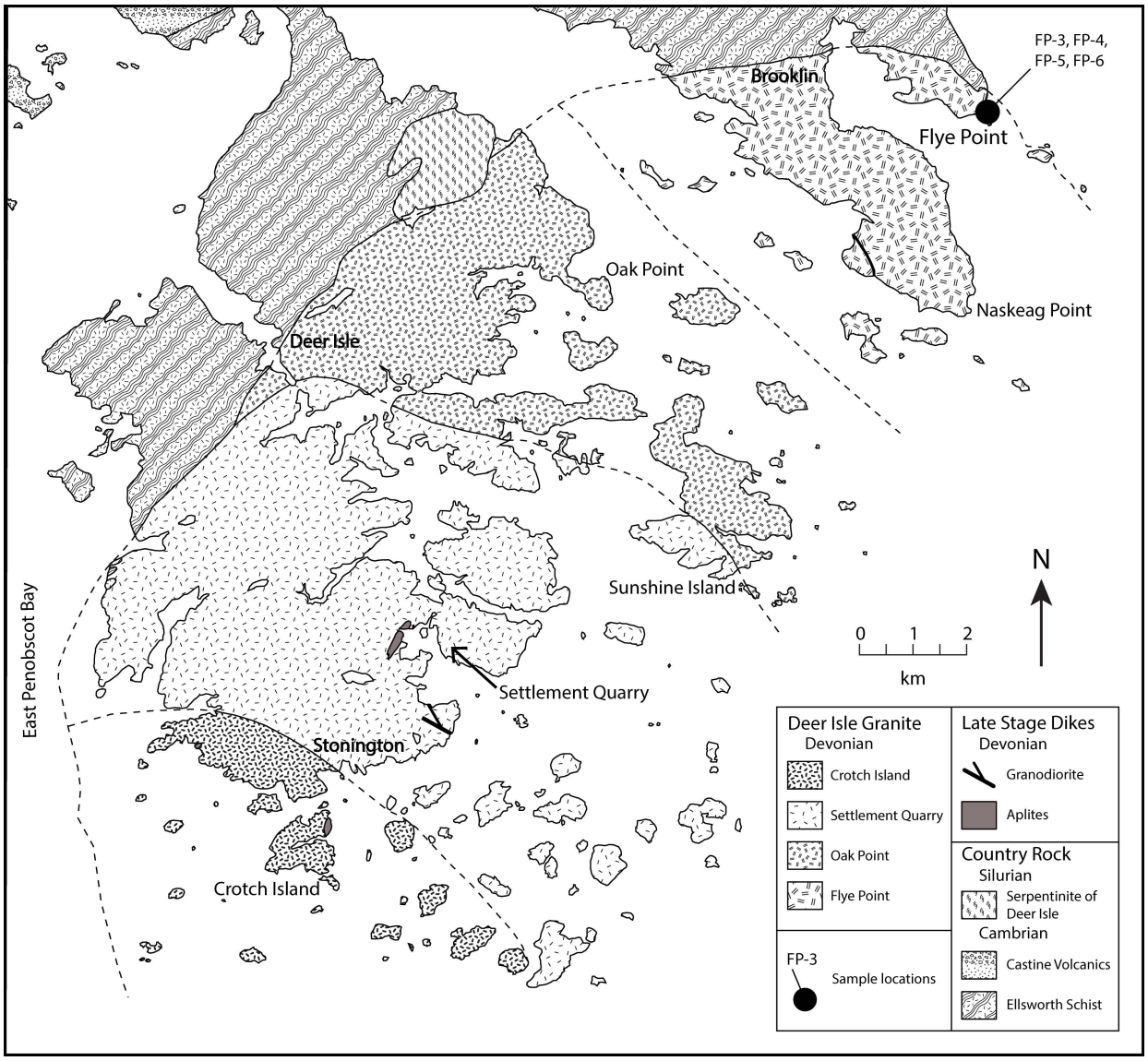

Figure 2. Geological map of the Deer Isle Granite Complex (after Lux *et al.,* 2007).

Other minerals present are quartz phenocrysts and form anhedral to subhedral crystals up to ~1.5 cm across. Mafic phases include biotite, hornblende, and minor amounts of titanite, zircon, apatite, allanite, ilmenite, and magnetite; all these are also typically found as inclusions within feldspars (Lux et al., 2007).

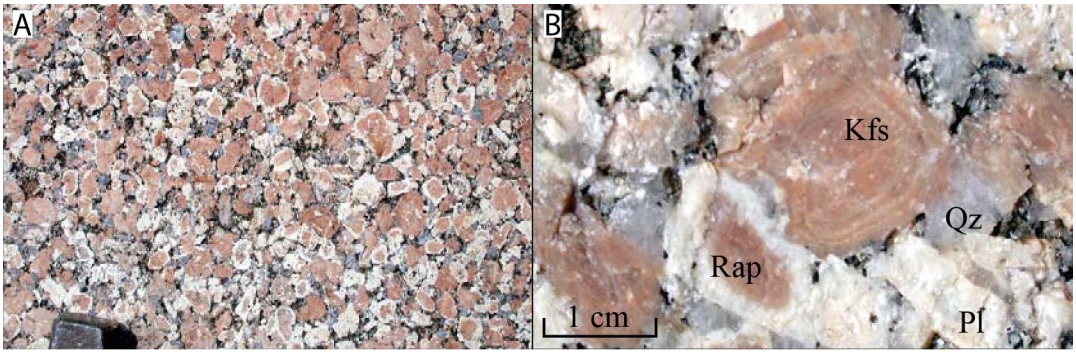

Figure 3. Field photographs of the Flye Point facies (from Lux et al., 2007). (A) Outcrop with framework of touching phenocrysts of feldspar with abundant rapakivi feldspars present. (B) Close-up of same outcrop showing rapakivi feldspar (Rap) touching a zoned alkali feldspar (Kfs), and next to plagioclase phenocrysts (Pl).

The Oak Point facies has the same mineral assemblage as the Flye Point facies, but is classified as a coarse-grained, seriate, biotite-hornblende monzogranite. In addition, the Oak Point facies contains much larger quartz phenocrysts (0.3 – 1.5 cm) than the Flye Point. (Lux *et al*., 2007).

The Settlement Quarry Facies is a coarse-grained, leucocratic, biotite monzogranite (Lux *et al.*, 2007). Its mineral assemblage is similar to the previous facies with the noted rarity in hornblend as an accessory phase. Also present in this facies are aplite and granodiorite dikes. Schlieren are abundant in this facies and form planar, ring, and ladder dike structures (Lux *et al.*, 2007).

The Crotch Island facies is a coarse-grained, leucocratic, biotite monzogranite and has a hypidiomorphic texture. Like the other facies it has a similar mineral assemblage with the exception of hornblende, which is absent. Enclaves are rare, and schlieren and aplite dikes are uncommon (Lux *et al.*, 2007).

Mafic, intermediate, and felsic enclaves are present throughout the pluton, with abundances decreasing upward (mimicking the pattern found for the rapakivi feldspar concentrations). They are angular to disc-shaped to almost spherical and range from 1 cm to

several meters in size. Alignment of these enclaves generally parallel feldspar foliations found throughout the Flye Point and Oak Point facies (Johnston, 2001). Porphyritic enclaves often contain rounded (resorbed) plagioclase, alkali feldspars, rapakivi feldspars, and quartz ocelli (Lux *et al.*, 2007). Fine-grained quartz diorite and diorite enclaves are generally smaller (<20 cm) and rounded compared to the more felsic ones. Accessory minerals within the intermediate enclaves include apatite, titanite (matrix and ocelli), zircon and allanite (Hooks, 2003; Lux et al., 2007).

The decrease of rapakivi feldspars (Lux et al., 2007) and the decrease in the size of plagioclase mantles (Stewart, 1956) proved the Stonington Quarry and Crotch Island facies to be less viable for this study.

METHODS

Rapakivi and alkali feldspars analyzed were collected from the type locality for the Flye Point facies (Flye Point, Deer Isle, Maine; Fig. 2). Seven hand samples (*e.g.* FP-1, FP-2, FP-3, etc.) were collected, sectioned into ~ 1cm wide slabs, and labeled (*e.g.* FP-4-1, FP-4-2, etc.). Thick sections, and matching thin sections, were made from five different slabs (FP-3-1, FP-4-1, FP-4-7, FP-5-8 and FP-6-1). Where two feldspars were analyzed from the same thick section, grains were numbered additionally (*e.g.* FP-4-7R1 and FP-4-7R2).

Electron microprobe analyses and imagery for feldspars were conducted at Brigham Young University using a Cameca SX50 electron microprobe. Analyses used a 15 kV accelerating voltage, 10 nA beam current with a 10 μm beam diameter. Calibration standards consisted of all natural minerals and are listed in Appendix 1. Data reduction followed the procedures outlined in Pouchou and Pichoir (1985). Major elements analyzed consisted of Na,

Al, Si, K, Ca, and Fe for plagioclase and the same suite of elements, along with Ba for K-feldspar. See Appendix 2 for complete electron microprobe data.

Wavelength-dispersive X-ray spectroscopy element maps of feldspars were constructed for Si Kα, Ca Kα, K Kα, and Ba Lα and are presented in Figures 1 – 8. Element maps were obtained using a 15 kV accelerating voltage, a 40 nA beam current (Ba Lα used 100 nA), a 10 μm beam diameter. Images were obtained by stage scanning and, depending on the size of the grain imaged, map sizes were either 9.5 x 9.5 mm, or 21 x 21 mm.

In situ trace element LA-ICP-MS analyses of plagioclase were carried out at the W.M. Keck Collaboratory for Plasma Mass Spectrometry at Oregon State University using a Photon Machines Analyte G2 193 nm excimer laser coupled to a Thermo X-Series II quadrupole ICP-MS and followed analytical techniques outlined by Kent et al. (2004). Spot analyses had a diameter of 50 μm, a pulse frequency of 7 Hz, and an ablation time of 30-45 seconds. Background measurements were taken for 30 seconds prior to start of each run with a 30 second signal washout period between each ablation. Trace elements analyzed, and dwell times for each element are presented in Table 1.

U.S. Geological Survey glass standards GSE-1G, BHVO-2G, BCR-2G, and National Institute of Standards NIST-612 and NIST-613 were used during each run of analyses, with GSE-1G used to standardize between every 8-10 unknowns to monitor accuracy and precision of analytical run. Analyses are generally below 5% standard error (SE) for most elements with the following exceptions: ^{25}Mg, ^{85}Rb, ^{89}Y ^{147}Sm, and ^{157}Gd >10%, ^{146}Nd >15%, and ^{90}Zr, ^{93}Nb, ^{159}Tb, and ^{172}Yb generally below detection limits. Raw data was processed using the in-house LaserTram and LaserCalc software (Kent et al., 2004) using ^{43}Ca as the internal standard.

Electron microprobe analyses for CaO concentrations of each sample spot were used to reduce the data. See Appendix 3 for complete trace element data.

Element	Dwell Time (ms)	Element	Dwell Time (ms)
^{25}Mg	10	^{93}Nb	10
^{29}Si	10	^{137}Ba	10
^{43}Ca	10	^{138}Ba	10
^{47}Ti	10	^{139}La	20
^{56}Fe	10	^{140}Ce	20
^{66}Zn	10	^{146}Nd	20
^{69}Ga	10	^{147}Sm	20
^{85}Rb	10	^{153}Eu	20
^{86}Sr	10	^{157}Gd	20
^{88}Sr	10	^{159}Tb	20
^{89}Y	20	^{172}Yb	20
^{90}Zr	20	^{208}Pb	10

Table 1. Element and associated dwell times for analyzed elements.

In situ Pb isotope compositions of plagioclase and alkali feldspar were analyzed by LA-MC-ICP-MS, using a Photon Machines Analyte G2 193 nm excimer laser coupled to a Nu Plasma Multi Collector ICP Mass Spectrometer at the W.M. Keck Collaboratory for Plasma Mass Spectrometry at Oregon State University. Analytical techniques followed those used by Kent et al. (2008) and glass standards NIST-612 and BCR-2G were used as standards. Each analysis consisted of a 135 μm spot diameter, a pulse frequency of 10 Hz, and a shot count of 225. Pb-isotope measurements obtained consisted of ^{206}Pb, ^{207}Pb, and ^{208}Pb; the minor ^{204}Pb isotope was also measured but is not presented here due to difficulty in its detection above background in these samples. See Appendix 4 for all isotopic data. Because of variable alteration

of the feldspars, continuous linear traverses from core to rim were not permitted for LA-ICP-MS analyses of most grains. Where this was the case, analyses are graphically ordered on the graphs according to their relative positions from core to rim (Figs. 12, 14-15).

Cathodoluminescence (CL) imagery was conducted at Brigham Young University using a FEI/Philips XL30 FEG environmental scanning electron microscope with a GATAN MiniCL detector. An accelerating voltage of 15 kV and a spot size of 6 μm were used for each image with the stage tilted 12-15° from horizontal. Scanning rates were at 116 ms/line scan resulting in images roughly 1,700 x 2,300 μm. Because grains were much larger than maximum image size (e.g. >2 cm^2), multiple images were taken of selected grains and then later stitched together into one composite image (e.g. Fig. 10).

RESULTS

Petrography

Rapakivi Grains

Representative rapakivi feldspars from the Flye Point facies ranged from 1.5 – 2 cm across with generally tabular shapes reflective of their idiomorphic nature (Figs. 4-6). Equant rapakivi grains were also present (Fig. 7) and are most likely due to their orientations during sectioning. The alkali feldspar cores are salmon in color and perthitic with a composition of about Or_{95}. Contacts between the alkali feldspar cores and plagioclase mantles are generally irregular; however, euhedral faces developed on some alkali feldspar cores where quartz forms a boundary between the mantle and core (Figs. 4A and 6A).

Mantling these alkali feldspar cores is at least one generation of plagioclase (~An_{20}) up to 3 mm thick with its outermost edge more albitic (An_{8-14}). Plagioclase generally forms a complete mantle around a central alkali feldspar; however, partial mantling was seen in thin section and

outcrop as well. Plagioclase is partly or completely optically continuous around the alkali feldspar cores. Simple twining of alkali feldspar cores are continuous across core/mantle boundary and into the plagioclase mantle (*c.f.* Vernon, 2016). When multiple mantles are present, some inner most mantles display a coarse-sieve texture (Fig. 6) and are compositionally similar to subsequent mantle generations (An $_{19\text{-}22}$). Mantling by plagioclase, either by one or two generations, gives a subhedral to euhedral shape to most grains.

Inclusions within the alkali feldspar cores are predominantly plagioclase. However, quartz, occasional biotite and apatite, and rare Fe-Ti oxides are also present in both cores and mantles. These inclusions are generally <1 mm in size and occasionally are found in discrete zones that parallel primary growth zones within both alkali feldspar cores and plagioclase mantles. Plagioclase inclusions in the alkali feldspar cores are variably altered and dusty in thin-section, and are generally more easily detected in Ca X-ray maps (Fig. 4-7). Occasionally larger (~1 mm), and less altered, plagioclase inclusions are partially encased in quartz (Fig. 4). Some of these plagioclase inclusions rarely appear to be in optical continuity with the plagioclase in the mantle and may be re-entrants into the alkali feldspar core from the third dimension. For some rapakivi grains, quartz also forms thin pockets that separate plagioclase mantles from alkali feldspar cores and are usually optically continuous with other proximal quartz inclusions (Figs. 4-6). When quartz is present, euhedral faces form on both alkali feldspar cores and plagioclase mantles (Fig. 6).

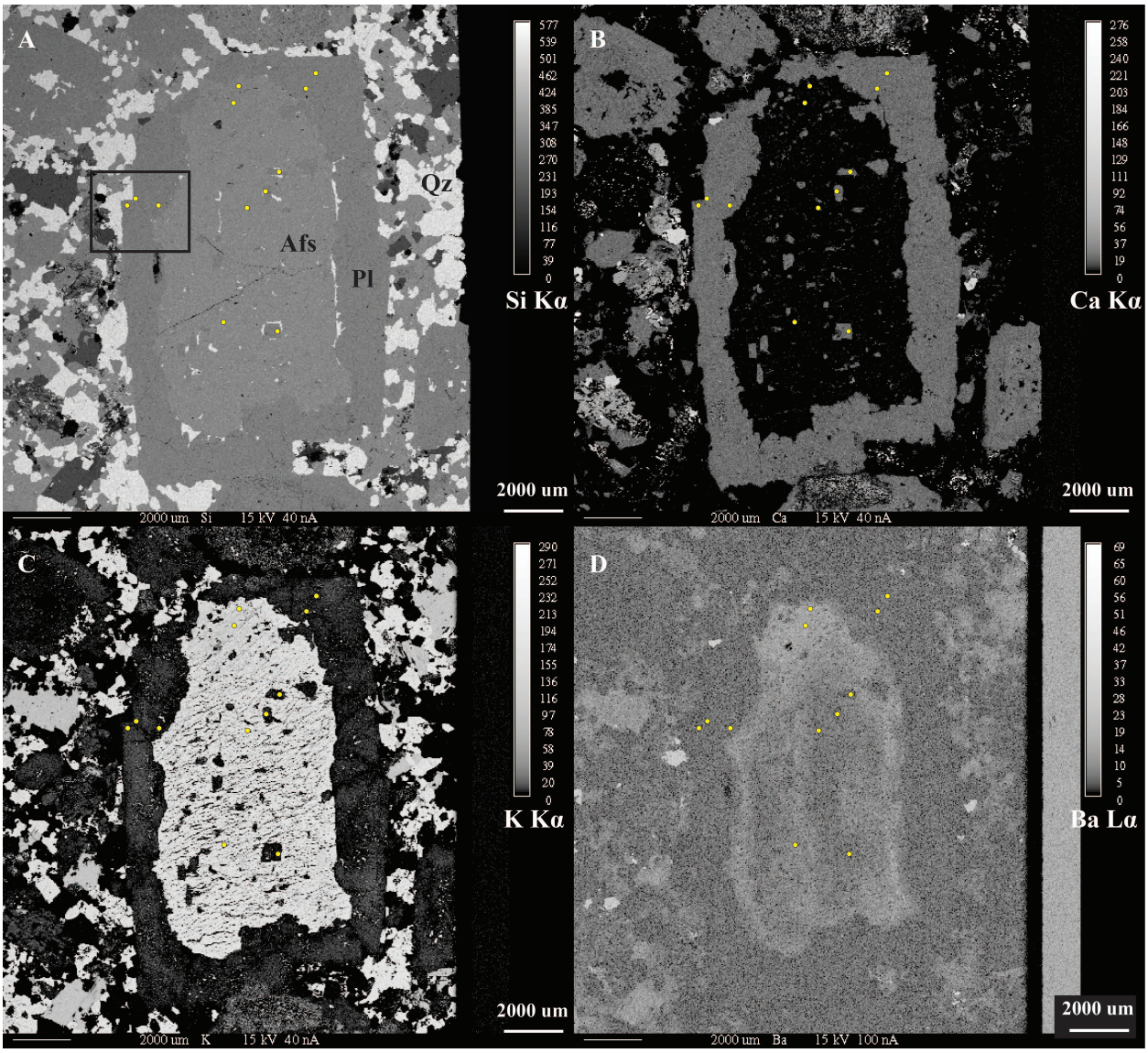

Figure 4. X-ray element maps of rapakivi grain FP-4-1R1. Greyscale element maps of Si (a), Ca (b), K (c), and Ba (d) with Pb isotope analysis locations marked with yellow circles. Major phases are plagioclase (Pl), alkali feldspar (Afs), and quartz (Qz). Rectangle in (a) shows location of Figure 16.

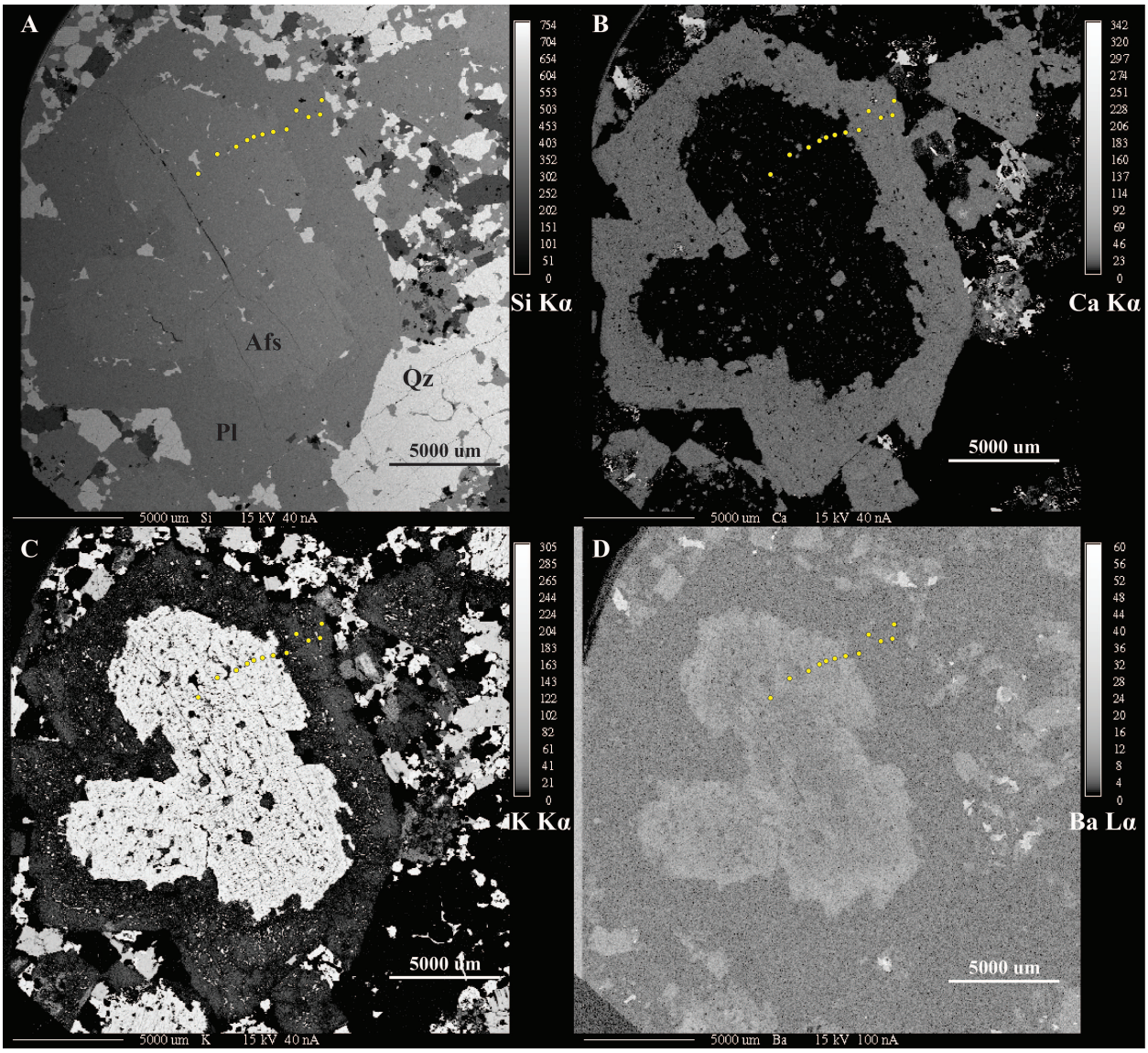

Figure 5. X-ray element maps of rapakivi grain FP-4-7R2. Greyscale element maps of Si (a), Ca (b), K (c), and Ba (d) with Pb isotope analysis locations marked with yellow circles. Major phases include plagioclase (Pl), alkali feldspar (Afs), and quartz (Qz).

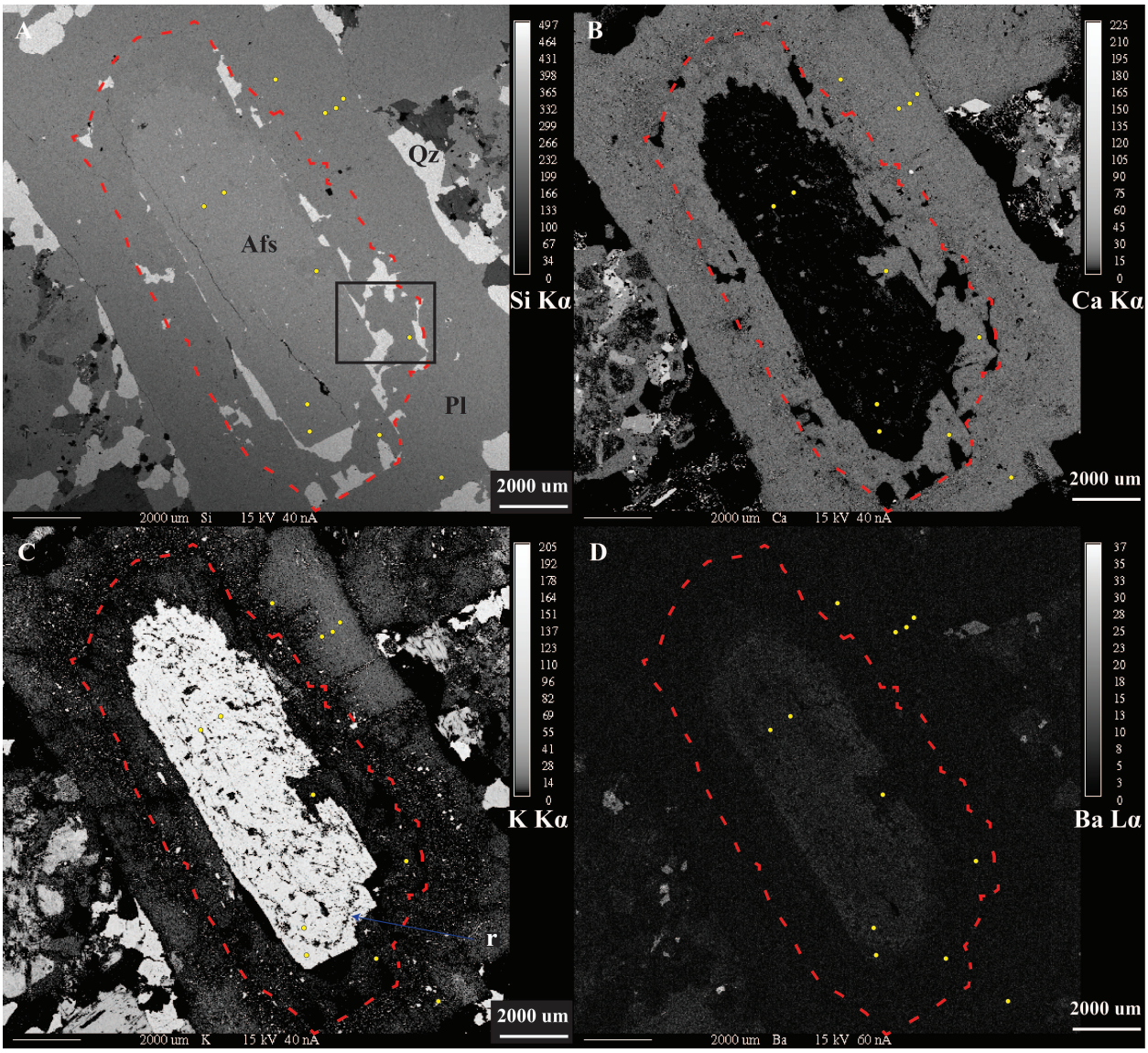

Figure 6. X-ray element maps of rapakivi grain FP-3-1R1. Greyscale element maps of Si (a), Ca (b), K (c), and Ba (d) with Pb isotope analysis locations marked with yellow circles. Major phases included plagioclase (Pl), alkali feldspar (Afs), and quartz (Qz). Internal contact between inner, coarse sieve textured plagioclase mantle (1st mantle) and outer, oscillatory zoned plagioclase mantle (2nd mantle) is marked by dashed line. Resorption surface (r) marked in (c). Rectangle in (a) shows location of Figure 17.

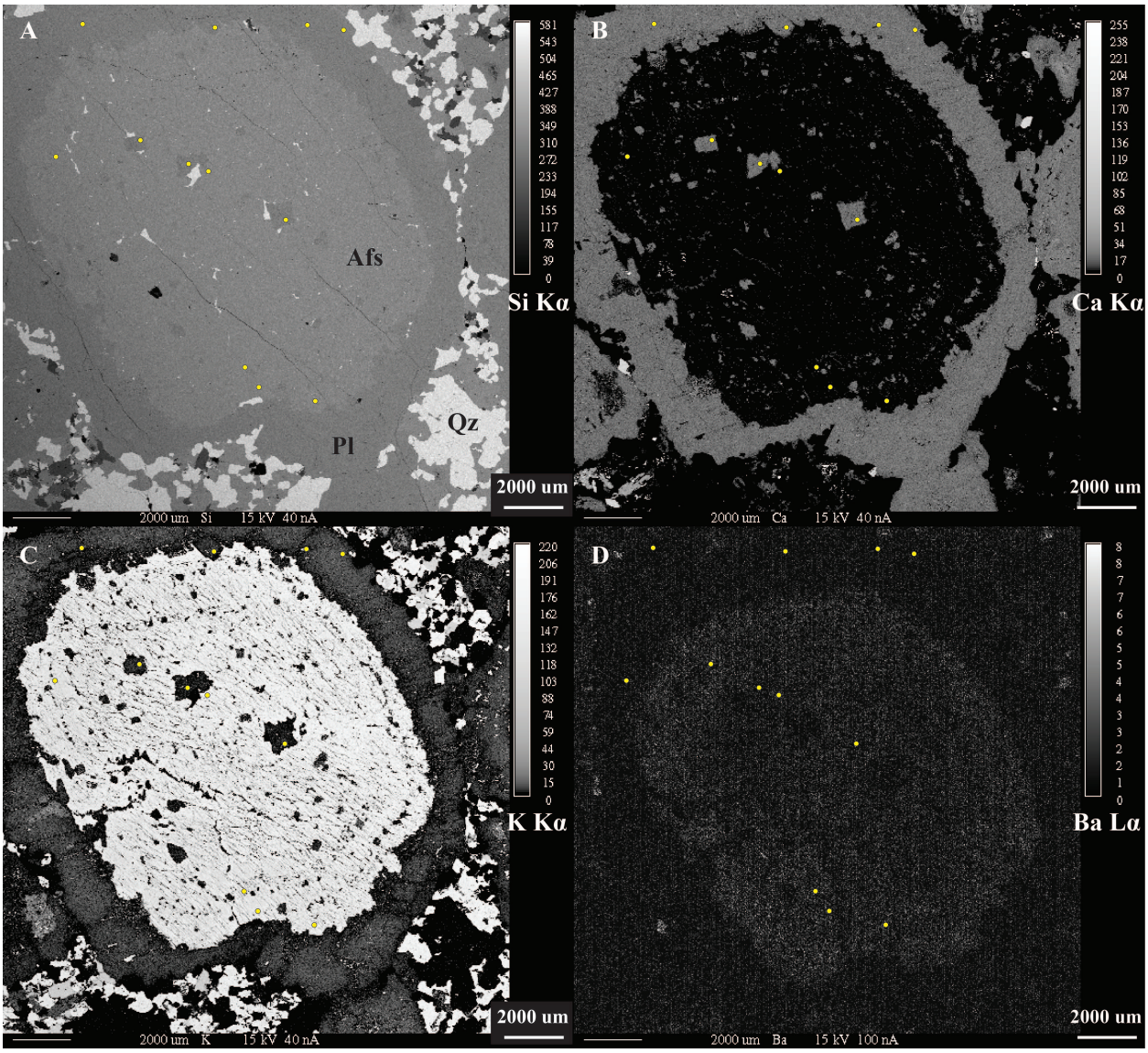

Figure 7. X-ray element maps of rapakivi grain FP-5-8R1. Greyscale element maps of Si (a), Ca (b), K (c), and Ba (d) with Pb isotope analysis locations marked with yellow circles. Major phases include plagioclase (Pl), alkali feldspar (Afs), and quartz (Qz). Note the cyclic zoning of plagioclase inclusions easily seen in (b) and (c).

Plagioclase Phenocrysts

Separate from rapakivi feldspars are discrete grains of plagioclase feldspar that sometimes are mantle by a second generation of plagioclase. These generally larger phenocrysts are tabular and can be found up to 2.5 cm long (Fig. 8). Examined phenocrysts have cores of oligoclase (An_{23} to An_{27}) that are slightly more calcic than the plagioclase mantles (~An_{20}). The cores have a coarse-sieve texture, much like the inner mantle of FP-3-1R1 (Fig. 6), with quartz infilling irregularly shaped voids (poikilitic grains of Lux *et al.,* 2007). Also abundant in the cores are mafic silicate inclusions, typically biotite, with occasional amphibole, titanite, and Fe-Ti-oxides.

Plagioclase mantles are between 0.5 – 1.5 mm thick, generally pristine and inclusion-free. These euhedral to subhedral mantles are more sodic than the cores and range from An_{20} to An_{24} with minor oscillatory zoning. The outermost edge of these mantles are more albitic (~An_{14}) along the contact with matrix material, similar to that found on rapakivi feldspars.

Alkali Feldspar Phenocrysts

Unmantled alkali feldspars up to 2 cm across are common in the Deer Isle Granite (Fig. 9). These grains are salmon colored and perthitic and typically display Carlsbad twins. Internal oscillatory zoning is defined by variations in color from salmon pink to a more creamy pink. This appears to reflect changes in Ba concentrations as is evidenced by the element maps (Fig. 9d). These alkali feldspar grains are typically mantled by a ~1 mm rim of Ba-rich (~ 0.7 % BaO) alkali feldspar that formed after an inferred resorption event ("r" in Fig. 9d). Continued growth by Ba-poor alkali feldspar over Ba-rich mantle gives a subhedral appearance to most gains. Where Ba concentrations are relatively high, exsolution lamellae are less abundant compared to other parts of the grain (Fig. 9).

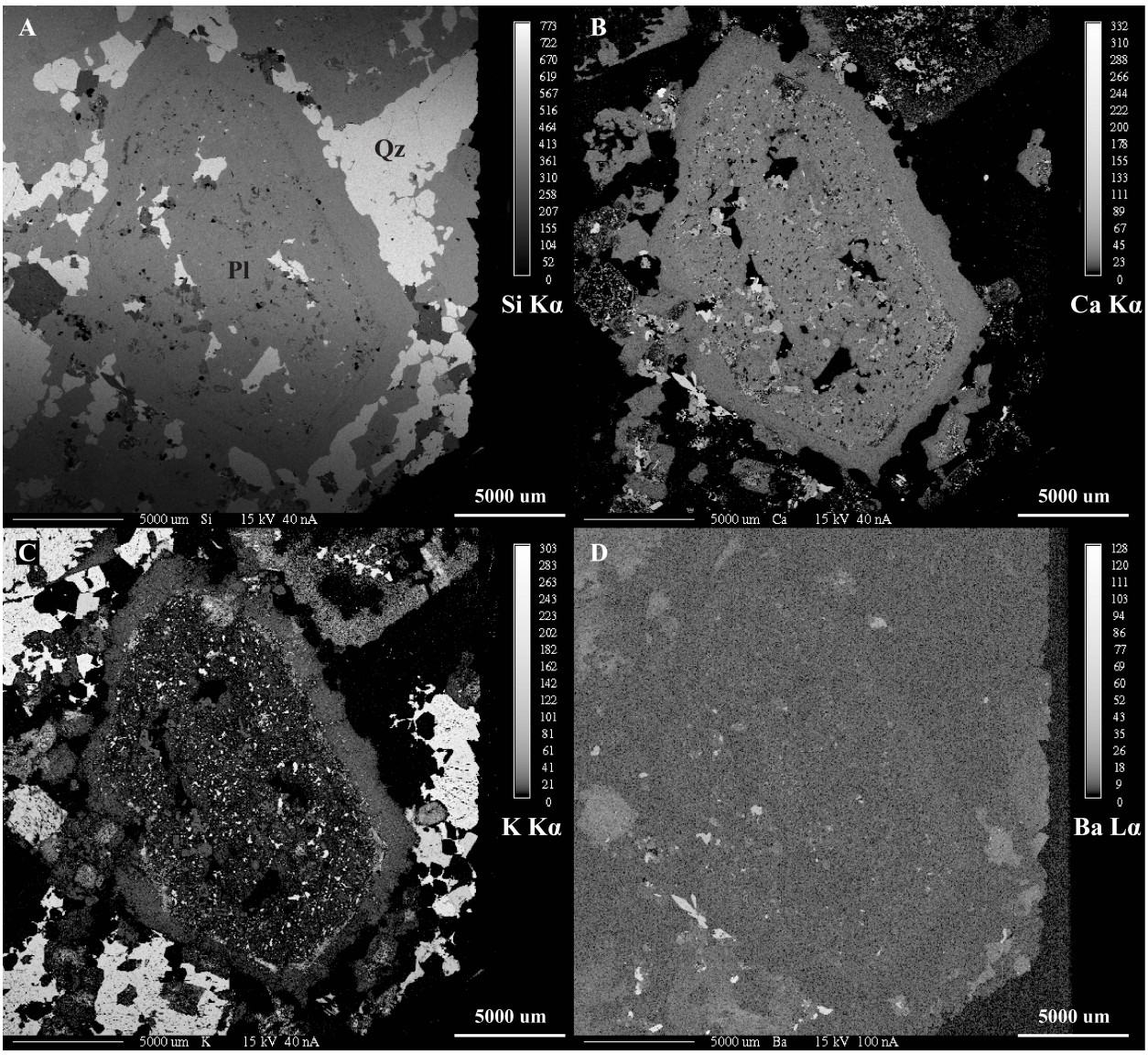

Figure 8. X-ray element maps of plagioclase phenocryst FP-6-1P1. Greyscale element maps of Si (a), Ca (b), K (c), and Ba (d). Major phases present are plagioclase (Pl) and quartz (Qz).

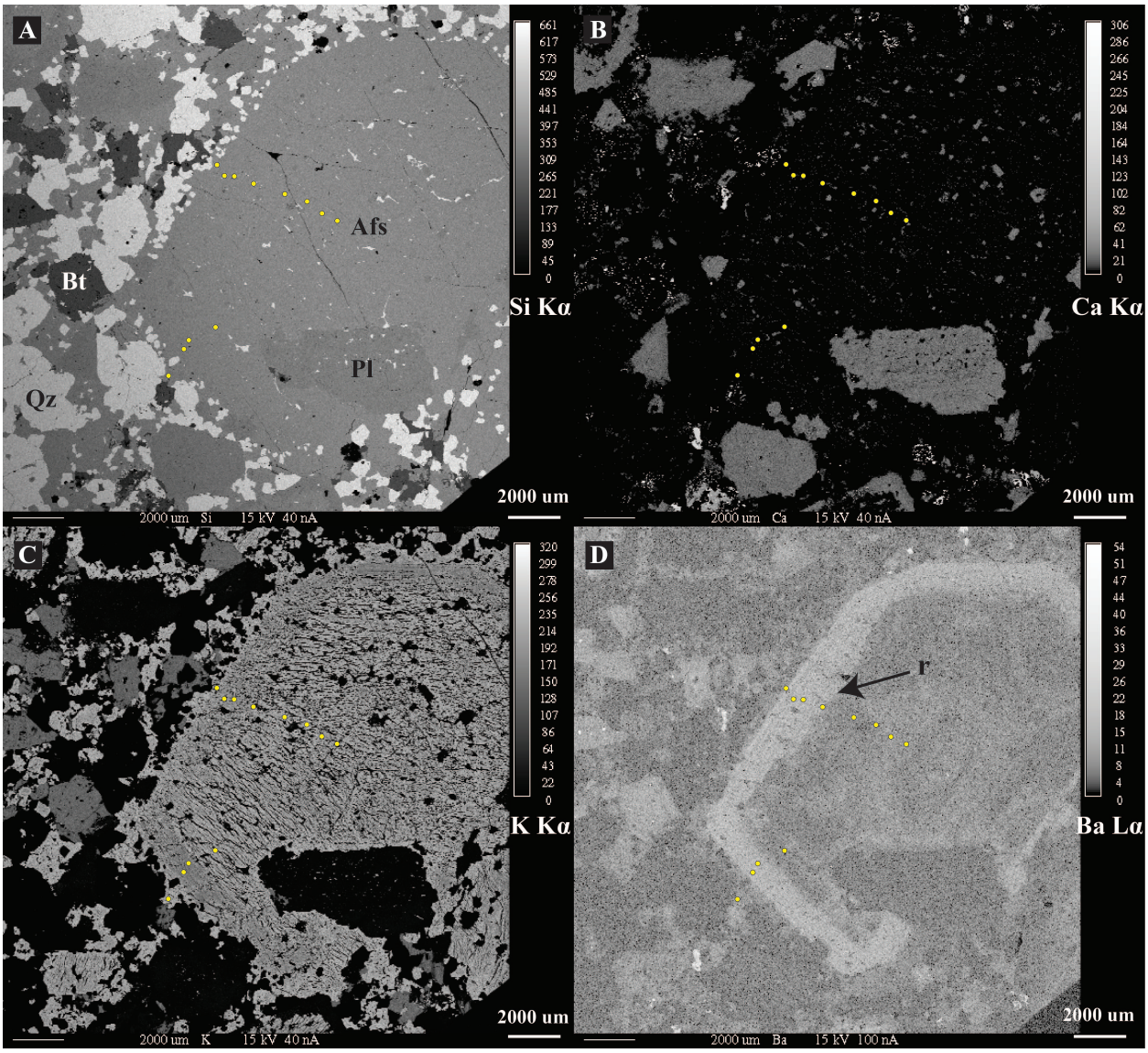

Figure 9. X-ray element maps of unmantled alkali feldspar phenocryst FP-4-7R1. Greyscale element maps of Si (a), Ca (b), K (c), and Ba (d) with Pb isotope analysis locations marked with yellow circles. Major phases include plagioclase (Pl), alkali feldspar (Afs), quartz (Qz), and biotite (Bt). Perthitic nature of alkali feldspar is clearly seen in K map (c). Ba-rich zone is easily seen in Ba map (d) and highlights an inferred resorption surface (r), marked by arrow.

Quartz Phenocrysts

Quartz phenocrysts are found up to 1 cm in size forming anhedral to subhedral, poorly rounded to rounded grains. Grains are seen as either amalgamations of several distinct grains, with generally a central or dominant grain making up the majority of the phenocryst, or as single distinct grains (Fig. 10). Cathodoluminescence (CL) imagery of several quartz grains revealed primary growth zonation that includes normal (bright to dark), and reverse (dark to light) step zoning (Fig. 10); zoning trends are based on the assumption that the brighter zones are richer in Ti than the lighter ones (e.g. Müller *et al.*, 2005). Quartz grains exhibiting distinct oscillatory zoning have successions of brighter and darker growth domains around central cores. These domains generally exhibit a euhedral crystal habit that is accentuated by normal and reverse zoning. Contacts are sharp and irregular with newer domains truncating older ones along an inferred resorption surface (arrows in Fig. 10).

Secondary features found in all CL images of quartz grains are fine, dark wispy bands that appear to represent healed brittle fractures ("f" in Fig. 10). These are over printed by nearly non-luminescence quartz that surrounds fluid inclusions giving the appearance of dark fractures to the images ("i" in Fig. 10). The last quartz to mantle these phenocrysts generally exhibit a darker luminescence than that seen internally and produces an anhedral texture.

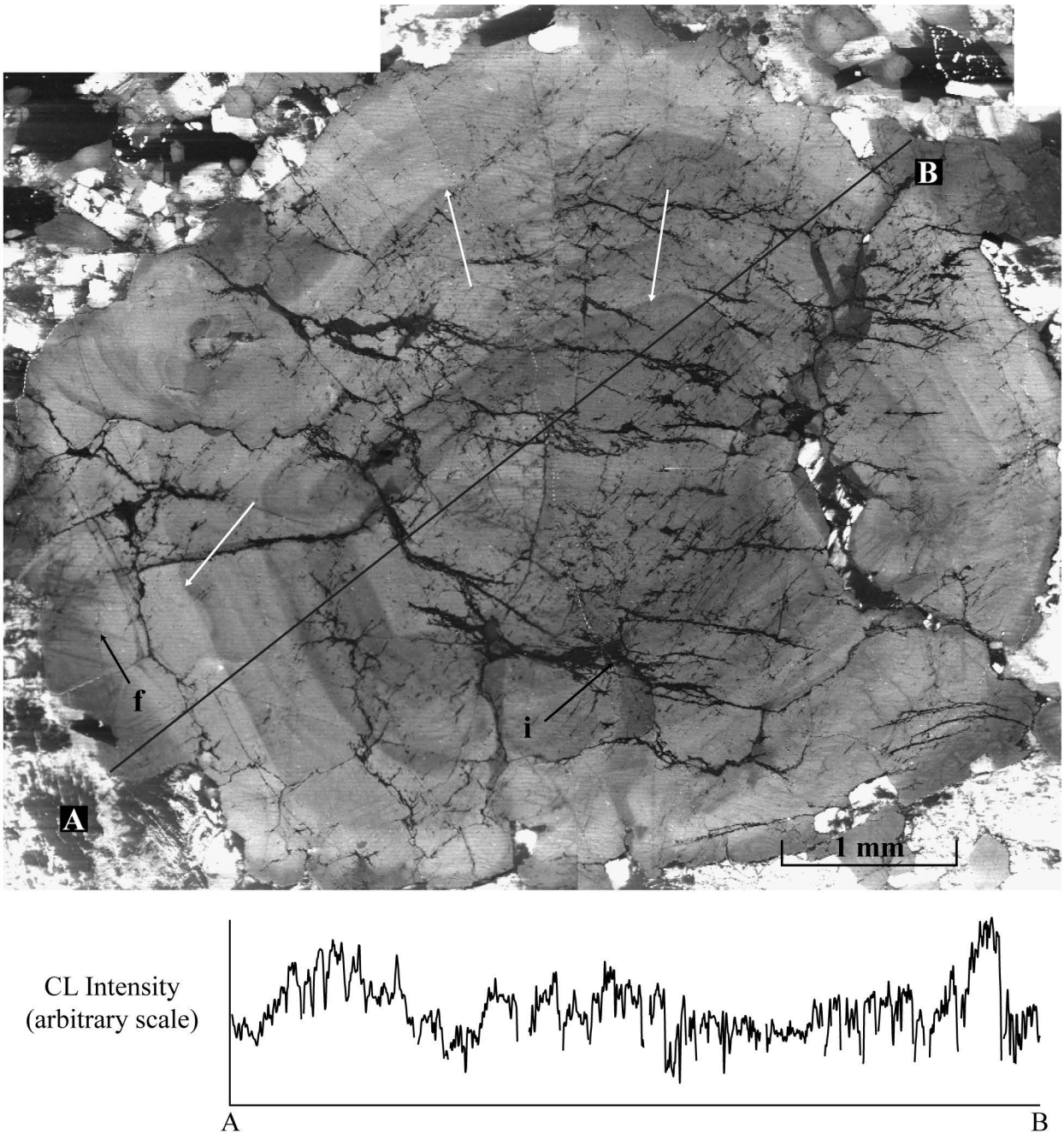

Figure 10. Cathodoluminescence image of quartz phenocryst from the Flye Point facies (FP-5-6) showing distinct bright growth zones; an inferred response to changing Ti concentrations. Brittle fractures (f) and fluid inclusions (i) are present throughout. White arrows mark resorption surfaces that have been over grown by a more luminescent quart (Note truncated zone below left most arrow). Line represents transect across phenocryst, which is shown below. Gaps in profile represent where transect intersected fluid inclusion-rich zones.

Geochemistry

Major elements

For all alkali feldspar cores, compositions typically varied between Or_{90} to Or_{97} (Fig. 11). Compared to volcanic alkali feldspar (typically less than $<Or_{75}$), these have significantly higher Or and show that Ab has exsolved (Tuttle, 1952). Rimward towards the core-mantle boundary, Ba concentrations are typically higher (>0.3% BaO) relative to the inner core (~0.1 % BaO) (e.g. FP-4-7R2, Fig. 5). In these Ba-rich zones, Or is generally much lower and exhibits a larger degree of variability ($Or_{62} - Or_{90}$). Perthitic and microperthitic textures are present in all samples with lamellae ranging from 91-99 mol % Ab (Fig. 11). Perthite is less developed in areas of the cores where the BaO concentration is higher (>0.5 wt %) and is believed to be the reason for the lower mol % Or values noted above. Higher BaO content must have inhibited albite exsolution from the alkali feldspar.

Plagioclase phenocrysts are the most An-rich with cores of up to An_{27}. Plagioclase mantles, on both plagioclase phenocrysts and rapakivi grains, have a mean composition of An_{20} and are typically oscillatory zoned with maximum amplitudes of 3 mol % An. Albitic plagioclase ($An_{<14}$) forms the outermost edge on both rapakivi and plagioclase phenocrysts as a result of melt fractionation. Plagioclase inclusions within alkali feldspar cores of rapakivi grains have a mean value of An_{20} and, like the mantles, have more albitic rims (An_{13}). Within the coarse-sieve textured regions of both plagioclase phenocrysts (Fig. 8) and double mantled rapakivi feldspars (Fig. 6), albitic plagioclase (An14-17) is found along contacts with quartz pockets. Isolated albitic patches are also noted within this region and are believed to represent the same contact with quartz, only in the third dimension.

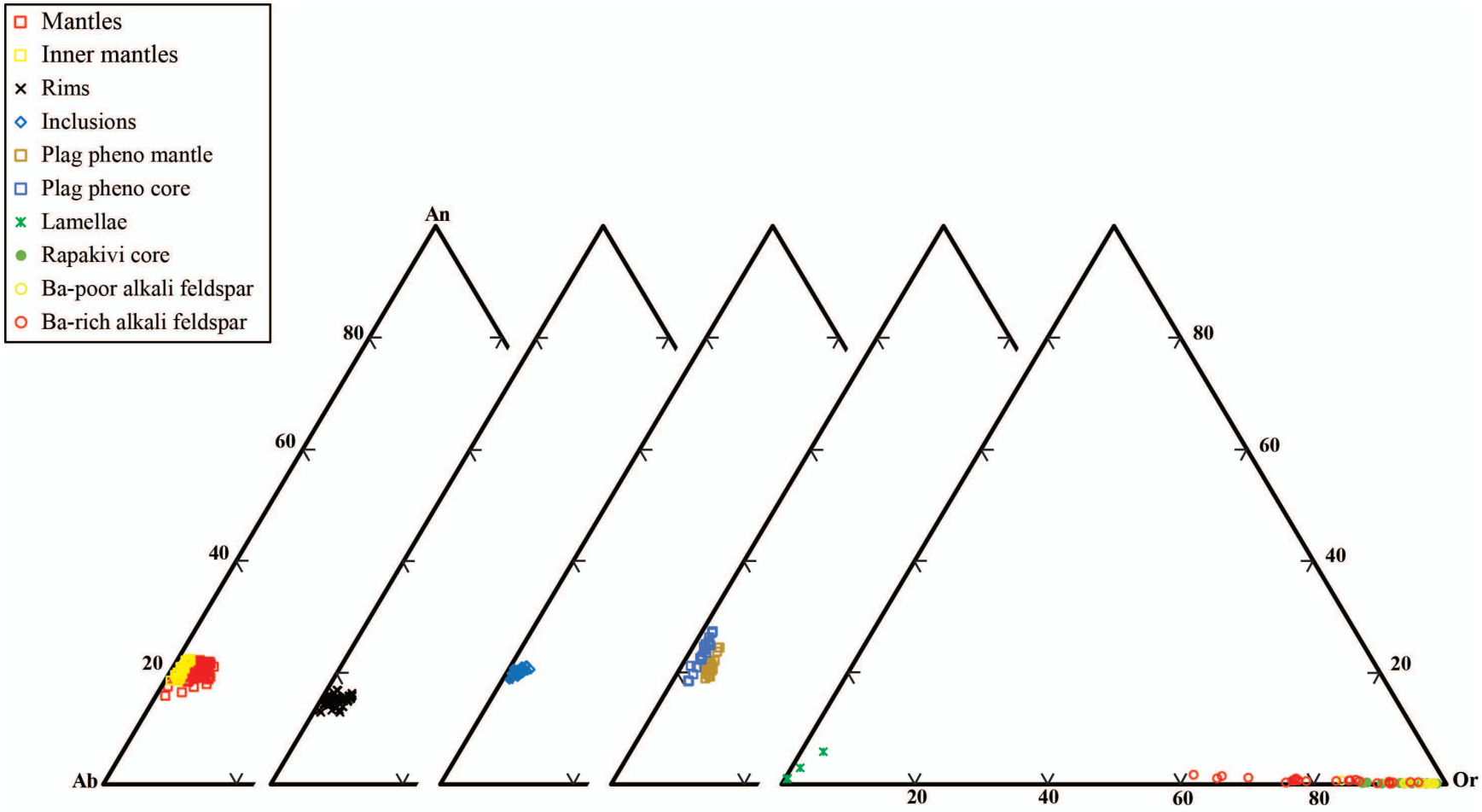

Figure 11. Feldspar ternary diagram of rapakivi cores (alkali feldspar), mantles (plagioclase), plagioclase phenocrysts, and alkali feldspar phenocrysts from the Flye Point facies of the Deer Isle Granite Complex.

Trace Elements

Trace element analyses by LA-ICP-MS (Figs. 12-15) were conducted on plagioclase mantles of rapakivi grains, plagioclase inclusions in the alkali feldspar cores, and plagioclase phenocrysts. Alkali feldspar cores and phenocrysts were not analyzed using LA-ICP-MS so comparisons of rapakivi alkali feldspar cores and alkali feldspar phenocrysts were done using major element maps (Figs. 4-9) and spot analyses with the electron microprobe (Appendix 2). Below, we describe the elemental variations in 5 grains from 3 hand samples of the Flye Point facies of the Deer Isle Granite Complex.

Rapakivi FP-4-1R1

Trace element concentrations in rapakivi grain FP-4-1R1 (portrayed in Fig. 4) are presented in Figure 12a-c. Plagioclase inclusions within the Ba-poor alkali feldspar core have lower concentrations of Ba, La, and Ce than plagioclase in the mantle. This lower abundance is independent of An content since both plagioclase inclusions and plagioclase mantle are ~An_{20}. Inclusions within the Ba-rich alkali feldspar zone of the core were not analyzed but the zone is marked in Figure 12 using element maps (Fig. 4) and CL imagery (Fig. 16).

Variations in trace element concentrations, seen especially in its Ba content (Fig. 12a), indicate oscillatory zoning of the plagioclase mantle. This oscillatory zoning is not expressed in major element changes but is easily seen in CL imagery of the rapakivi grain (Fig 16). We interpret the oscillatory zonation to be the result of plagioclase crystallization from melts with time-varying compositions. Ba concentrations appear to be more sensitive to changes in melt composition than La or Ce, probably because of the much higher partition coefficients for Ba in plagioclase than for the LREE. Superimposed on the oscillation is a decrease in Ba concentration from approximately 400 ppm to 200 ppm. This probably indicates a fractionation trend rimward

from the core-mantle boundary as Ba-rich phases (alkali feldspar and biotite) fractionated from the magma.

Rapakivi FP-4-7R2

The relatively small size and minor alteration of plagioclase inclusions within the alkali feldspar core of rapakivi grain FP-4-7R2 deterred their analysis, however it is noted that a plagioclase-rich inclusion zone is discernable in element maps (Fig. 5). A Ba-rich zone within the outer part of the alkali feldspar core is also observed in element maps (Fig. 5d) and has been marked in Figure 13.

Within the plagioclase mantle of the grain, Ba, La, and Ce concentrations are relatively low along the core-mantle boundary (Fig 13a-c). Also within this zone the An content is atypically lower (An_{18-19}) than that found in the rest of the mantle (An_{20-22}). Rimward distinctive increases in Ba and LREE concentrations occur such that a double mantle is evident. Most notably Ba concentrations double to 300 ppm (Fig 13a), something not evident in its element map (Fig. 5d). For Ba, this increase in concentration is then followed by an abrupt decrease to values comparable to those along the core-mantle boundary (~150 ppm). La and Ce concentrations form a similar pattern of low, high, and low concentrations rimward in the mantle. However, the second zone of relatively low concentrations are on average slightly higher than those along the core-mantle boundary (Fig. 13b-c). It is noted that the increase and then decrease in trace element concentrations is not accompanied by a change in An concentrations and values remain consistently ~An_{21}.

Rapakivi FP-3-1R1

A texturally distinct double mantle of plagioclase on this rapakivi grain is seen optically and in X-ray element maps (Fig. 6). Much like FP4-7R2, Ba, La, and Ce concentrations are

relatively low within the inner most part of the coarse-sieve textured plagioclase mantle (Fig. 14a-c). Rimward, concentrations increase in a zone of elemental enrichment, followed by a decrease in the outer part of the plagioclase mantle. As in FP-4-7R2, the changes are most notably seen in Ba concentrations. Within the inner mantle values average ~150 ppm for Ba (Fig. 14a). Ba concentrations more than double to about ~320 ppm in a zone also enriched in La and Ce. The punctuated decrease in Ba, La and Ce concentrations within the outer part of the second plagioclase mantle are nearly identical to that seen in the mantle of FP-4-7R2.

Ba, La, Ce are all strongly depleted along the most outer edge of the second mantle where plagioclase becomes more albitic (~An_{14}). The declining An and concentrations of Ba, La, and Ce are again most likely due to fractionation of the host magma with the continued growth of plagioclase, alkali feldspar, and the accessory phases allanite and titanite. Albitic rims of plagioclase in contact with quartz are also found within the coarse-sieve textured area of the first mantle (Figs. 6 & 17). These albitic rims may reflect continued feldspar growth accompanying fractionation of trapped melt, or subsolidus growth during the exsolution of alkali feldspar. Due to their size, plagioclase inclusions within the alkali feldspar core were not analyzed.

Rapakivi FP-5-8R1

Although not as pronounce as in some of the previous grains, the alkali feldspar core of rapakivi grain FP-5-8R1 has a zone of plagioclase inclusions near its outer edge (Fig. 7). Ba, La, and Ce concentrations in these inclusions on average are much higher than concentrations in inclusions found within rapakivi grain FP-4-1R1 (Fig. 15). For Ce and La, no major change in their concentrations is observed toward the edge of the alkali feldspar core. Ba, however, may form a fractionation trend (decreasing from 267 ppm to 117 ppm) within the inner half of the core. This decrease is followed by a jump back to ~250 ppm Ba in plagioclase inclusions closer

to the rim. A plagioclase inclusion within the core-mantle boundary records values of 357 ppm Ba in its inner region followed by 253 ppm towards its outer edge (Fig. 15a). Trace element concentrations within albitic rims plagioclase inclusions were the lowest observed.

In the plagioclase mantle, trace element concentrations are relatively constant for over half the width of the mantle, after which a distinct fractionation trend is observed with declining Ba, La, and Ce. It is noted that oscillatory zones seen optically in the plagioclase mantle are very narrow (< 50 μm). This caused spatial resolution issues with analyses as a single laser spot sometimes sampled two to three oscillatory zones at once and so provided more of an average over the area analyzed. This could have "smeared" out any variations in trace element concentrations caused by the oscillatory growth.

Alkali Feldspar Phenocryst FP-4-7R1

Although LA-ICP-MS trace element analyses were not conducted on this alkali feldspar phenocryst, BaO was analyzed by electron microprobe (Appendix 2). Due to the observed correlation of Ba to La and Ce in previous grains, the Ba data is used here for comparison.

The core of this alkali feldspar grain has an average BaO concentration of ~0.1 wt % with only minor zoning seen in its element map (Fig. 9). A resorption surface (r in Fig. 9) marks the boundary between a Ba poor core and a 2 mm wide Ba-rich rim. This rim has oscillatory zoning with an average BaO concentration of 0.51 wt %, with concentrations reaching as high as 0.79 wt % (Fig 9; Appendix 2).

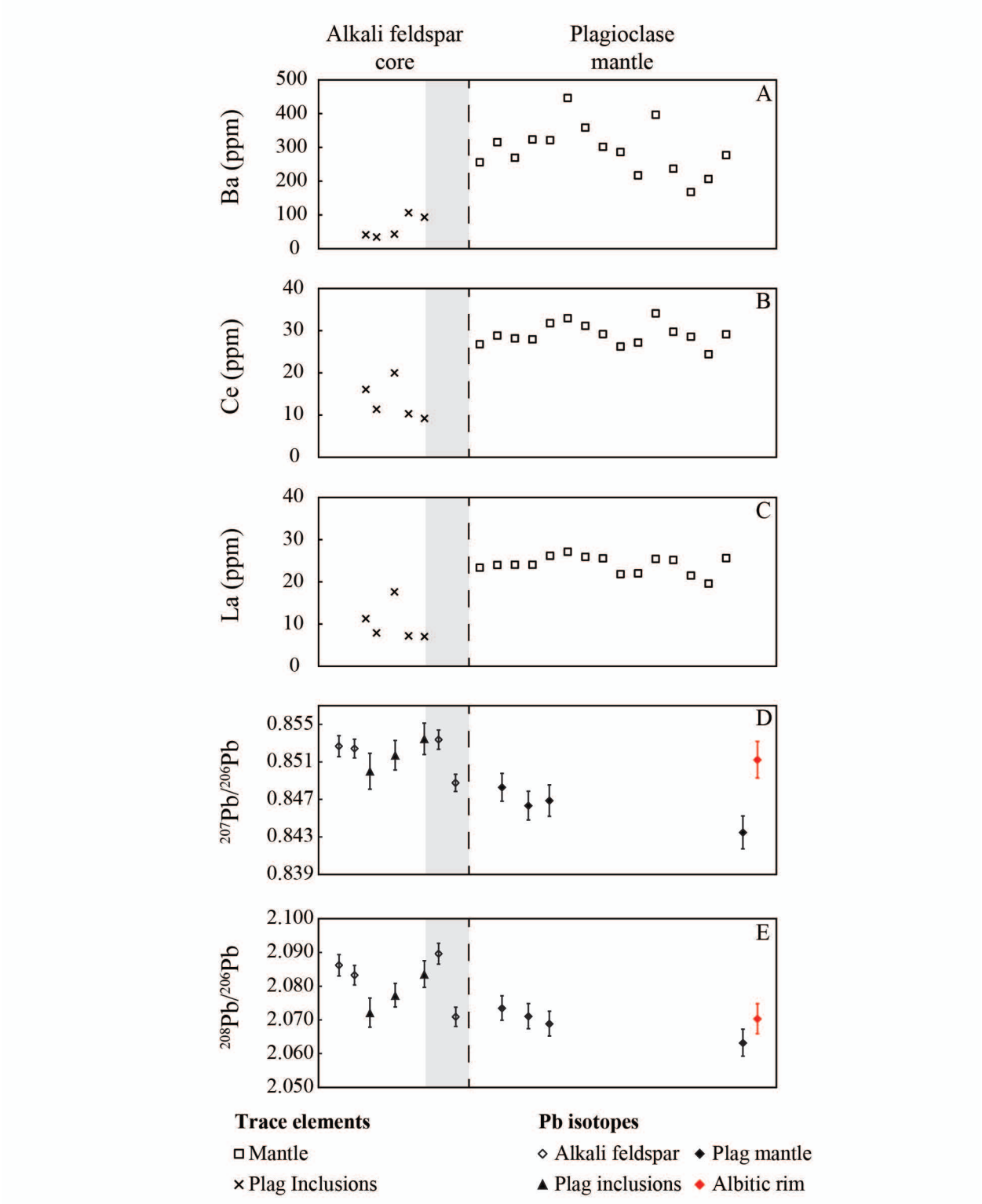

Figure 12. Trace element and Pb isotope core to rim profiles of rapakivi grain FP-4-1R1 (Fig. 4). Bold dashed line represents core-mantle boundary (alkali feldspar-plagioclase contact) within grain. Gray area marks Ba-rich alkali feldspar zone revealed in Ba element map (Fig. 4d). Trace element uncertainties are smaller than symbols and Pb isotope ratio uncertainties show 2σ error bars.

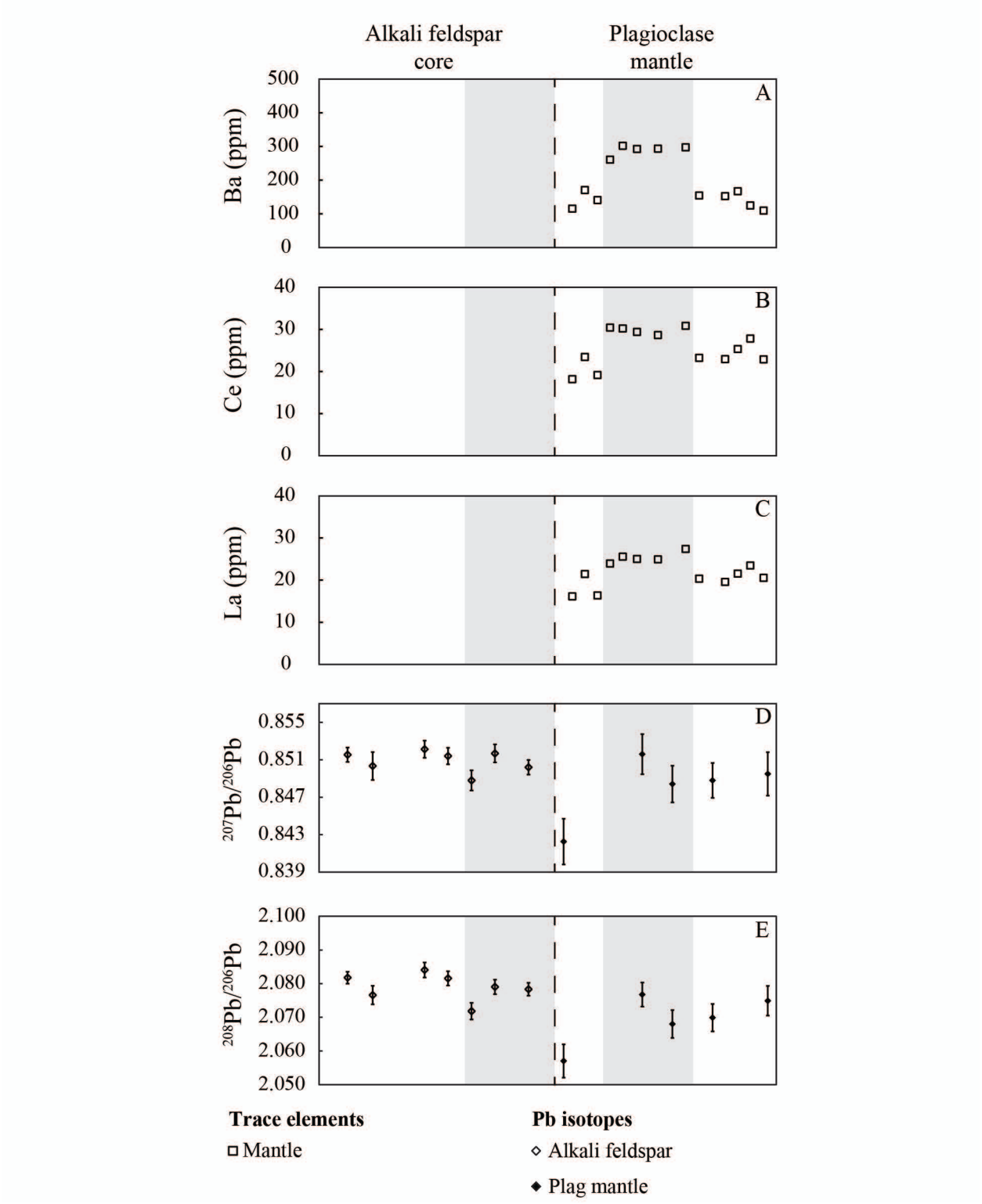

Figure 13. Trace element and Pb isotope core to rim profiles of rapakivi grain FP-4-7R2 (Fig. 5). Bold dashed line represents core-mantle boundary (alkali feldspar-plagioclase contact) within grain. Gray areas mark zones of Ba-rich alkali feldspar (core) and plagioclase (mantle) within grain. Trace element errors are smaller than symbol and Pb isotope uncertainties show 2σ error bars.

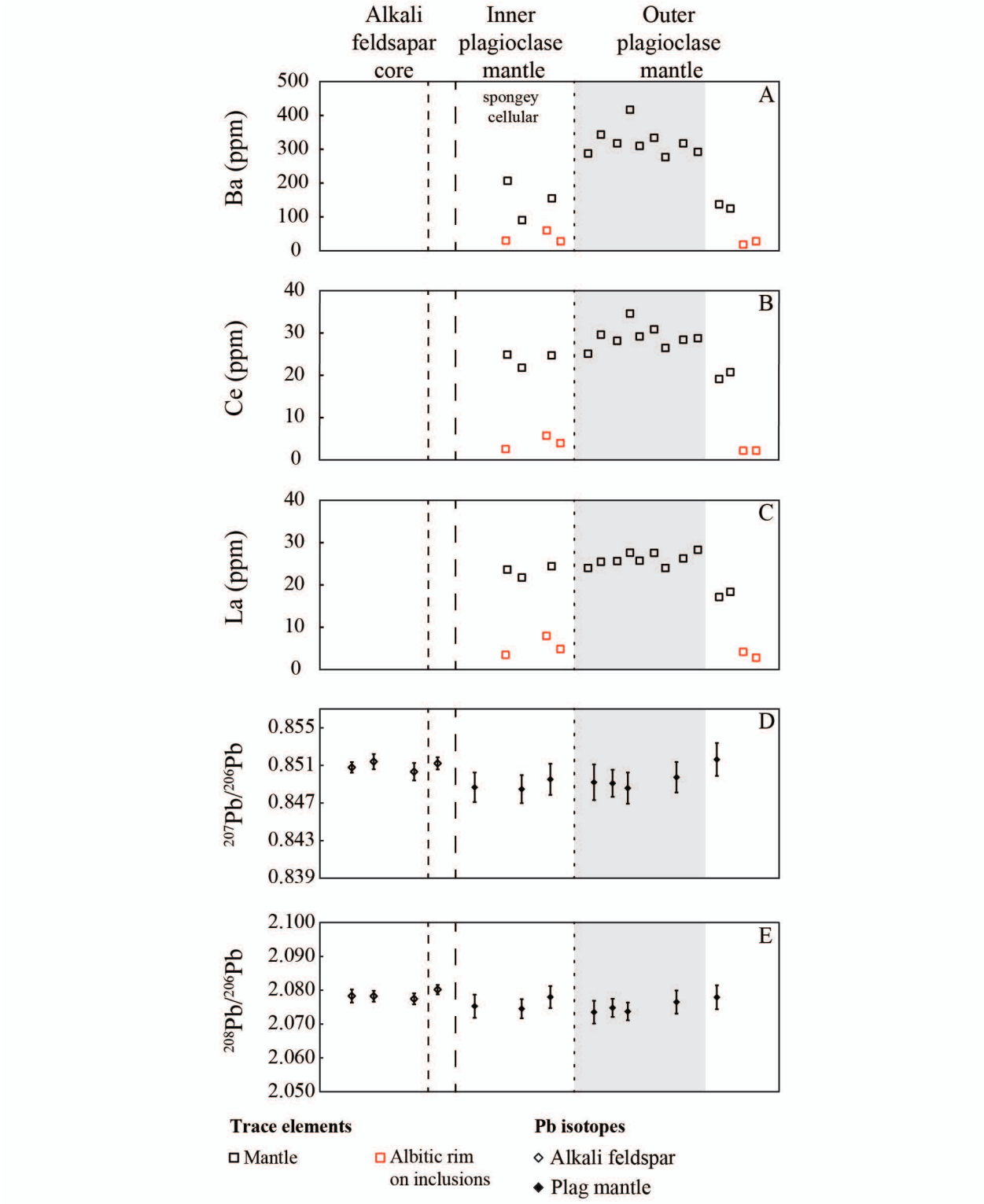

Figure 14. Trace element and Pb isotope core to rim profiles of rapakivi grain FP-3-1R1 (Fig. 6). Bold dashed line represents core-mantle boundary (alkali feldspar-plagioclase contact) within grain. Dashed line represents resorption surface (r) in Figure 6c. Dotted line represents contact between the first and second plagioclase mantles. Gray areas mark zone of Ba-rich plagioclase within mantle. Trace element errors are smaller than symbol and Pb isotope uncertainties show 2σ error bars.

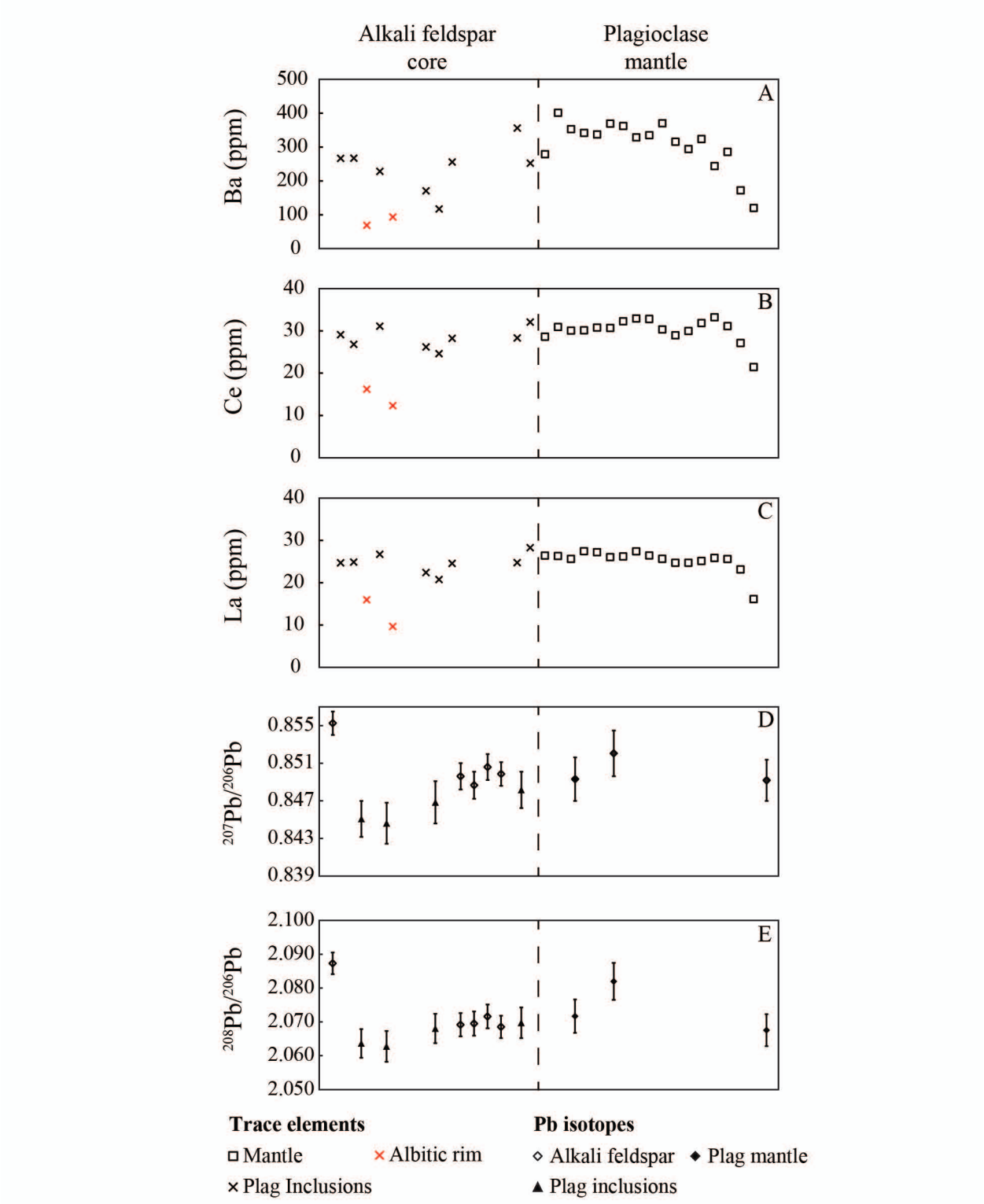

Figure 15. Trace element and Pb isotope core to rim profiles of rapakivi grain FP-5-8R1 (Fig. 7). Bold dashed line represents core-mantle boundary (alkali feldspar-plagioclase contact) within grain. Trace element errors are smaller than symbol and Pb isotope uncertainties show 2σ error bars.

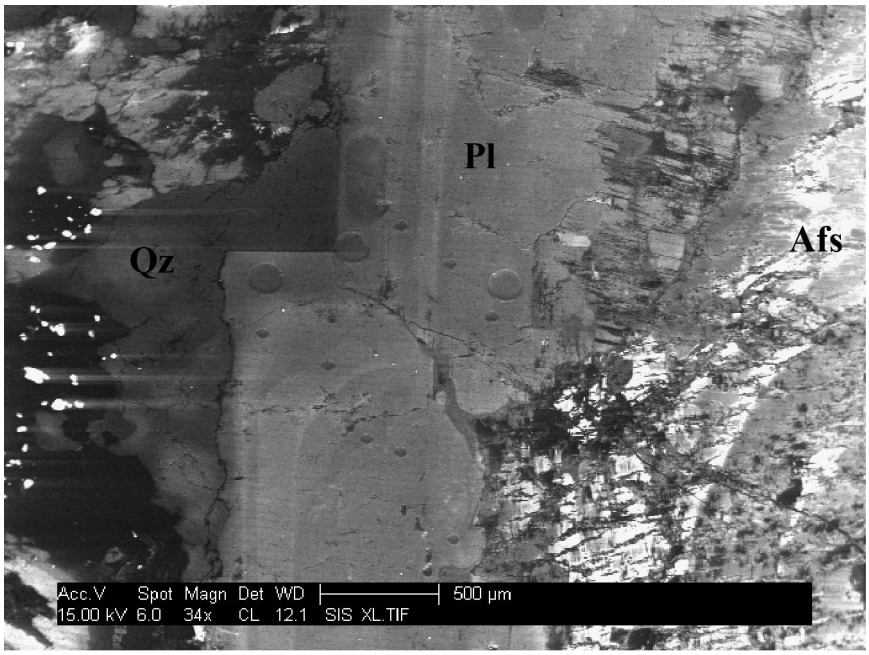

Figure 16. CL image showing oscillatory zoning in plagioclase mantle (Pl) and within the alkali feldspar core (Afs) of rapakivi grain FP-4-1R1 (see Fig. 4 for location. Note subhedral/euhedral plagioclase growth where in contact with quartz (Qz). Relative brighter regions indicate increases in either rare earth elements (e.g. Ce^{3+} or Eu^{3+}) or defects in crystal lattice that may be due to ion substitutions (e.g. Al^{3+} for Si^{4+}) (Boggs and Krinsley, 2006 and citations within).

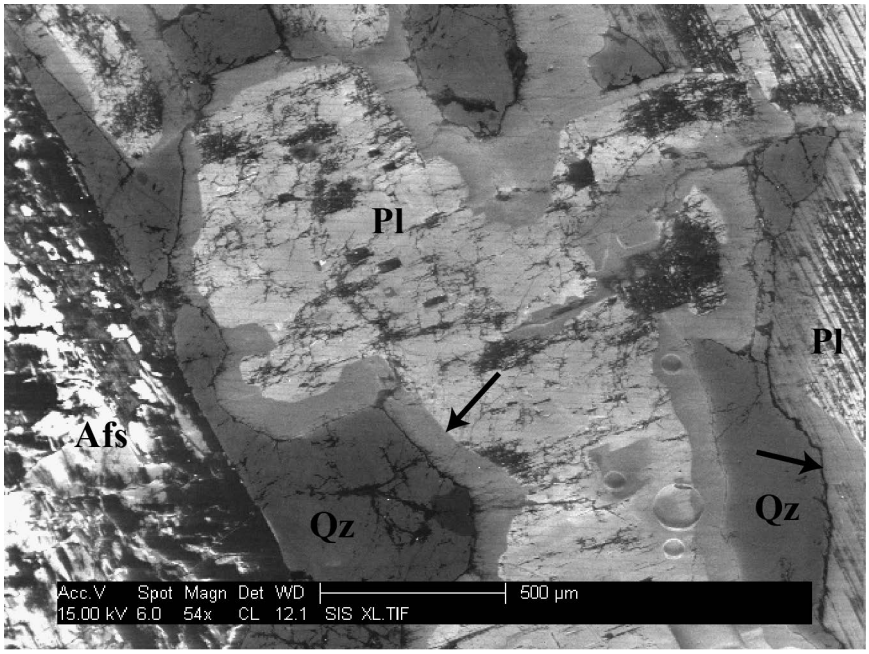

Figure 17. CL image showing coarse sieve texture of the 1st plagioclase mantle in rapakivi grain FP-3-1R1 (See Fig. 6 for location). Note the euhedral face of alkali feldspar core (Afs) in contact with quartz (Qz). Plagioclase (Pl) of both the coarse-sieve textured 1st (center) and 2nd (far right) mantle shows growth of more albitic phase (arrows) where it is in contact with quartz.

Pb Isotopes

Rapakivi FP-4-1R1

The inner Ba-poor alkali feldspar core of this rapakivi grain (Fig. 4) has average $^{207}Pb/^{206}Pb$ of ~0.853 and $^{208}Pb/^{206}Pb$ of ~2.085 (Fig. 12d, e). Plagioclase inclusions within the innermost Ba-poor core have a slightly more primitive isotopic signature ($^{207}Pb/^{206}Pb = 0.850$ and $^{208}Pb/^{206}Pb = 2.072$), but then trend increasingly back to values similar to those found within the inner most area of the alkali feldspar core. The most rimward plagioclase inclusion falls along the contact where the Ba-poor alkali feldspar core is overgrown by a more Ba-rich alkali feldspar. Isotopic ratios within this inclusion and those proximal to, and within the Ba-rich overgrowth, are comparable with each other. Rimward (i.e. towards the core-mantle boundary), there is a marked decrease in isotopic ratios ($^{207}Pb/^{206}Pb = 0.848$ and $^{208}Pb/^{206}Pb = 2.071$; Fig. 12d, e) that drops to values similar to those found within the inner most plagioclase inclusion.

Across the core-mantle boundary, isotopic values continue to drop rimward to the lowest values found within the grain ($^{207}Pb/^{206}Pb = 0.843$ and $^{208}Pb/^{206}Pb = 2.063$). Along the most outer edge of the mantle, which is marked by a decrease in mol % An (An_{15}), isotopic Pb ratios increase ($^{207}Pb/^{206}Pb = 0.851$ and $^{208}Pb/^{206}Pb = 2.070$). Of note, is the disparity between the relative increases in ratios of these outermost analyses.

Rapakivi FP-4-7R2

Like FP-3-1R1, this grain also has a relatively Ba-poor alkali feldspar inner core that is overgrown by more Ba-rich alkali feldspar (Fig. 5). Within the Ba-poor inner core, there is a weak decreasing trend in the Pb isotope ratios rimward (Fig. 13d, e). This is marked by two minor steps where there is a drop in isotopic ratios. The second of these minor drops is located

on the contact between the Ba-poor and Ba-rich alkali feldspar core. Outward from here, toward the core-mantle boundary, ratios return to the slightly higher inner core values.

Outward from the core-mantle boundary, the plagioclase mantle's isotopic ratios drop to the lowest values seen in any of the analyzed grains ($^{207}Pb/^{206}Pb$ =0.842 and $^{208}Pb/^{206}Pb$ = 2.057). Again, it is noted that here the molar An content of the inner most mantle is slightly lower (An_{18-19}) and atypical of the more constant An_{20-22} seen in the rest of the mantle. As stated above, Ba, La, and Ce are also depleted within this zone.

Rimward, within a Ba-rich zone (see above), isotope ratios jump to values similar to those seen throughout most of the alkali feldspar core ($^{207}Pb/^{206}Pb$ =0.852 and $^{208}Pb/^{206}Pb$ = 2.077), but then drop to relative moderate values ($^{207}Pb/^{206}Pb$ =0.848 and $^{208}Pb/^{206}Pb$ = 2.068). From here, and within another zone of depleted Ba, La, and Ce, Pb isotopic ratios gently increase rimward (Fig. 13d, e).

Rapakivi FP-3-1R1

As seen in Figure 6, this rapakivi grain has a double plagioclase mantle with the inner mantle possessing a coarse sieve texture and the outer mantle showing normal oscillatory zoning. Within the alkali feldspar core Pb isotopic ratios are similar to those seen in other grains ($^{207}Pb/^{206}Pb$ =0.851 and $^{208}Pb/^{206}Pb$ = 2.079) however, they have limited variability rimward (Fig. 14d, e). Also unique to this grain is an inferred resorption surface within the outer edge (proximal to the core-mantle boundary) of the core ("r" in Fig. 6c). Only a slight increase in $^{208}Pb/^{206}Pb$ ratios exists between the inner and outer (after resorption surface) core, but this difference is within error of the other analyses (Fig. 14e).

A minor decrease in Pb isotopic ratios occur with the transition across the core-mantle boundary into the first plagioclase mantle. Within this innermost mantle values average 0.849

and 2.076, $^{207}Pb/^{206}Pb$ and $^{208}Pb/^{206}Pb$ respectively, with a hint at a minor increase along the contact with the second mantle. Ratios within the second plagioclase mantle also show limited variability with an average of 0.849 and 2.074, $^{207}Pb/^{206}Pb$ and $^{208}Pb/^{206}Pb$ respectively, with the last three analyses rimward indicating a trend of increasing isotopic ratios that match the values of the alkali feldspar core.

Rapakivi FP-5-8R1

Unlike other rapakivi gains, FP-5-8R1 displays a distinct ovoidal morphology, possibly caused by sectioning perpendicular to the c-axis Fig. 7). The innermost alkali feldspar analysis has the highest Pb isotope ratios measured in any of the alkali feldspar cores ($^{207}Pb/^{206}Pb = 0.855$ and $^{208}Pb/^{206}Pb = 2.087$). Rimward, within zonally (crystallographically) arranged euhedral plagioclase inclusions, there is a large decrease in isotopic ratios ($^{207}Pb/^{206}Pb = 0.845$ and $^{208}Pb/^{206}Pb = 2.064$) (Fig. 15d, e). Pb isotopic values within these plagioclase inclusions display a slightly increasing trend toward the core-mantle boundary. Average ratio values of 0.849 and 2.070 ($^{207}Pb/^{206}Pb$ and $^{208}Pb/^{206}Pb$ respectively) for the outer part of the alkali feldspar core appears to lie along trend with the increase seen in these plagioclase inclusions.

Within the plagioclase mantle, Pb isotope ratios closest to the core-mantle boundary appear to be the same as those found in the outer core. Within the very center of the plagioclase mantle however there is a minor increase in Pb isotopic ratios with no associated change in Ba, La, or Ce concentrations or An content. It is noted again the size of oscillatory zoning was < 50 μm for some areas of the mantle and caused spatial resolution issues (laser spot size = 50 μm). Following this increase, isotopic ratios drop to values comparable to the outer core average ($^{207}Pb/^{206}Pb = 0.849$ and $^{208}Pb/^{206}Pb = 2.068$) (Fig. 19).

Alkali Feldspar Phenocryst FP-4-7R1

Although not a rapakivi, this alkali feldspar phenocryst displays an inner core that has been overgrown by a rim of Ba-rich alkali feldspar (Fig. 9). Much like the rapakivi feldspars, the inner alkali feldspar core has average Pb isotope ratios of 0.851 and 2.090 ($^{207}Pb/^{206}Pb$ and $^{208}Pb/^{206}Pb$ respectively; Fig. 18). These ratios show marked decreases proximal to the contact with the Ba-rich rim. Crossing the boundary, this drop is followed by the increase of Pb isotope ratios back to values similar to the inner core ($^{207}Pb/^{206}Pb$ = 0.852 and $^{208}Pb/^{206}Pb$ = 2.084).

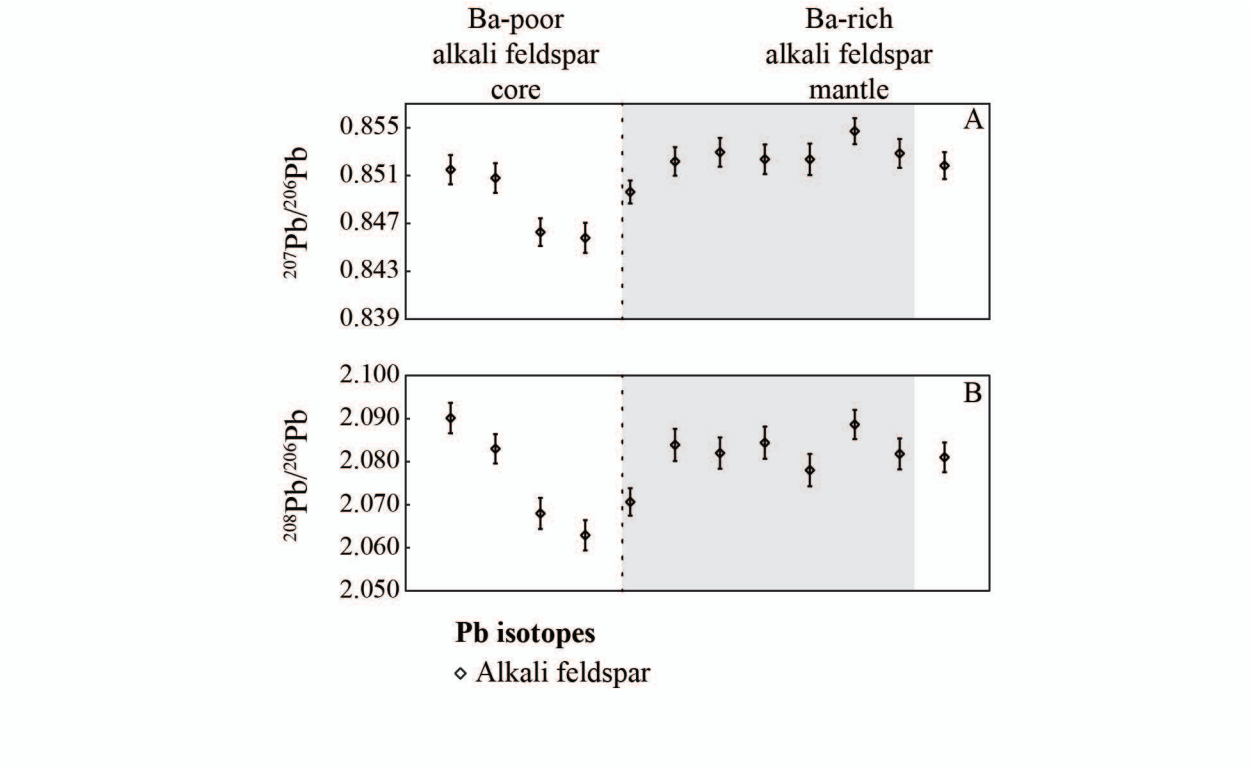

Figure 18. Pb isotope core to rim profiles of rapakivi grain FP-4-7R1. Dashed line marks contact between Ba-poor inner core and Ba-rich rim (gray area). Pb isotope uncertainties show 2σ error bars.

DISCUSSION

The formation of rapakivi feldspars has been explained by both isothermal decompression of a granitic magma (e.g. Nekvasil, 1991) and by magma mixing (e.g. Wark and Stimac, 1992). To review, isothermal decompression of a granitic magma has been shown to cause alkali feldspar and quartz to destabilized, while plagioclase remains stable. During ascent, the resorbed alkali feldspar and quartz provide the nuclei for additional growth of plagioclase and quartz (respectively). Because there is no contamination of the host magma, isothermal decompression is considered a closed system hypothesis.

Magma mixing on the other hand, represents an open system. Here, the host magma is contaminated by another magma (or magmas) during crystallization. If crystallization of alkali feldspar has occurred in the host magma when mixing begins, the injection of a hotter, and/or chemically different, magma can create disequilibrium in the host and cause resorption of alkali feldspar. As cooling (equilibration) again begins, these partially resorbed alkali feldspars act as nucleation surfaces for plagioclase.

In a closed system, because there are no external inputs into the magma system, the host magma's Pb isotopic composition does not change during crystallization. Thus, minerals that crystallized prior to decompression will have the same isotopic signatures as those that formed after ascent and emplacement of the magma. In an open system, the host magma's bulk chemistry may be changed with the subsequent addition of new batches of magma. The resulting minerals may therefore show trace element and isotopic zoning or mantling that reflects the dynamic nature of the open system from which they crystallized.

The observed ranges of isotopic values in the feldspar grains from the Deer Isle Granite Complex, especially between the alkali feldspar cores and their plagioclase mantles, demand that

there was contamination of the system during formation (not just simple growth) of these minerals. Outward from the inner core each of the studied grains has a different crystallization history as revealed by its isotopic and trace element compositions. Figure 19 shows the crystal growth (and resorption) histories of each grain in Ba/Pb* space (Pb* = isotopic Pb). We suggest that these different compositional histories are indicative of open system development and were caused by the relative movement of each grain through a compositionally varied magma as discussed below.

Formation of feldspars

Alkali feldspar and rapakivi cores

Compositions of the most inner cores of all grains examined, both rapakivi and unmantled alkali feldspars, have similar initial Pb isotope compositions (Fig. 19, pt. 1). An exception to this observation may be with rapakivi grain FP-5-8R1, which possess slightly higher isotopic Pb values in its inner alkali feldspar core ($^{208}Pb/^{206}Pb = 0.855$ and $^{207}Pb/^{206}Pb = 2.087$); however, this observation is based on only one analysis. Each grain (rapakivi and alkali feldspar phenocrysts) also have relatively low Ba concentrations within their inner alkali feldspar cores (Figs. 4d, 5d, 6d, 7d & 9d). This suggests they all initially crystallized from a common Ba-poor and relatively isotopically evolved magma.

As growth continued, most of the feldspar grains recorded lower Pb isotope ratios rimward with minor to little change in Ba concentrations (Fig. 19, pt. 2). This drop is more noticeable in grains FP-5-8R1 and FP-4-7R1 with only a limited decrease in grains FP-4-1R1 and FP-4-7R2 (Fig. 19). Mixing of the host with an isotopically more primitive and relatively Ba-poor magma could account for this change. Each grain's relative proximity to a zone of mixing between magmas described above could account for the differences in their isotopic Pb

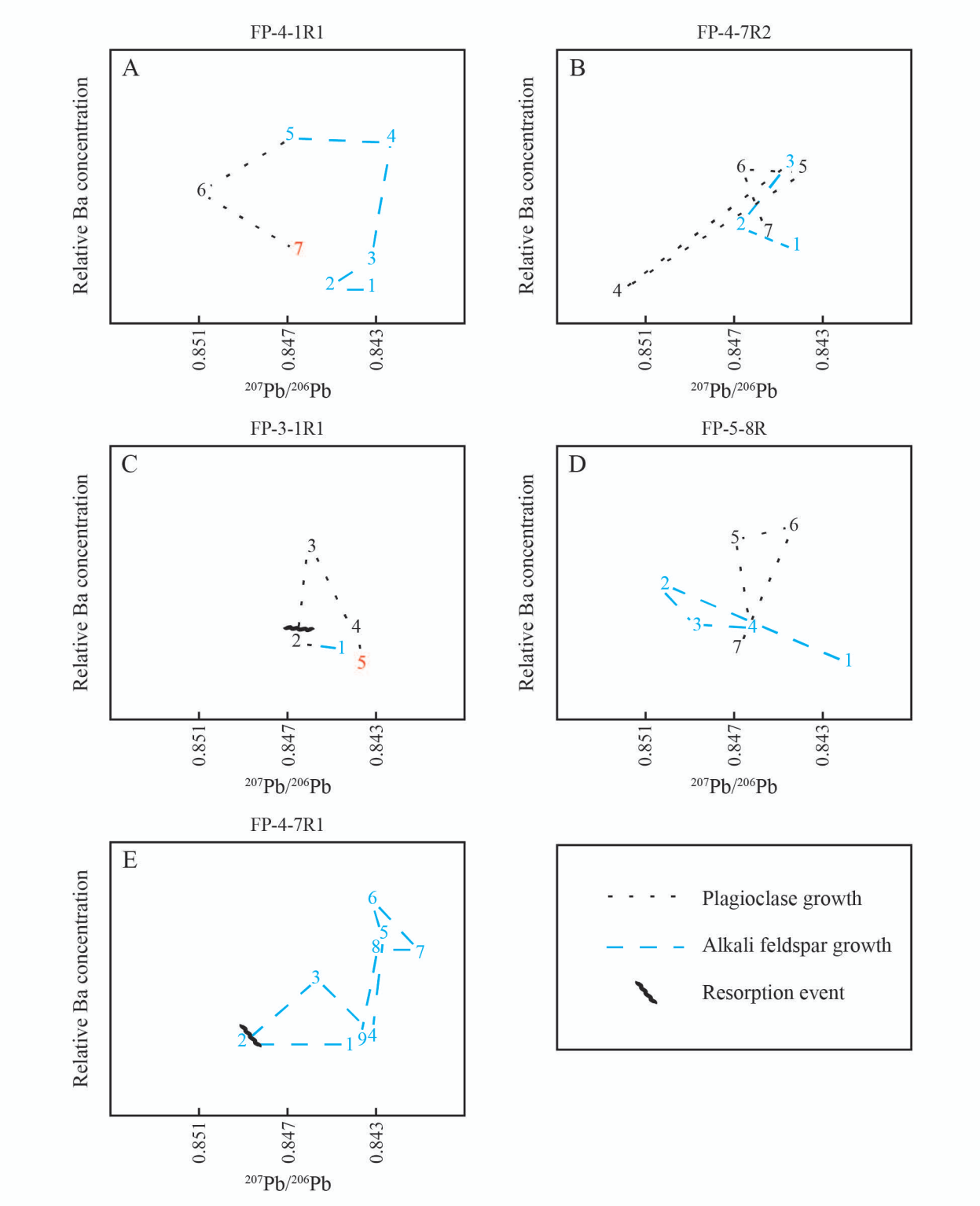

Figure 19. Crystal growth/resorption histories in Relative Ba / $^{207}Pb/^{206}Pb$ space for rapakivi (a-d) and alkali feldspar (e) grains from the Flye Point facies of the Deer Isle Granite Complex. Scale for Relative Ba concentrations is 0 to 500 ppm for plagioclase and 0 to 60 counts per second for alkali feldspars (taken from Ba element maps). Red indicates albitic growth.

values. A grain more proximal to this inferred mixing zone would acquire an isotopic signature more similar to the injected magma than would a grain more distal to the zone of hybridization.

From this point in their growth, the compositions of most of the grains indicate different crystallization histories. For rapakivi grain FP-5-8R1, it experiences an increase in its isotopic Pb ratios back to values similar to the host magmas, just prior to its inferred resorption and mantling event (Fig. 19d, pt. 3&4). The concentric zonation of plagioclase inclusions (Fig. 7) supports the idea that the grain may have remained proximal to the zone of mixing. Cyclic periods of rapid growth, brought on by its relative movement in and out of the zone of mixing, caused plagioclase crystals to become trapped along the crystallizing front of the alkali feldspar (Fig. 19d, pts. 2-4).

Grains FP-4-1R1 and FP-4-7R2 indicate they became entrained into a batch of Ba-rich magma isotopically similar to the host prior to becoming resorbed and then mantled by plagioclase (Fig. 19a, pt. 4 & b, pt. 3). Within some magma chambers there is evidence for chemical stratification occurring (e.g. Bateman and Chappell, 1979). The introduction of these grains into a batch of less fractionated host magma (i.e. still rich in Ba and isotopically similar) could account for the observed crystal growth. Just prior to being resorbed and then mantled, FP-4-1R1 was introduced into a batch of relatively isotopically primitive magma that was rich in Ba (Fig. 19a, pt. 5).

It is noted that although these grains seem to indicate they experienced different growth histories prior to being mantled, there is an inferred resorption event. The degree of resorption for each grain could have been different for each grain and so any common crystallization histories they may have shared just prior to mantling may have been removed. It is therefore not intended to suggest that the crystallization histories of these grains is completely captured in Figure 19.

Rapakivi and alkali feldspar mantles

Magma sources responsible for mantle growth of all grains appear to be just as varied as sources involved with growth of the outer parts of their cores. FP-4-7R2 for instance shows a large drop isotopically when initial growth of its mantle started (Fig. 19b. pt. 4). For FP-3-1R1, growth of its first mantle was in a Ba-poor and isotopically moderate magma (Fig. 19c, pt. 2); these values being only slightly lower than ones seen throughout its core (Fig. 19c. pt. 1). Its second, or outermost mantle, grew from a Ba-rich and isotopically moderate magma, which appears to be the same magma from which FP-4-1R1 and FP-5-8R1 initially crystallized their mantles (Figs. 19a, pt. 5, & 19d, pt.5, respectively).

Both rapakivi grains FP-3-1R1 and FP-4-7R2 have two distinct mantle growing events. After initial resorption and then mantling of the alkali feldspar core by plagioclase, FP-3-1R1's newly formed plagioclase mantle experienced a major disequilibrium event, resulting in the coarse-sieve texture of its inner mantle (Figs. 6 & 17). For FP-4-7R2, no major resorption occurred between its first and second mantling events. Each grains relative proximity to a zone of mixing/hybridization could account for this difference in textures. While FP-3-1R1 could have been entrained more thoroughly into the replenishing (hotter) magma, FP-4-7R2 remained more distal.

When equilibrium was again attained, crystallization of a second mantle initially was from a magma rich in Ba and LREE's, and moderately enriched isotopically. However then both grains appear to have been exposed to a melt that was now depleted in Ba and LREE's with no change isotopically. This punctuated decrease in trace elements is independent of changes in the mantle's An content, which remains ~An_{20} for both (Figs. 13 & 14).

Noticeably different than these rapakivi grains is the isotopic profile of FP-4-7R1 (alkali feldspar phenocryst). Again growth of its core was within an isotopically more evolved, Ba-poor, magma. As crystallization continued, the magma became progressively more primitive (Fig. 18; Fig. 19, pt. 2). At this point crystallization stopped and minor resorption of the grain occurred ("r" Fig. 9). When equilibrium was again attained, its rim (which we interpret to be the equivalent of the plagioclase mantle on the rapakivi feldspars) started growing from an isotopically evolved and Ba-rich magma (Fig. 19e, pt. 3). Isotopically this rim doesn't change during its growth but Ba concentrations fluctuate. This grain must have initially experienced the thermal and compositional perturbation from an injecting magma, but because it was more distal from the zone of mixing than others (i.e. the precursors of rapakivi grains) it never developed into a rapakivi feldspar. This suggests that the injection of magma into the chamber and the proximity of each grain to the chemically diverse and thermally charged magmas was key to the formation of the rapakivi grains.

The final trend of all the grains appear to indicate that as fractional crystallization of the host continued, Ba, La, and Ce became depleted and the magma became increasingly more radiogenic. As accumulation continued each grain became separated from the active mixing area of the chamber and essentially became shut off from any further contamination by newer injections of magma. This would allow the interstitial melts to evolve by fractionation of Ba-rich (alkali feldspar and biotite) and LREE-rich (titanite and allanite) phases, creating the trace element depletion trends seen in the margins of these grains.

Thus, a plausible scenario immerges from the evidence that calls on an initial alkali feldspar-plagioclase-quartz crystalizing magma, relatively isotopically enriched with low Ba and LREE concentrations, being actively mixed with (but not limited to) a Ba- and LREE-rich,

isotopically primitive magma. According to Ayuso and Bevier (1991), the neighboring Devonian Blue Hill granite has $^{208}Pb/^{206}Pb$ and $^{207}Pb/^{206}Pb$ values of 0.837 and 2.059 respectively. Mixing between a parent melt and a melt that was similar to that which formed the Blue Hill granite, could have created the changes in the Pb isotope ratios seen in the analyzed feldspar grains of the Deer Isle Granite. No publish elemental data was found for the Blue Hill granite and thus a comparison of major or trace elements could not be made.

Quartz phenocrysts

Ti concentrations in quartz have been used to indicate changes in temperature during crystallization (Wark & Watson, 2006). CL intensity in quartz is typically related to Ti concentrations and provides an image of the crystalline results of changing temperatures. Normal zoning (Ti poor, darker rims) indicates the natural decrease of temperature during cooling and crystallization and the opposite trend indicates quartz crystallized from progressively hotter magmas. Thus, as suggested by Müller *et al.* (2008), Ti-rich mantles on quartz phenocrysts (i.e. more luminescent in cathodoluminescence imaging) might represent the quartz equivalent of a rapakivi feldspar. Thus quartz phenocrysts should provide evidence of the same events recorded by the rapakivi feldspars. In fact, the reverse zonation of quartz seen in Figure 10 suggests that temperatures (and/or concentrations of Ti) oscillated but were higher when the rims crystallized, a pattern similar to that seen in the plagioclase mantled grains of alkali feldspar.

Resorption events, indicated by truncation of internal growth zones (Fig. 10, white arrows), suggest that the temperature of the magma was hot enough to cause repeated episodes of disequilibrium between the mama and the quartz phenocryst. These thermal perturbations suggest that this quartz grain crystallized near a mixing zone in the chamber. With each pulse of hotter magma Ti concentrations within the quartz increased either solely due to the thermal

change or possibly also due to an increase in Ti within the magma. Ti enrichment of quartz can be analogous to Ba enrichment in alkali feldspar or plagioclase crystals seen in the Deer Isle Granite and thus a similar mechanism is also suggested for the growth of these quartz phenocrysts.

Chamber dynamics

Lux *et al*. (2007) presented a dynamic model for the formation of the Deer Isle Granite Complex from field observations and elemental geochemistry (Fig. 20). In it they describe a vertically zoned magma chamber, with each zone represented by the individual facies of the granite complex (Fig. 2). According to this model, the Flye Point facies represents the bottom most portion of the chamber where crystals first started to cumulate. A framework of touching phenocrysts of alkali feldspars, plagioclase and quartz, with finer grains of the same phases and mafics infilling the interstitial spaces, is consistent with this idea (Chappell and Wyborn, 2004, Collins *et al.*, 2006). As cumulates continued to be deposited, the floor of the chamber moved upward with the Oak Point facies representing the last active cumulate surface prior to solidification.

Within the outcrops of the Flye Point facies neighboring minerals show very different growth zonations (Fig. 3). Rapakivi feldspars are seen in contact with unmantled alkali feldspars and discrete phenocrysts of plagioclase. Like other granitic bodies studied around the world (*e.g.* Gagnevin *et al.,* 2007) neighboring alkali and rapakivi feldspars (*e.g.* FP-4-7R1 and FP-4-7R2) have zoning with different Pb isotopes and trace element concentrations indicating they experienced different growth histories. FP-4-7R2, FP-3-1R1, and FP-6-1P1 show two growth events of plagioclase feldspar yet FP-5-8R1 and FP-4-1R1 don't show this in their mantles. This juxtaposition of grains with disparate histories therefore indicates that they did not grow *in situ*

and must have originated from different parts of the chamber and were subsequently deposited next to each other.

As crystals grew, evidence of their proximity to a zone of hybridization, and the geochemical composition of the magma in which they formed, was texturally and chemically imprinted on each grain. Replenishment of the magma chamber by new magmas caused both the thermal perturbation and locally changed the composition of the chamber over time. Due to the size of the chamber, crystals could have experienced either mild resorption (*e.g.* FP-4-7R1), severe resorption (*e.g.* FP-3-1R1) or possibly no resorption at all depending on how close they were to the center of mixing. Their interaction with varying amounts of this new magma, and to what extent thorough mixing had occurred, resulted in the differences in their inherited geochemical signatures.

Lux *et al.* (2007) envisioned that within the chamber as magma cooled, a solidification front migrated in from the top and sides of the chamber. Along this front, crystal-rich batches of magma formed and created a density inversion with relatively cooler crystal-rich magma over top hotter crystal-poor magma. These relatively cooler batches of magmas then settled "*en masse*" creating gravity currents. As these currents of crystal-rich magma reached the floor of the chamber, crystals separated out and were deposited. Subsequent depositions of new batches of could potentially carry with them minerals from very different parts of the chamber, allowing for the juxtaposition of two or more minerals with different crystallization histories.

As accumulation increased, compaction caused filter pressing of the cumulate pile, removing interstitial melt. This silica-rich and less dense interstitial melt rose, through dikes (apalites), into the hotter and more active core of the chamber. This recycling of melt lead to the leucocratic nature of the Settlement Quarry and Crotch Island facies (Lux et al., 2007).

Interaction of this melt, as it traversed the cumulate pile, most likely formed the more albitic outer edges seen on the plagioclase mantles. Compaction of the cumulate pile also developed the framework of touching feldspars and feldspar foliation seen within the Flye Point and Oak Point facies (Lux *et al.*, 2007).

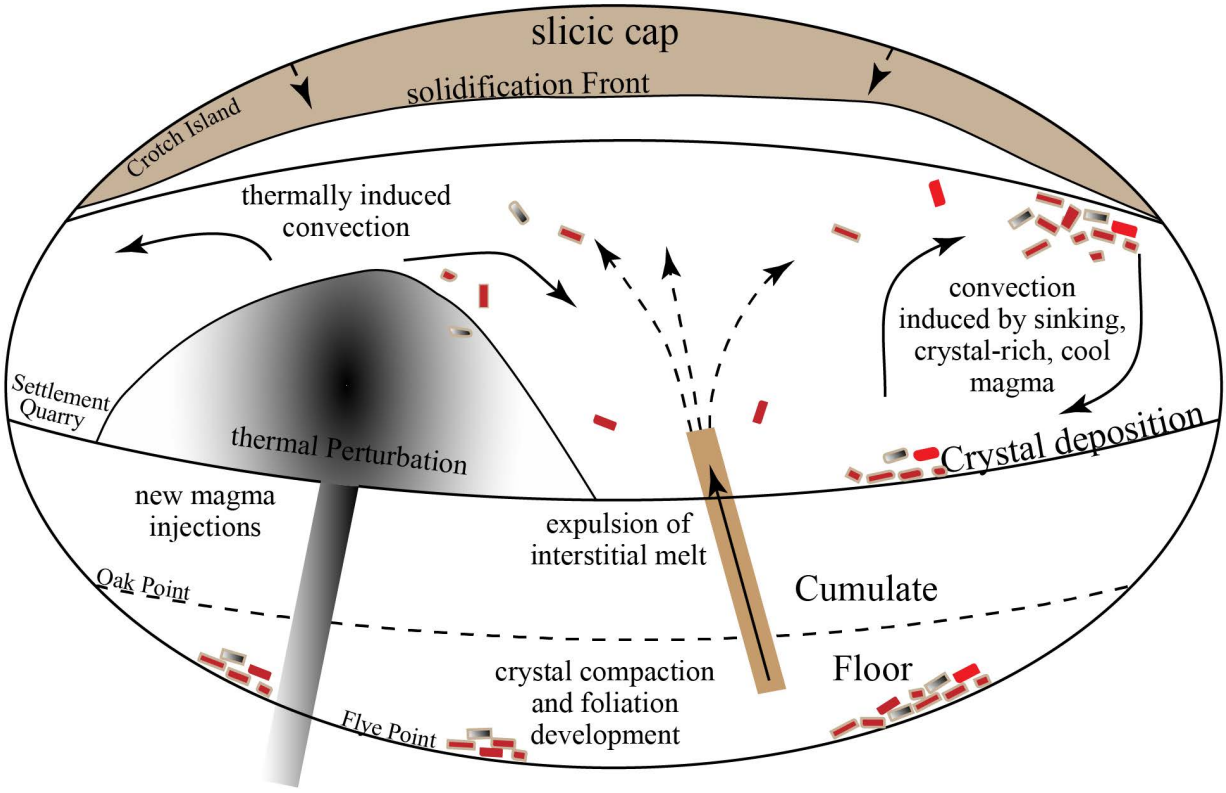

Figure 20. Theoretical Cross-section of the Deer Isle Granite Complex (modified from Lux et al., 2007).

Glazner *et al.* (2004) presents the idea of incremental emplacement as a mechanism for the formation of some plutons. In their model, only a small percentage of the pluton contains melt at any one time. Growth of the pluton occurs by amalgamation of small injections of magma (e.g., sheeted dikes) over millions of years. Glazner *et al.* (2004) further state that the pluton is "homogenized" after emplacement; thus, concealing the contacts of these sheeted dikes. It is evident that for the Deer Isle Granite Complex there needed to be a large enough chamber so

that several grains could experience completely different histories, be transported away from these sites of magma mixing, and then accumulate together on the floor of the chamber (Fig. 20).

CONCLUSIONS

The Devonian Deer Isle Granite Complex of the Coastal Maine magmatic province contains abundant rapakivi feldspars and zoned quartz. Detailed trace element and Pb isotopic profiles and CL images of its felsic minerals indicate magmatic changes occurred as rapakivi and unmantled alkali feldspar grew. These changes required an open system (i.e. magma mixing) and are inconsistent with the isothermal decompression model for the origin of rapakivi textures in this complex. Evidences from rapakivi feldspars, alkali feldspars, and quartz phenocrysts show that repeated episodes of magma mixing/replenishment (along with more normal fractional crystallization) caused significant temperature and chemical changes during the growth of the pluton. Due to the similarities in their Pb isotopic ratios, one of possible several different magmas that mixed with the Deer Isle host magma, could have shared a common source with the nearby Devonian Blue Hill granite. The proximity of grains to these mixing zones varied the extent to which each grain was affected by thermal perturbation, thereby permitting the crystallization of rapakivi feldspar with different crystallization histories from the same magma. While some alkali feldspars became mantled with Ba-rich mantles, others experienced one or more mantling events by plagioclase (forming rapakivi feldspar). *En masse* settling of crystal-rich mushes brought crystals from different parts of the chamber together and formed the cumulate texture seen within. Juxtaposition of these grains, with different crystallization histories, suggests a magma chamber of sufficient size must have existed.

REFERENCES

Anderson, A. T., 1984. Probable relations between plagioclase zoning and magma dynamics, Fuego Volcano, Guatemala. *American Mineralogist*, vol. 69, pp. 660-676.

Ayuso, R. A., and Bevier, M. L., 1991. Regional differences in Pb isotopic compositions of feldspars in plutonic rocks of the Northern Appalachian Mountains, U. S. A., and Canada: A geochemical method of terrane correlation. *Tectonics*, vol. 10, no. 1, pp. 191-212.

Bateman, P. C., and Chappell, B. W., 1979. Crystallization, fractionation, and solidification of the Tuolumne Intrusive Series, Yosemite National Park, California. *Geological Society of America Bulletin*, vol. 90, pp. 465–482

Boggs, S., Jr., and Krinsley, D., 2006. Application of Cathodoluminescence Imaging to the study of Sedimentary Rocks. *Cambridge University Press*, Cambridge, U.K.

Bussy, F., 1990. The rapakivi texture of feldspars in a plutonic mixing environment: A dissolution-recrystallization process? *Geological Journal*, vol. 25, iss. 3, pp. 319-324.

Castro, A., 2001. Plagioclase morphologies in assimilation experiments. Implications for disequilibrium melting in the generation of granodiorite rocks. *Mineralogy and Petrology*, vol. 71, pp. 31-49.

Chapman, C. A., 1962. Bays-of-Maine igneous complex. *Geological Society of America Bulletin*, vol. 73, no. 7, pp. 883-888.

Chappell, B. W., and Wyborn, D., 2004. Cumulate and cumulative granites and associated rocks. *Resource Geology*, vol. 54, no. 3, pp. 227-240.

Collins, W. J., Wiebe, R. A., Healy, B., and Richards, S. W., 2006. Replenishment, crystal accumulation and floor aggradation in the megacrystic Kameruka Suite, Australia. *Journal of Petrology*, vol. 47, no. 11, pp. 2073-2104.

Dempster, T.J., Jenkin, G.R.T., and Rogers, G., 1994. The origin of rapakivi texture. *Journal of Petrology*, vol. 35, pt. 4, pp. 963-981.

Eklund, O., and Shebanov, A.D., 1999. The origin of rapakivi texture by sub-isothermal decompression. *Precambrian Research*, vol. 95, pp. 129-146.

Gagnevin, D., Waight, T. E., Daly, J. S., Poli, G., and Conticelli, S., 2007. Insights into magmatic evolution and recharge history in Capraia Volcano (Italy) from chemical and isotopic zoning in plagioclase phenocrysts. *Journal of Volcanology and Geothermal Research*, vol. 168, iss. 1, pp. 28-54.

Gibson, D., Lux, D.R., and Choate, M.A., 2003. Petrography of a “cryptic” mixed magma system – the Mount Waldo granite, coastal Maine. *Atlantic Geology*, vol. 39, pp. 163-173.

Gibson, D., and Lux, D.R., 2009. Geochemical signatures of Early to Late Devonian plutons of the Piscataquis magmatic belt, central Maine. *Geological Society of America Abstracts with Programs*, vol. 41, no. 3, pp. 80.

Glazner, A. F., Bartley, J. M., Coleman, W. G., and Taylor, R. Z., 2004. Are plutons assembled over millions of years by amalgamation from small magma chambers? *Geological Society of America Today*, vol. 14, no. 4/5, pp. 4-11.

Haapala, I., and Rämö, O. T., 1992. Tectonic setting and origin of the Proterozoic rapakivi granites of southeastern Fennoscandia. *Transactions of the Royal Society of Edinburgh: Earth Sciences*, vol. 83, pp. 165-171.

Heinonen, A. P., Andersen, T., and Rämö, O. T., 2010. Re-evaluation of rapakivi petrogenesis: Source constraints from the Hf isotope composition of zircon in the rapakivi granites and associated mafic rocks of Southern Finland. *Journal of Petrology*, vol. 51, no. 8, pp. 1687-1709.

Hibbard, M. J., 1981. The magma mixing origin of mantled feldspars. *Contributions to Mineralogy and Petrology*, vol. 76, iss. 2, pp. 158-170.

Hogan, J. P., and Sinha, A. K., 1989. Compositional variation of plutonism in the Coastal Mine Magmatic Province: mode of origin and tectonic setting: a model. *Maine Geological Survey, Studies in Maine Geology*, vol. 4, pp. 1-33.

Hogan, J. P., and Mataragio, J. P., 2006. Temporal evolution of crustal sources for granitic magmatism in Maine. *Geological Society of America, Abstracts with Programs*, vol. 38, no. 2, p. 32.

Hooks, B. P., 2003. Petrology of the Deer Isle Pluton, coastal Maine: a complex mixed magma system [Master's thesis]: University of Maine, Orono, Maine.

Johnston, B., 2001. Magmatic enclaves and evidence for magma mixing in the Oak Point Granite, Deer Isle, Maine, U.S.A. [Master's thesis]: University of Maine, Orono, Maine.

Kent, A. J. R., Jacobsen, B., Peate, D. W., Waight, T. E., and Baker, J. A., 2004. Isotope dilution MC-ICP-MS rare earth element analysis of geochemical reference materials NIST SRM 610, NIST SRM 612, NIST SRM 614, BHVO-2G, BHVO-2, BRC-2G, JB-2, WS-E, W-2, AGV-1 and AGV-2. *Geostandards and Geoanalytical Research*, v. 28, no. 3, p. 417–429.

Kent, A. J. R., 2008. In-situ analysis of Pb isotope ratios using laser ablation MC-ICP-MS: Controls on precision and accuracy and comparison between Faraday cup and ion counting systems. Journal of Analytical Atomic Spectrometry, vol. 23, Iss. 7, pp. 968-975.

Lux, D. R., Hooks, B., Gibson, D., and Hogan, J. P., 2007. Magma interactions in the Deer Isle Granite complex, Maine: Field and textural evidence. *The Canadian Mineralogist*, vol. 45, pp. 131-146.

Miller, J. A. and Kent, A. J. R., 2009. The determination of maternal run time in juvenile Chinook salmon (Oncorhynchus tshawytscha) based on Sr/Ca and 87Sr/86Sr within otolith cores. *Fisheries Research*, vol. 95, iss. 2-3, pp. 373-378.

Müller, A., Breiter, K., Seltmann, R., and Pécskay, Z., 2005. Quartz an dfeldspar zoning in the eastern Erzgebirge volcano-plutonic complex (Germany, Czech Republick): evidence of multiple magma mixing. *Lithos*, vol. 80, iss. 1-4, pp. 201-227

Müller, A., Seltmann, R., Kober, B., Eklund, O., Jeffries, T., and Kronz, A., 2008. Compositional zoning of rapakivi feldspars and coexisting quartz phenocrysts. *The Canadian Mineralogist*, vol. 46, pp. 1417-1442.

Narayana, B. L., Mallikharjuna Rao, J., Subba Rao, M. V., Murthy, N. N., and Divakara Rao, V., 2000. Geochemistry and origin of Early Proterozoic Dongargarh rapakivi granite complex, Central India – An example for magma mixing and differentiation. *Gondwana Research*, vol. 3, no. 4, pp. 507-520.

Nekvasil, H., 1991. Ascent of felsic magmas and formation of rapakivi. *American Mineralogist*, vol. 76, pp. 1279-1290.

Pouchou J. L., Pichoir F., 1985. 'PAP' (phi-rho-z) procedure for improved quantitative microanalysis. In: Armstrong J.T. (Ed.), *Microbeam Analysis*. San Francisco Press, San Francisco, California, pp. 104–106.

Rämö, O. T., and Haapala, I., 2005. Rapakivi granites. In: Lehtinen, M., Murmi, P.A. and Rämö, O. T. (Eds.), *Precambrian Geology of Finland – Key to the Evolution of the Fennoscandian Shield*. Elsivier B. V., Amsterdam, pp. 533-562.

Schulz, K. J., Stewart, D. B., Tucker, R. D., Pollock, J. C., and Ayuso, R. A., 2008. The Ellsworth terrane, coastal Maine: Geochronology, geochemistry, and Nd-Pb isotopic composition – Implications for the rifting of Ganderia. *Geological Society of America Bulletin*, vol. 120, no. 9-10, pp. 1134-1158.

Senderholm, J. J., 1891. Ueber die finnlänndischen Rapakiwigesteine. *Tschermaks Mineralogisch-Petrographische Mitteilungen*, vol. 12, pp. 1-31.

Stewart, D. B., 1956. Rapakivi Granite of the Deer Isle Region, Maine [Ph.D. thesis]: Harvard University, Cambridge, Massachusetts.

Stewart, D. B., Tucker, R. C., and West D. P., Jr., 1995. Genesis of Silurian composite terrane in northern Penobscot Bay, *New England Intercollegiate Geological Conference, 87th Annual Meeting.* Guidebook, pp. 29-49.

Stewart, D. B., and Tucker, R.D., 1998. Geology of northern Penobscot Bay, Maine. *U. S. Geological Survey, Miscellaneous Investigations Series Map I-2251* (scale 1:62,500).

Stimac, J. A., and Wark, D. A., 1992. Plagioclase mantles on sanidine in slicic lavas, Clear Lake, California: Implications for the origin of Rapakivi texture. *Geological Society of America Bulletin*, vol. 104, pp. 728-744.

Stull, R. J., 1979. Mantled feldspars and synneusis. *American Mineralogist*, vol. 64, no. 5, pp. 514-518.

Tuttle, O. F., 1952. Origin of the Contrasting Mineralogy of Extrusive and Plutonic Salic Rocks. *Journal of Geology*, vol. 60, no. 2, pp. 107-124.

Vernon, R., 2016. Rapakivi granite problems: plagioclase mantles and ovoid megacrysts. *Australian Journal of Earth Sciences*, vol. 63, iss. 6, pp. 675-700.

Vorma, A., 1976. On the petrochemistry of Rapakivi granites with special reference to the Laitila massif, southwestern Finland. *Geological Survey of Finland Bulletin*, vol. 285, pp. 1-98.

Waight, T. E., Wiebe, R. A., and Krogstad, E. J., 2007. Isotopic evidence for multiple contributions to felsic magma chambers: Gouldsboro Granite, Coastal Maine. *Lithos*, vol. 93, iss. 3, pp. 234-247

Wang, X., Wang, T., Haapala, I., and Mao, J., 2008. P-T conditions of crystallization and origin of plagioclase-mantled K-feldspar megacrysts in the Mesozoic granitoids in the Qinling orogeny (China). *Lithos*, vol. 103, iss. 3, pp. 289-308.

Wark, D. A., and Stimac, J. A., 1992. Origin of mantled (rapakivi) feldspars: experimental evidence of a dissolution- and diffusion-controlled mechanism. *Contributions to Mineralogy and Petrology*, vol. 111, iss. 3, pp. 345-361.

Wark, D. A., and Watson, E. B., 2006. TitaniQ: a titanium-in-quartz geothermometer. *Contributions to Mineralogy and Petrology*, vol. 152, iss. 6, pp. 743-754.

Whitney, J. A., 1975. The effects of pressure, temperature and X_{H2O} on phase assemblage in four synthetic rock compositions. *Journal of Geology*, vol. 83, no.1, pp. 1-31.

Wiebe, R. A., Manon, M. R., Hawkins, D. P., and McDonough, W.F., 2004. Late-stage mafic injection and thermal rejuvenation of the Vinalhaven Granite, Coastal Maine. *Journal of Petrology*, vol. 45, no. 11, pp. 2133-2153.

APPENDIX 1

Electron Microprobe Calibration Standards

Oxide	Standard	Crystal
SiO_2	Orthoclase, Wollastonite	TAP
Al_2O_3	Anorthite, Labradorite	TAP
CaO	Wollastonite	PET
FeO	Grunerite	LIF
BaO	Barite	PET
Na	Jadeite	PC0
K	Orthoclase	PET

APPENDIX 2

Electron microprobe analyses

Sample: FP-4-1R1

	Plagioclase Inclusions											
Analysis:	28	28A	29A	29B	30	30A	30C	31	31A	32	32B	47
SiO_2	62.964	62.981	62.717	62.61	62.4	62.657	62.79	63.344	63.135	62.472	63.373	63.272
Al_2O_3	23.253	23.388	23.314	23.136	23.143	23.672	23.423	22.913	22.837	23.19	23.123	23.291
CaO	4.446	4.397	4.193	4.394	4.534	4.608	4.549	4.065	4.055	4.484	4.332	4.464
FeO	0.191	0.216	0.153	0.179	0.225	0.24	0.249	0.198	0.182	0.184	0.208	0.197
BaO	-	-	-	-	-	-	-	-	-	-	-	-
Na	9.512	9.536	9.569	9.411	9.313	9.205	9.335	9.782	9.811	9.249	9.525	9.216
K	0.311	0.206	0.272	0.288	0.405	0.432	0.435	0.211	0.185	0.409	0.389	0.495
Total	100.677	100.724	100.218	100.018	100.02	100.814	100.781	100.513	100.205	99.988	100.95	100.935
Si	2.777	2.775	2.776	2.778	2.773	2.762	2.769	2.795	2.794	2.775	2.787	2.782
Al	1.209	1.214	1.216	1.21	1.212	1.23	1.217	1.191	1.191	1.214	1.198	1.207
Ca	0.21	0.208	0.199	0.209	0.216	0.218	0.215	0.192	0.192	0.213	0.204	0.21
Fe	0.007	0.008	0.006	0.007	0.008	0.009	0.009	0.007	0.007	0.007	0.008	0.007
Ba	-	-	-	-	-	-	-	-	-	-	-	-
Na	0.813	0.815	0.821	0.81	0.802	0.787	0.798	0.837	0.842	0.796	0.812	0.786
K	0.018	0.012	0.015	0.016	0.023	0.024	0.024	0.012	0.01	0.023	0.022	0.028
Total	5.034	5.032	5.033	5.03	5.034	5.03	5.032	5.034	5.036	5.028	5.031	5.02
Ab	78.135	78.804	79.31	78.238	77.062	76.482	76.927	80.399	80.594	77.098	78.236	76.748
Or	1.684	1.118	1.486	1.575	2.203	2.361	2.358	1.14	1.001	2.245	2.101	2.711
An	20.181	20.079	19.204	20.187	20.735	21.156	20.715	18.461	18.405	20.656	19.663	20.54
Cs	-	-	-	-	-	-	-	-	-	-	-	-

Sample: FP-4-1R1 (continued)

	Plagioclase Mantle											
Analysis:	33	33B	34	34A	35	35A	36	36A	37	PB1	PB1A	PB12
SiO_2	62.461	62.822	62.85	62.665	62.519	62.901	63.163	62.909	63.025	62.973	62.742	64.437
Al_2O_3	23.369	23.504	23.465	23.366	23.084	23.2	23.115	23.086	23.41	23.116	23.332	22.164
CaO	4.711	4.571	4.447	4.436	4.497	4.44	4.255	4.242	4.2	4.32	4.643	3.254
FeO	0.206	0.267	0.24	0.278	0.242	0.265	0.253	0.199	0.161	0.19	0.245	0.139
BaO	-	-	-	-	-	-	-	-	-	-	-	-
Na	9.03	9.027	9.202	9.232	9.075	9.215	9.451	9.596	9.488	9.499	9.073	9.949
K	0.645	0.631	0.675	0.669	0.651	0.511	0.325	0.249	0.232	0.466	0.671	0.588
Total	100.422	100.822	100.879	100.646	100.068	100.532	100.562	100.281	100.516	100.564	100.706	100.531
Si	2.766	2.769	2.77	2.77	2.777	2.779	2.787	2.784	2.779	2.782	2.771	2.837
Al	1.22	1.221	1.219	1.217	1.209	1.208	1.202	1.204	1.217	1.203	1.214	1.15
Ca	0.224	0.216	0.21	0.21	0.214	0.21	0.201	0.201	0.198	0.204	0.22	0.154
Fe	0.008	0.01	0.009	0.01	0.009	0.01	0.009	0.007	0.006	0.007	0.009	0.005
Ba	-	-	-	-	-	-	-	-	-	-	-	-
Na	0.775	0.772	0.786	0.791	0.782	0.789	0.808	0.823	0.811	0.814	0.777	0.849
K	0.036	0.035	0.038	0.038	0.037	0.029	0.018	0.014	0.013	0.026	0.038	0.033
Total	5.029	5.023	5.032	5.036	5.028	5.025	5.025	5.033	5.024	5.036	5.029	5.028
Ab	74.89	75.428	76.027	76.15	75.7	76.761	78.654	79.281	79.322	77.903	75.105	81.992
Or	3.519	3.468	3.669	3.629	3.573	2.799	1.777	1.352	1.274	2.517	3.656	3.189
An	21.591	21.105	20.304	20.221	20.726	20.44	19.569	19.368	19.404	19.58	21.239	14.819
Cs	-	-	-	-	-	-	-	-	-	-	-	-

Sample: FP-4-1R1 (continued)

	Plagioclase Mantle											
Analysis:	PB12A	38	39	40	41	42	43	44	45	45A	46	46A
SiO_2	64.7	62.507	62.906	62.446	62.797	62.734	63.263	63.196	62.929	62.828	62.903	62.913
Al_2O_3	22.296	23.363	23.24	23.426	23.476	23.33	23.12	23.183	23.334	23.079	23.59	23.381
CaO	3.27	4.663	4.35	4.561	4.628	4.489	4.293	4.314	4.645	4.545	4.429	4.49
FeO	0.143	0.269	0.2	0.217	0.263	0.215	0.24	0.24	0.269	0.245	0.251	0.179
BaO	-	-	-	-	-	-	-	-	-	-	-	-
Na	9.9	9.005	9.181	8.867	8.964	9.201	9.204	9.093	9.154	9.27	9.341	9.333
K	0.63	0.636	0.824	0.967	0.768	0.53	0.615	0.844	0.534	0.525	0.358	0.235
Total	100.939	100.443	100.701	100.484	100.896	100.499	100.735	100.87	100.865	100.492	100.872	100.531
Si	2.837	2.768	2.778	2.766	2.769	2.773	2.788	2.785	2.773	2.779	2.769	2.776
Al	1.152	1.219	1.21	1.223	1.22	1.216	1.201	1.204	1.212	1.203	1.224	1.216
Ca	0.154	0.221	0.206	0.217	0.219	0.213	0.203	0.204	0.219	0.215	0.209	0.212
Fe	0.005	0.01	0.007	0.008	0.01	0.008	0.009	0.009	0.01	0.009	0.009	0.007
Ba	-	-	-	-	-	-	-	-	-	-	-	-
Na	0.842	0.773	0.786	0.762	0.766	0.789	0.786	0.777	0.782	0.795	0.797	0.798
K	0.035	0.036	0.046	0.055	0.043	0.03	0.035	0.047	0.03	0.03	0.02	0.013
Total	5.025	5.027	5.033	5.031	5.027	5.029	5.022	5.026	5.026	5.031	5.028	5.022
Ab	81.671	75.04	75.706	73.745	74.532	76.481	76.821	75.576	75.825	76.444	77.685	77.98
Or	3.421	3.485	4.472	5.292	4.202	2.899	3.379	4.613	2.912	2.847	1.958	1.29
An	14.908	21.475	19.821	20.963	21.266	20.62	19.8	19.811	21.263	20.709	20.357	20.73
Cs	-	-	-	-	-	-	-	-	-	-	-	-

Sample: FP-4-7R2

	Plagioclase Mantle											
Analysis:	48	48A	48B	48C	49	49A	50	50A	50B	51	51A	52
SiO_2	62.759	63.577	62.854	63.562	63.691	63.185	63.293	63.415	64.152	62.379	62.668	61.859
Al_2O_3	23.606	22.941	23.158	23.215	23.043	23.265	23.19	23.002	22.406	23.453	23.342	23.645
CaO	4.511	3.772	4.18	4.223	4.243	4.234	4.136	4.032	3.567	4.714	4.568	4.812
FeO	0.195	0.213	0.251	0.258	0.242	0.258	0.227	0.269	0.26	0.238	0.247	0.285
BaO	-	-	-	-	-	-	-	-	-	-	-	-
Na	9.321	9.232	9.451	9.279	9.216	9.267	9.114	9.267	9.475	8.87	9.045	8.845
K	0.184	0.884	0.169	0.194	0.423	0.42	0.638	0.654	0.645	0.61	0.622	0.615
Total	100.576	100.619	100.063	100.731	100.858	100.629	100.598	100.639	100.505	100.264	100.492	100.061
Si	2.768	2.803	2.784	2.794	2.798	2.785	2.791	2.796	2.827	2.765	2.772	2.751
Al	1.227	1.192	1.209	1.202	1.193	1.209	1.205	1.195	1.164	1.225	1.217	1.239
Ca	0.213	0.178	0.198	0.199	0.2	0.2	0.195	0.19	0.168	0.224	0.216	0.229
Fe	0.007	0.008	0.009	0.009	0.009	0.01	0.008	0.01	0.01	0.009	0.009	0.011
Ba	-	-	-	-	-	-	-	-	-	-	-	-
Na	0.797	0.789	0.812	0.791	0.785	0.792	0.779	0.792	0.809	0.762	0.776	0.763
K	0.01	0.05	0.01	0.011	0.024	0.024	0.036	0.037	0.036	0.034	0.035	0.035
Total	5.022	5.02	5.022	5.006	5.009	5.02	5.014	5.02	5.014	5.019	5.025	5.028
Ab	78.102	77.591	79.606	79.033	77.842	77.985	77.11	77.706	79.815	74.688	75.508	74.274
Or	1.012	4.889	0.939	1.09	2.353	2.325	3.551	3.609	3.578	3.378	3.419	3.396
An	20.886	17.52	19.456	19.877	19.804	19.69	19.339	18.685	16.607	21.934	21.073	22.33
Cs	-	-	-	-	-	-	-	-	-	-	-	-

Sample: FP-4-7R2 (continued)

	Plagioclase Mantle											
Analysis:	53	53A	54	55	56	56A	57	58	58A	59	60	Pb 1a
SiO_2	62.752	62.609	62.75	62.739	63.056	62.837	62.692	63.059	63.009	63.085	62.59	61.554
Al_2O_3	23.233	23.104	23.444	23.33	23.425	23.664	23.406	23.408	23.585	23.193	23.363	23.34
CaO	4.592	4.356	4.707	4.499	4.245	4.439	4.495	4.535	4.542	4.275	4.543	4.356
FeO	0.258	0.236	0.243	0.215	0.188	0.271	0.236	0.236	0.186	0.274	0.229	0.17
BaO	-	-	-	-	-	-	-	-	-	-	-	0
Na	8.952	8.944	8.85	9.203	9.426	9.286	9.142	8.98	8.951	9.021	8.93	9.276
K	0.683	0.661	0.645	0.502	0.308	0.344	0.453	0.655	0.644	0.723	0.545	0.656
Total	100.47	99.91	100.639	100.488	100.648	100.841	100.424	100.873	100.917	100.571	100.2	99.352
Si	2.776	2.782	2.771	2.774	2.778	2.766	2.772	2.777	2.772	2.785	2.773	2.757
Al	1.211	1.21	1.22	1.216	1.216	1.228	1.22	1.215	1.223	1.207	1.22	1.232
Ca	0.218	0.207	0.223	0.213	0.2	0.209	0.213	0.214	0.214	0.202	0.216	0.209
Fe	0.01	0.009	0.009	0.008	0.007	0.01	0.009	0.009	0.007	0.01	0.008	0.006
Ba	-	-	-	-	-	-	-	-	-	-	-	0
Na	0.768	0.771	0.758	0.789	0.805	0.793	0.784	0.767	0.764	0.772	0.767	0.806
K	0.039	0.037	0.036	0.028	0.017	0.019	0.026	0.037	0.036	0.041	0.031	0.037
Total	5.022	5.016	5.017	5.028	5.023	5.025	5.024	5.019	5.016	5.017	5.015	5.047
Ab	74.983	75.888	74.521	76.566	78.719	77.607	76.67	75.354	75.314	76.067	75.683	76.57
Or	3.764	3.687	3.575	2.751	1.692	1.893	2.499	3.615	3.566	4.012	3.041	3.561
An	21.254	20.424	21.904	20.683	19.589	20.5	20.832	21.031	21.12	19.921	21.276	19.869
Cs	-	-	-	-	-	-	-	-	-	-	-	0

Sample: FP-4-7R2 (continued)

	Plagioclase Mantle											
Analysis:	Pb 1b	Pb 1c	Pb 1d	Pb 1e	Pb 2a	Pb 2b	Pb 2c	Pb 2d	Pb 3a	Pb 3b	Pb 3c	Pb 4a
SiO_2	61.659	61.094	61.443	61.719	61.695	61.091	61.424	61.188	61.977	62.133	61.915	62.282
Al_2O_3	23.093	23.681	22.922	22.941	23.124	23.599	23.348	23.109	23.093	23.225	22.911	23.261
CaO	4.399	4.511	4.035	4.033	4.549	4.568	4.583	4.534	4.348	4.274	4.192	4.511
FeO	0.221	0.271	0.174	0.271	0.186	0.147	0.186	0.221	0.252	0.221	0.159	0.205
BaO	0.017	0.01	0	0	0	0.035	0.005	0.035	0.022	0.02	0.008	0
Na	9.116	9.095	9.311	9.404	8.985	8.889	9.168	9.056	9.05	9.136	9.335	8.971
K	0.644	0.643	0.579	0.608	0.666	0.727	0.44	0.711	0.658	0.598	0.534	0.599
Total	99.149	99.305	98.464	98.976	99.205	99.056	99.154	98.854	99.4	99.607	99.054	99.829
Si	2.767	2.741	2.773	2.773	2.766	2.745	2.755	2.757	2.772	2.772	2.777	2.772
Al	1.221	1.252	1.219	1.215	1.222	1.25	1.234	1.227	1.217	1.221	1.211	1.22
Ca	0.211	0.217	0.195	0.194	0.219	0.22	0.22	0.219	0.208	0.204	0.201	0.215
Fe	0.008	0.01	0.007	0.01	0.007	0.006	0.007	0.008	0.009	0.008	0.006	0.008
Ba	0	0	0	0	0	0.001	0	0.001	0	0	0	0
Na	0.793	0.791	0.815	0.819	0.781	0.775	0.797	0.791	0.785	0.79	0.812	0.774
K	0.037	0.037	0.033	0.035	0.038	0.042	0.025	0.041	0.038	0.034	0.031	0.034
Total	5.037	5.048	5.042	5.046	5.033	5.039	5.038	5.044	5.029	5.029	5.038	5.023
Ab	76.131	75.713	78.103	78.155	75.27	74.705	76.454	75.236	76.113	76.804	77.762	75.655
Or	3.54	3.52	3.196	3.323	3.671	4.02	2.415	3.888	3.643	3.309	2.927	3.322
An	20.3	20.749	18.701	18.522	21.059	21.215	21.123	20.818	20.206	19.853	19.298	21.023
Cs	0.03	0.017	0	0	0	0.059	0.008	0.059	0.038	0.034	0.013	0

Sample: FP-4-7R2 (continued)

	Plagioclase Mantle								Alkali Feldspar Core			
Analysis:	Pb 4b	Pb 4c	Pb 4d	Pb 4e	Pb 5a	Pb 5b	Pb 5c	Pb 5d	Pb 6a	Pb 6b	Pb 6c	Pb 7a
SiO_2	62.116	62.131	62.556	62.486	63.189	63.416	62.745	64.392	63.168	63.196	63.628	64.15
Al_2O_3	23.516	23.348	23.426	23.662	23.094	22.787	23.425	22.559	18.408	18.656	18.491	18.572
CaO	4.528	4.464	4.833	4.533	4.133	3.858	4.497	3.487	0.022	0	0	0
FeO	0.256	0.194	0.205	0.225	0.217	0.085	0.147	0.155	0.131	0	0.092	0.05
BaO	0.013	0.005	0.018	0	0	0.002	0.028	0	0.42	0.202	0.302	0.267
Na	8.902	9.13	8.942	8.976	9.522	9.838	9.275	9.983	0.68	0.221	0.216	0.168
K	0.647	0.626	0.575	0.589	0.31	0.174	0.197	0.252	16.228	16.75	16.824	16.774
Total	99.978	99.898	100.555	100.471	100.465	100.16	100.314	100.828	99.057	99.025	99.553	99.981
Si	2.762	2.765	2.766	2.763	2.789	2.803	2.774	2.825	2.969	2.968	2.975	2.981
Al	1.232	1.225	1.221	1.233	1.201	1.187	1.22	1.166	1.02	1.033	1.019	1.017
Ca	0.216	0.213	0.229	0.215	0.195	0.183	0.213	0.164	0.001	0	0	0
Fe	0.01	0.007	0.008	0.008	0.008	0.003	0.005	0.006	0.005	0	0.004	0.002
Ba	0	0	0	0	0	0	0	0	0.008	0.004	0.006	0.005
Na	0.767	0.788	0.767	0.77	0.815	0.843	0.795	0.849	0.062	0.02	0.02	0.015
K	0.037	0.036	0.032	0.033	0.017	0.01	0.011	0.014	0.973	1.004	1.004	0.995
Total	5.024	5.034	5.023	5.022	5.025	5.029	5.018	5.024	5.038	5.029	5.028	5.015
Ab	75.234	76.024	74.55	75.631	79.285	81.406	77.97	82.67	5.932	1.955	1.906	1.493
Or	3.598	3.43	3.154	3.265	1.7	0.947	1.091	1.371	93.218	97.683	97.556	98.028
An	21.146	20.538	22.267	21.104	19.015	17.643	20.892	15.958	0.107	0	0	0
Cs	0.022	0.008	0.029	0	0	0.004	0.047	0	0.742	0.362	0.537	0.479

Sample: FP-4-7R2 (continued)

	Alkali Feldspar Core											
Analysis:	Pb 7b	Pb 8a	Pb 8b	Pb 9a	Pb 9b	Pb 9c	Pb 9d	Pb 10	Pb 10b	Pb 10d	Pb 11a	Pb 11b
SiO_2	64.049	64.588	64.565	64.654	63.471	64.09	64.865	64.515	64.416	64.255	63.837	64.044
Al_2O_3	18.702	18.471	18.584	18.503	18.206	18.357	18.431	18.494	18.238	18.38	18.698	18.344
CaO	0.025	0	0	0	0	0	0.022	0.003	0.019	0	0.02	0.005
FeO	0.058	0.085	0.143	0.023	0.015	0.112	0.139	0.069	0.093	0.069	0.123	0.1
BaO	0.302	0.331	0.209	0.198	0.279	0.243	0.326	0.154	0.163	0.131	0.218	0.207
Na	0.39	0.348	1.11	0.931	0.311	0.593	1.441	0.225	0.763	0.46	0.324	0.253
K	16.511	16.606	15.566	15.796	16.231	16.272	15.142	16.75	16.01	16.455	16.599	16.872
Total	100.037	100.429	100.177	100.105	98.513	99.667	100.366	100.21	99.702	99.75	99.819	99.825
Si	2.974	2.987	2.982	2.988	2.989	2.985	2.989	2.988	2.993	2.988	2.972	2.984
Al	1.024	1.007	1.012	1.008	1.01	1.008	1.001	1.009	0.999	1.007	1.026	1.007
Ca	0.001	0	0	0	0	0	0.001	0	0.001	0	0.001	0
Fe	0.002	0.003	0.006	0.001	0.001	0.004	0.005	0.003	0.004	0.003	0.005	0.004
Ba	0.005	0.006	0.004	0.004	0.005	0.004	0.006	0.003	0.003	0.002	0.004	0.004
Na	0.035	0.031	0.099	0.083	0.028	0.054	0.129	0.02	0.069	0.041	0.029	0.023
K	0.978	0.98	0.917	0.931	0.975	0.967	0.89	0.99	0.949	0.976	0.986	1.003
Total	5.019	5.014	5.02	5.015	5.008	5.022	5.021	5.013	5.018	5.017	5.023	5.025
Ab	3.441	3.07	9.742	12.55	8.195	2.816	5.229	1.991	6.728	4.065	2.865	2.221
Or	95.897	96.34	89.887	86.773	91.453	96.673	94.339	97.716	92.888	95.701	96.647	97.386
An	0.123	0	0	0.104	0	0.002	0	0.017	0.093	0	0.099	0.027
Cs	0.538	0.59	0.371	0.573	0.352	0.51	0.432	0.276	0.29	0.234	0.39	0.367

Sample: FP-4-7R2 (continued)

	Alkali Feldspar Core		
Analysis:	Pb 12a	Pb 12b	Pb 12c
SiO_2	63.552	64.196	67.423
Al_2O_3	18.432	18.673	20.501
CaO	0.007	0	0.641
FeO	0.123	0.023	0.081
BaO	0.172	0.119	0.03
Na	0.272	0.206	11.591
K	16.826	16.9	0.247
Total	99.384	100.117	100.514
Si	2.976	2.978	2.943
Al	1.017	1.021	1.055
Ca	0	0	0.03
Fe	0.005	0.001	0.003
Ba	0.003	0.002	0.001
Na	0.025	0.019	0.981
K	1.005	1	0.014
Total	5.031	5.021	5.027
Ab	2.388	1.819	95.684
Or	97.274	97.969	1.34
An	0.033	0	2.926
Cs	0.305	0.212	0.05

Sample: FP-3-1R1

	Plagioclase Mantle											
Analysis:	1 w	1 s	2 ne	2 w	2 se	2nw	2se	3 e	3 w	4 sw	4 ne	4 nw
SiO_2	62.864	62.27	63.169	63.161	63.05	63.081	62.571	62.326	62.111	62.05	62.32	62.771
Al_2O_3	23.048	22.359	22.942	22.503	22.591	22.955	22.902	22.781	22.972	23.151	22.937	22.366
CaO	4.275	4.207	4.48	3.97	4.162	4.195	4.124	4.671	4.798	4.882	4.692	4.228
FeO	0.177	0.214	0.209	0.209	0.198	0.23	0.187	0.247	0.241	0.207	0.236	0.214
BaO	-	-	-	-	-	-	-	-	-	-	-	-
Na	9.229	9.224	9.045	9.18	9.071	8.886	9.026	8.871	8.909	8.946	8.924	9.132
K	0.982	0.941	1.072	1.216	1.114	1.174	1.186	1.127	0.994	0.909	0.973	1.05
Total	100.575	99.215	100.917	100.239	100.186	100.521	99.996	100.023	100.025	100.145	100.082	99.761
Si	2.782	2.794	2.787	2.804	2.8	2.791	2.785	2.778	2.769	2.763	2.775	2.8
Al	1.202	1.182	1.193	1.177	1.182	1.197	1.202	1.197	1.207	1.215	1.204	1.176
Ca	0.203	0.202	0.212	0.189	0.198	0.199	0.197	0.223	0.229	0.233	0.224	0.202
Fe	0.007	0.008	0.008	0.008	0.007	0.008	0.007	0.009	0.009	0.008	0.009	0.008
Ba	-	-	-	-	-	-	-	-	-	-	-	-
Na	0.792	0.802	0.774	0.79	0.781	0.762	0.779	0.767	0.77	0.772	0.77	0.79
K	0.055	0.054	0.06	0.069	0.063	0.066	0.067	0.064	0.057	0.052	0.055	0.06
Total	5.041	5.042	5.034	5.037	5.031	5.023	5.037	5.038	5.041	5.043	5.037	5.036
Ab	75.415	75.807	73.982	75.408	74.943	74.193	74.688	72.754	72.939	73.076	73.406	75.103
Or	5.28	5.086	5.769	6.571	6.054	6.452	6.456	6.079	5.356	4.887	5.264	5.683
An	19.305	19.107	20.249	18.021	19.003	19.356	18.856	21.167	21.705	22.037	21.331	19.214
Cs	-	-	-	-	-	-	-	-	-	-	-	-

Sample: FP-3-1R1 (continued)

	Plagioclase Mantle											
Analysis:	4 & Pb 2	4se	pt4a	pt4b	pt5	5 se	5 sw	5 nw	6 s	6 w	6 e	6n edge
SiO_2	62.067	62.435	62.924	62.469	62.73	62.205	62.488	62.303	62.975	64.653	64.158	64.726
Al_2O_3	23.439	23.698	23.269	23.512	23.431	23.213	23.057	23.169	22.194	21.594	22.249	22.211
CaO	4.805	4.737	4.428	4.75	4.461	4.591	4.744	4.547	3.541	3.306	3.466	3.167
FeO	0.214	0.191	0.252	0.333	0.283	0.272	0.218	0.258	0.114	0.137	0.103	0
BaO	-	-	0.023	0.005	0.037	-	-	-	-	-	-	-
Na	8.794	8.766	8.813	8.703	8.999	9.079	9.051	9.188	9.808	9.965	9.768	10.225
K	0.927	0.947	0.958	0.88	0.791	0.756	0.753	0.698	0.785	0.762	0.783	0.339
Total	100.246	100.774	100.667	100.652	100.732	100.116	100.311	100.163	99.417	100.417	100.527	100.668
Si	2.758	2.758	2.78	2.763	2.77	2.767	2.773	2.769	2.813	2.853	2.829	2.841
Al	1.228	1.234	1.211	1.226	1.22	1.217	1.206	1.214	1.168	1.123	1.156	1.149
Ca	0.229	0.224	0.21	0.225	0.211	0.219	0.226	0.217	0.169	0.156	0.164	0.149
Fe	0.008	0.007	0.009	0.012	0.01	0.01	0.008	0.01	0.004	0.005	0.004	0
Ba	-	-	0	0	0.001	-	-	-	-	-	-	-
Na	0.758	0.751	0.755	0.746	0.771	0.783	0.779	0.792	0.849	0.853	0.835	0.87
K	0.053	0.053	0.054	0.05	0.045	0.043	0.043	0.04	0.045	0.043	0.044	0.019
Total	5.034	5.027	5.019	5.022	5.028	5.039	5.035	5.042	5.048	5.033	5.032	5.028
Ab	72.923	73.006	74.091	73.086	75.04	74.95	74.382	75.561	79.859	81.062	80.074	83.827
Or	5.057	5.191	5.298	4.863	4.34	4.108	4.073	3.776	4.206	4.078	4.225	1.827
An	22.02	21.802	20.572	22.043	20.557	20.942	21.544	20.663	15.935	14.86	15.701	14.346
Cs	-	-	0.039	0.008	0.063	-	-	-	-	-	-	-

Sample: FP-3-1R1 (continued)

	Plagioclase Mantle											
Analysis:	6sw	6ne	7 se	7 sw	7 nw	8 ne	8 sw	8 se	8 e	9 se	9 nw	9nw
SiO_2	64.045	64.211	63.087	62.885	62.972	62.687	62.454	62.469	62.368	63.65	64.348	63.982
Al_2O_3	22.479	22.541	22.89	22.62	22.814	22.611	22.979	23.127	22.987	22.367	22.095	22.519
CaO	3.454	3.391	4.499	4.342	4.418	4.223	4.598	4.681	4.656	3.536	3.201	3.23
FeO	0.199	0.222	0.251	0.227	0.254	0.202	0.189	0.213	0.234	0.135	0.144	0.195
BaO	-	-	-	-	-	-	-	-	-	-	-	-
Na	9.841	9.839	8.934	9.19	9.06	9.35	8.996	8.871	8.928	10.281	10.289	10.288
K	0.789	0.792	0.99	0.969	0.953	0.818	0.98	0.968	0.988	0.112	0.244	0.229
Total	100.807	100.996	100.651	100.233	100.471	99.891	100.196	100.329	100.161	100.081	100.321	100.443
Si	2.819	2.82	2.789	2.793	2.789	2.792	2.776	2.773	2.774	2.817	2.837	2.82
Al	1.166	1.167	1.193	1.184	1.191	1.187	1.204	1.21	1.205	1.167	1.148	1.17
Ca	0.163	0.16	0.213	0.207	0.21	0.202	0.219	0.223	0.222	0.168	0.151	0.153
Fe	0.007	0.008	0.009	0.008	0.009	0.008	0.007	0.008	0.009	0.005	0.005	0.007
Ba	-	-	-	-	-	-	-	-	-	-	-	-
Na	0.84	0.838	0.766	0.791	0.778	0.807	0.775	0.763	0.77	0.882	0.88	0.879
K	0.044	0.044	0.056	0.055	0.054	0.046	0.056	0.055	0.056	0.006	0.014	0.013
Total	5.039	5.037	5.026	5.038	5.031	5.042	5.037	5.032	5.036	5.045	5.035	5.042
Ab	80.21	80.422	74.009	75.163	74.701	76.502	73.848	73.349	73.478	83.527	84.212	84.167
Or	4.233	4.261	5.396	5.213	5.171	4.403	5.293	5.265	5.349	0.598	1.313	1.232
An	15.557	15.317	20.595	19.624	20.128	19.095	20.859	21.386	21.173	15.875	14.476	14.601
Cs	-	-	-	-	-	-	-	-	-	-	-	-

Sample: FP-3-1R1 (continued)

	Plagioclase Mantle											
Analysis:	9n	9sse	9 w	10 ne	10 w	11 nw	11 ne	11 s	11 w	12 n	12 w	12 sw
SiO_2	64.186	64.181	64.32	62.712	62.52	62.857	62.832	62.939	62.527	62.566	62.546	61.947
Al_2O_3	22.843	22.656	22.268	22.966	22.723	22.767	22.497	22.9	22.723	23.151	23.114	22.856
CaO	3.39	3.461	3.37	4.186	4.263	4.436	4.212	4.207	4.256	4.405	4.581	4.649
FeO	0.132	0.129	0.164	0.18	0.182	0.209	0.22	0.245	0.247	0.166	0.196	0.247
BaO	-	-	-	-	-	-	-	-	-	-	-	-
Na	10.26	10.153	10.237	9.344	9.306	9.632	9.676	9.632	9.454	9.742	9.578	9.513
K	0.112	0.235	0.212	0.74	0.734	0.25	0.36	0.348	0.454	0.185	0.253	0.211
Total	100.923	100.815	100.571	100.128	99.728	100.151	99.797	100.271	99.661	100.215	100.268	99.423
Si	2.813	2.818	2.83	2.784	2.788	2.788	2.797	2.787	2.788	2.773	2.773	2.771
Al	1.18	1.172	1.155	1.202	1.194	1.19	1.18	1.195	1.194	1.209	1.208	1.205
Ca	0.159	0.163	0.159	0.199	0.204	0.211	0.201	0.2	0.203	0.209	0.218	0.223
Fe	0.005	0.005	0.006	0.007	0.007	0.008	0.008	0.009	0.009	0.006	0.007	0.009
Ba	-	-	-	-	-	-	-	-	-	-	-	-
Na	0.872	0.864	0.873	0.804	0.805	0.828	0.835	0.827	0.817	0.837	0.823	0.825
K	0.006	0.013	0.012	0.042	0.042	0.014	0.02	0.02	0.026	0.01	0.014	0.012
Total	5.035	5.035	5.035	5.038	5.04	5.039	5.041	5.038	5.037	5.044	5.043	5.045
Ab	84.051	83.085	83.644	76.943	76.625	78.644	79.047	79.041	78.102	79.216	78.022	77.842
Or	0.604	1.265	1.138	4.009	3.978	1.341	1.938	1.881	2.47	0.99	1.355	1.136
An	15.345	15.65	15.218	19.048	19.396	20.015	19.016	19.079	19.428	19.795	20.623	21.023
Cs	-	-	-	-	-	-	-	-	-	-	-	-

Sample: FP-3-1R1 (continued)

	Plagioclase Mantle											
Analysis:	13 s	13 w	13 ne	14 w	14 s	14 ne	14w	14ne	14sw	15 n2	15 e	15 w
SiO_2	63.031	62.179	62.447	64.361	63.948	64.221	63.92	64.819	64.522	61.654	62.149	61.802
Al_2O_3	22.866	22.442	23.122	21.603	21.695	22.236	22.531	22.136	22.429	23.547	23.603	23.15
CaO	4.387	4.448	4.576	2.948	3.388	3.308	3.476	2.958	3.281	4.887	4.885	4.873
FeO	0.202	0.216	0.198	0.101	0.126	0.103	0.156	0.152	0.164	0.158	0.114	0.162
BaO	-	-	-	-	-	-	-	-	-	-	-	-
Na	9.444	9.318	9.416	10.355	9.98	10.165	10.042	10.185	10.061	9.23	9.322	9.203
K	0.444	0.497	0.283	0.47	0.619	0.372	0.398	0.671	0.47	0.299	0.232	0.375
Total	100.374	99.1	100.042	99.838	99.756	100.405	100.523	100.921	100.927	99.775	100.305	99.565
Si	2.789	2.789	2.773	2.853	2.841	2.831	2.817	2.843	2.83	2.749	2.754	2.761
Al	1.192	1.187	1.21	1.128	1.136	1.155	1.17	1.144	1.159	1.237	1.233	1.219
Ca	0.208	0.214	0.218	0.14	0.161	0.156	0.164	0.139	0.154	0.233	0.232	0.233
Fe	0.007	0.008	0.007	0.004	0.005	0.004	0.006	0.006	0.006	0.006	0.004	0.006
Ba	-	-	-	-	-	-	-	-	-	-	-	-
Na	0.81	0.81	0.811	0.89	0.86	0.869	0.858	0.866	0.856	0.798	0.801	0.797
K	0.025	0.028	0.016	0.027	0.035	0.021	0.022	0.038	0.026	0.017	0.013	0.021
Total	5.031	5.036	5.035	5.042	5.038	5.036	5.037	5.036	5.031	5.04	5.037	5.037
Ab	77.66	76.991	77.623	84.231	81.407	83.06	82.143	83.066	82.578	76.109	76.571	75.791
Or	2.404	2.7	1.533	2.518	3.322	2	2.143	3.6	2.539	1.624	1.255	2.033
An	19.936	20.309	20.844	13.251	15.271	14.939	15.714	13.333	14.883	22.267	22.174	22.176
Cs	-	-	-	-	-	-	-	-	-	-	-	-

Sample: FP-3-1R1 (continued)

	Plagioclase Mantle											
Analysis:	15 ne	15n	15 & Pb 12	16 ne	16 nw	16 sw	16 nw	17 e	17 n	17	20 sw	20 ne
SiO_2	62.939	62.326	61.842	63.578	64.032	64.282	64.194	64.604	64.238	64.014	62.92	63.067
Al_2O_3	22.909	23.711	23.508	21.828	22.306	22.253	22.456	22.258	22.163	22.41	23.246	23.417
CaO	4.574	4.898	4.496	3.321	3.547	3.19	3.447	3.406	3.409	3.318	4.635	4.362
FeO	0.164	0.164	0.184	0.105	0.13	0.135	0.243	0.148	0.225	0.157	0.162	0.141
BaO	-	-	-	-	-	-	-	-	-	-	-	-
Na	9.365	9.128	9.466	10.38	10.206	10.39	10.256	10.212	10.101	10.314	9.516	9.772
K	0.333	0.32	0.295	0.169	0.121	0.144	0.208	0.194	0.394	0.233	0.202	0.187
Total	100.284	100.547	99.791	99.381	100.342	100.394	100.804	100.822	100.53	100.446	100.681	100.946
Si	2.786	2.755	2.755	2.833	2.824	2.832	2.821	2.834	2.831	2.822	2.775	2.773
Al	1.195	1.236	1.234	1.146	1.16	1.155	1.163	1.151	1.151	1.164	1.208	1.214
Ca	0.217	0.227	0.215	0.159	0.168	0.151	0.162	0.16	0.161	0.157	0.219	0.206
Fe	0.006	0.006	0.007	0.004	0.005	0.005	0.009	0.005	0.008	0.006	0.006	0.005
Ba	-	-	-	-	-	-	-	-	-	-	-	-
Na	0.804	0.787	0.818	0.897	0.873	0.887	0.874	0.869	0.863	0.881	0.814	0.833
K	0.019	0.018	0.017	0.01	0.007	0.008	0.012	0.011	0.022	0.013	0.011	0.011
Total	5.027	5.029	5.046	5.049	5.037	5.038	5.041	5.03	5.036	5.043	5.033	5.042
Ab	77.322	75.784	77.947	84.21	84.837	83.397	83.344	83.558	82.498	83.847	77.935	79.409
Or	1.811	1.746	1.596	0.904	0.772	1.115	0.651	1.042	2.116	1.247	1.086	1.002
An	20.867	22.47	20.458	14.886	14.391	15.488	16.006	15.4	15.386	14.906	20.978	19.589
Cs	-	-	-	-	-	-	-	-	-	-	-	-

Sample: FP-3-1R1 (continued)

	Plagioclase Mantle											
Analysis:	20 w	20se	20sw	21 w	21 e	21 n	21 s	21 nb	21NW	21E	21E	21sw
SiO_2	63.248	63.464	62.634	62.829	61.658	63.346	62.344	62.976	61.531	62.204	63.177	62.031
Al_2O_3	23.249	23.113	23.459	23.285	23.677	22.84	23.605	23.402	23.98	23.323	23.165	23.738
CaO	4.202	4.096	4.383	4.637	4.859	4.083	4.766	4.343	4.861	4.575	4.149	4.834
FeO	0.153	0.199	0.164	0.227	0.177	0.177	0.186	0.227	0.174	0.141	0.243	0.161
BaO	-	-	-	-	-	-	-	-	-	-	-	-
Na	9.638	9.818	9.548	9.538	9.346	9.726	9.317	9.508	9.293	9.42	9.608	9.35
K	0.253	0.153	0.216	0.338	0.278	0.367	0.285	0.369	0.242	0.343	0.378	0.269
Total	100.743	100.843	100.404	100.854	99.995	100.539	100.503	100.825	100.081	100.006	100.72	100.383
Si	2.784	2.79	2.769	2.77	2.744	2.796	2.757	2.774	2.735	2.764	2.784	2.748
Al	1.206	1.198	1.222	1.21	1.242	1.188	1.23	1.215	1.256	1.222	1.203	1.239
Ca	0.198	0.193	0.208	0.219	0.232	0.193	0.226	0.205	0.232	0.218	0.196	0.229
Fe	0.006	0.007	0.006	0.008	0.007	0.007	0.007	0.008	0.006	0.005	0.009	0.006
Ba	-	-	-	-	-	-	-	-	-	-	-	-
Na	0.823	0.837	0.818	0.815	0.806	0.832	0.799	0.812	0.801	0.812	0.821	0.803
K	0.014	0.009	0.012	0.019	0.016	0.021	0.016	0.021	0.014	0.019	0.021	0.015
Total	5.031	5.034	5.035	5.041	5.047	5.037	5.035	5.035	5.044	5.04	5.034	5.04
Ab	79.478	80.595	78.829	77.403	76.516	79.569	76.757	78.247	76.556	77.378	79.083	76.649
Or	1.372	0.826	1.173	1.805	1.5	1.973	1.547	2	1.313	1.853	2.049	1.452
An	19.15	18.58	19.998	20.792	21.984	18.458	21.696	19.752	22.131	20.768	18.868	21.898
Cs	-	-	-	-	-	-	-	-	-	-	-	-

Sample: FP-3-1R1 (continued)

	Plagioclase Mantle											
Analysis:	21ne	21s	21n	PB 9	Pb10 nw	Pb10 e	Pb 12 w	Pb12n	Pb12 w	Pb12 wb	Perthite	Perthite
SiO_2	62.132	62.121	62.655	62.363	61.603	64.148	63.974	62.707	64.391	63.963	68.333	67.711
Al_2O_3	23.25	23.02	23.583	23.162	23.658	22.633	22.689	23.324	22.652	22.759	19.939	19.801
CaO	4.606	4.162	4.652	4.582	4.877	3.406	3.476	4.387	3.428	3.685	0.204	0.235
FeO	0.184	0.238	0.143	0.119	0.176	0.176	0.156	0.214	0.105	0.14	0.045	0.043
BaO	-	-	-	-	-	-	-	-	-	-	-	-
Na	9.346	9.578	9.476	9.493	9.4	10.133	10.085	9.466	10.135	9.874	12.296	12.351
K	0.281	0.386	0.242	0.25	0.354	0.226	0.369	0.316	0.215	0.27	0.071	0.073
Total	99.799	99.505	100.751	99.969	100.068	100.722	100.749	100.414	100.926	100.691	100.888	100.214
Si	2.766	2.774	2.762	2.771	2.742	2.819	2.813	2.773	2.822	2.812	2.969	2.964
Al	1.22	1.212	1.225	1.213	1.241	1.172	1.176	1.216	1.17	1.179	1.021	1.022
Ca	0.22	0.199	0.22	0.218	0.233	0.16	0.164	0.208	0.161	0.174	0.01	0.011
Fe	0.007	0.009	0.005	0.004	0.007	0.006	0.006	0.008	0.004	0.005	0.002	0.002
Ba	-	-	-	-	-	-	-	-	-	-	-	-
Na	0.807	0.829	0.81	0.818	0.811	0.863	0.86	0.812	0.861	0.842	1.036	1.048
K	0.016	0.022	0.014	0.014	0.02	0.013	0.021	0.018	0.012	0.015	0.004	0.004
Total	5.036	5.045	5.036	5.038	5.054	5.033	5.04	5.035	5.03	5.027	5.042	5.051
Ab	77.389	78.951	77.636	77.882	76.25	83.301	82.339	78.244	83.27	81.685	98.718	98.578
Or	1.533	2.091	1.305	1.347	1.89	1.224	1.981	1.719	1.164	1.471	0.376	0.386
An	21.077	18.958	21.059	20.771	21.859	15.475	15.681	20.037	15.566	16.844	0.906	1.036
Cs	-	-	-	-	-	-	-	-	-	-	-	-

Sample: FP-3-1R1 (continued)

	Alkali Feldspar Core			
Analysis:	18 w	19 n	19 n	19 w
SiO_2	64.068	64.426	64.278	64.398
Al_2O_3	18.728	18.547	18.386	18.603
CaO	0.045	0.044	0.02	0
FeO	0.065	0.081	0.133	0.111
BaO	0.247	0.151	-	-
Na	1.336	0.956	0.788	0.72
K	15.004	15.917	15.834	16.1
Total	99.493	100.122	99.439	99.932
Si	2.975	2.981	2.989	2.982
Al	1.025	1.011	1.008	1.015
Ca	0.002	0.002	0.001	0
Fe	0.003	0.003	0.005	0.004
Ba	0.004	0.003	-	-
Na	0.12	0.086	0.071	0.065
K	0.889	0.94	0.939	0.951
Total	5.018	5.026	5.013	5.017
Ab	11.843	8.325	7.025	6.363
Or	87.495	91.198	92.875	93.637
An	0.219	0.212	0.1	0
Cs	0.443	0.265	-	-

Sample: FP-5-8R1

	Plagioclase Inclusions											
Analysis:	1A	1B	1 W	1 N	1ne	1se	1 nw	1e	1sw	2 n	2b s	3s
SiO_2	63.011	62.919	62.624	62.149	62.76	63.273	62.782	62.637	62.653	62.842	62.542	62.499
Al_2O_3	23.45	23.542	23.475	23.315	23.392	23.168	23.365	23.13	23.661	23.312	23.431	23.507
CaO	4.388	4.546	4.456	4.454	4.41	4.32	4.565	4.224	4.58	4.208	4.234	4.655
FeO	0.201	0.17	0.142	0.216	0.18	0.16	0.182	0.211	0.191	0.148	0.16	0.077
BaO	-	-	-	-	-	-	-	-	-	-	-	-
Na	9.388	9.509	9.531	9.465	9.566	9.585	9.648	9.492	9.532	9.837	9.563	9.757
K	0.25	0.29	0.297	0.34	0.316	0.368	0.305	0.342	0.338	0.252	0.376	0.138
Total	100.688	100.976	100.525	99.939	100.624	100.874	100.847	100.036	100.955	100.599	100.306	100.633
Si	2.776	2.768	2.767	2.764	2.77	2.784	2.768	2.779	2.759	2.774	2.769	2.76
Al	1.217	1.22	1.222	1.222	1.217	1.202	1.214	1.21	1.228	1.213	1.223	1.223
Ca	0.207	0.214	0.211	0.212	0.209	0.204	0.216	0.201	0.216	0.199	0.201	0.22
Fe	0.007	0.006	0.005	0.008	0.007	0.006	0.007	0.008	0.007	0.005	0.006	0.003
Ba	-	-	-	-	-	-	-	-	-	-	-	-
Na	0.802	0.811	0.816	0.816	0.819	0.818	0.825	0.817	0.814	0.842	0.821	0.835
K	0.014	0.016	0.017	0.019	0.018	0.021	0.017	0.019	0.019	0.014	0.021	0.008
Total	5.023	5.035	5.038	5.041	5.04	5.035	5.047	5.034	5.043	5.047	5.041	5.049
Ab	78.383	77.867	78.193	77.903	78.34	78.474	77.989	78.765	77.59	79.793	78.709	78.557
Or	1.372	1.562	1.604	1.839	1.703	1.98	1.621	1.866	1.809	1.343	2.037	0.731
An	20.246	20.571	20.202	20.258	19.957	19.545	20.39	19.37	20.601	18.864	19.255	20.712
Cs	-	-	-	-	-	-	-	-	-	-	-	-

Sample: FP-5-8R1 (continued)

	Plagioclase Inclusions											
Analysis:	3b w	3 s	3 n	3 w	3 e	4w	4e	4s	5w	5e	6w	6s
SiO_2	64.321	63.718	62.485	64.604	63.092	62.549	61.813	62.169	62.215	62.305	62.161	62.64
Al_2O_3	22.121	22.895	23.568	22.386	23.365	23.322	23.682	23.734	23.42	23.414	23.44	23.595
CaO	2.972	3.406	4.484	2.883	4.161	4.448	4.723	4.699	4.521	4.464	4.502	4.396
FeO	0.074	0.02	0.076	0.142	0.126	0.122	0.182	0.178	0.221	0.227	0.153	0.18
BaO	-	-	-	-	-	-	-	-	-	-	-	-
Na	10.655	10.52	9.623	10.619	9.733	9.649	9.343	9.485	9.281	9.344	9.599	9.428
K	0.122	0.106	0.236	0.19	0.199	0.253	0.426	0.326	0.616	0.543	0.348	0.464
Total	100.265	100.665	100.472	100.824	100.676	100.343	100.169	100.591	100.274	100.297	100.203	100.703
Si	2.837	2.803	2.762	2.833	2.779	2.769	2.747	2.75	2.761	2.763	2.759	2.764
Al	1.15	1.187	1.228	1.157	1.213	1.217	1.24	1.237	1.225	1.224	1.226	1.227
Ca	0.14	0.161	0.212	0.135	0.196	0.211	0.225	0.223	0.215	0.212	0.214	0.208
Fe	0.003	0.001	0.003	0.005	0.005	0.005	0.007	0.007	0.008	0.008	0.006	0.007
Ba	-	-	-	-	-	-	-	-	-	-	-	-
Na	0.911	0.897	0.825	0.903	0.831	0.828	0.805	0.813	0.799	0.804	0.826	0.807
K	0.007	0.006	0.013	0.011	0.011	0.014	0.024	0.018	0.035	0.031	0.02	0.026
Total	5.048	5.055	5.043	5.044	5.035	5.044	5.048	5.048	5.043	5.042	5.051	5.039
Ab	86.084	84.351	78.516	86.075	80.019	78.617	76.377	77.137	76.17	76.789	77.939	77.515
Or	0.648	0.558	1.268	1.013	1.075	1.357	2.289	1.743	3.326	2.938	1.861	2.512
An	13.268	15.091	20.216	12.912	18.905	20.026	21.335	21.12	20.504	20.272	20.2	19.973
Cs	-	-	-	-	-	-	-	-	-	-	-	-

Sample: FP-5-8R1 (continued)

	Plagioclase Inclusions											
Analysis:	7n	7s	7w	8w	8s	8s	9e	9w	17 se	17 n	17 nw	17 ne
SiO_2	62.596	62.091	63.058	62.619	64.007	63.717	62.354	62.841	62.653	62.417	62.787	62.431
Al_2O_3	23.774	23.447	23.245	23.576	21.949	22.716	23.499	23.009	23.456	23.114	23.289	23.189
CaO	4.402	4.415	4.391	4.397	3.158	3.647	4.454	4.143	4.619	4.435	4.547	4.361
FeO	0.187	0.189	0.146	0.119	0.112	0.099	0.112	0.182	0.186	0.148	0.171	0.182
BaO	-	-	-	-	-	-	-	-	-	-	-	-
Na	9.567	9.34	9.543	9.73	10.395	10.119	9.724	9.821	9.444	9.487	9.574	9.677
K	0.376	0.433	0.445	0.146	0.283	0.23	0.226	0.195	0.322	0.269	0.245	0.31
Total	100.902	99.915	100.828	100.587	99.904	100.528	100.369	100.191	100.68	99.87	100.613	100.15
Si	2.757	2.762	2.778	2.764	2.836	2.808	2.761	2.784	2.766	2.775	2.772	2.771
Al	1.234	1.229	1.207	1.226	1.146	1.18	1.226	1.201	1.22	1.211	1.212	1.213
Ca	0.208	0.21	0.207	0.208	0.15	0.172	0.211	0.197	0.218	0.211	0.215	0.207
Fe	0.007	0.007	0.005	0.004	0.004	0.004	0.004	0.007	0.007	0.005	0.006	0.007
Ba	-	-	-	-	-	-	-	-	-	-	-	-
Na	0.817	0.805	0.815	0.833	0.893	0.865	0.835	0.843	0.808	0.818	0.82	0.833
K	0.021	0.025	0.025	0.008	0.016	0.013	0.013	0.011	0.018	0.015	0.014	0.018
Total	5.044	5.038	5.037	5.043	5.045	5.042	5.05	5.043	5.037	5.035	5.039	5.049
Ab	78.119	77.414	77.826	79.391	84.332	82.366	78.838	80.245	77.358	78.31	78.169	78.734
Or	2.02	2.363	2.387	0.784	1.511	1.23	1.208	1.05	1.735	1.46	1.315	1.659
An	19.862	20.223	19.787	19.825	14.157	16.404	19.954	18.705	20.907	20.23	20.516	19.607
Cs	-	-	-	-	-	-	-	-	-	-	-	-

Sample:	FP-5-8R1 (continued)											
	Plagioclase Inclusions		Plagioclase Mantle									
Analysis:	pb 2 E	pb 4e	10s	10e	11s	11e	12e	12e	13 w	13 n	14 e	14 w
SiO_2	62.422	62.723	62.328	62.438	62.23	62.042	62.359	62.321	62.497	62.708	62.522	61.972
Al_2O_3	23.318	23.472	23.481	23.513	23.169	23.454	23.176	23.459	23.344	23.337	23.033	23.272
CaO	4.52	4.395	4.556	4.514	4.624	4.567	4.794	4.661	4.598	4.611	4.457	4.617
FeO	0.094	0.23	0.2	0.171	0.187	0.185	0.229	0.216	0.203	0.214	0.182	0.27
BaO	-	-	-	-	-	-	-	-	-	-	-	-
Na	9.65	9.462	9.219	9.302	9.143	9.259	9.019	9.072	9.37	9.135	9.306	9.28
K	0.188	0.434	0.584	0.506	0.7	0.623	0.762	0.812	0.569	0.659	0.484	0.6
Total	100.192	100.716	100.368	100.444	100.053	100.13	100.339	100.541	100.581	100.664	99.984	100.011
Si	2.767	2.768	2.762	2.763	2.768	2.758	2.768	2.761	2.765	2.771	2.778	2.76
Al	1.218	1.221	1.226	1.226	1.215	1.229	1.212	1.225	1.217	1.215	1.206	1.221
Ca	0.215	0.208	0.216	0.214	0.22	0.218	0.228	0.221	0.218	0.218	0.212	0.22
Fe	0.003	0.008	0.007	0.006	0.007	0.007	0.008	0.008	0.008	0.008	0.007	0.01
Ba	-	-	-	-	-	-	-	-	-	-	-	-
Na	0.829	0.81	0.792	0.798	0.789	0.798	0.776	0.779	0.804	0.783	0.802	0.801
K	0.011	0.024	0.033	0.029	0.04	0.035	0.043	0.046	0.032	0.037	0.027	0.034
Total	5.043	5.039	5.036	5.036	5.039	5.045	5.035	5.04	5.044	5.032	5.032	5.046
Ab	78.64	77.706	76.057	76.691	75.197	75.938	74.109	74.47	76.27	75.392	76.987	75.901
Or	1.006	2.346	3.171	2.746	3.787	3.364	4.12	4.386	3.047	3.58	2.636	3.231
An	20.353	19.948	20.772	20.564	21.016	20.698	21.771	21.145	20.683	21.029	20.378	20.868
Cs	-	-	-	-	-	-	-	-	-	-	-	-

Sample: FP-5-8R1 (continued)

	Plagioclase Mantle											
Analysis:	14 s	15b s	15 n	16 n	16 s	18 sw	18 e	19 s	19 nw	20 n	20 sw	21 e
SiO_2	62.641	63.117	62.662	62.56	62.477	62.636	62.741	62.459	62.007	62.781	62.492	62.365
Al_2O_3	23.338	23.006	23.114	23.106	23.369	23.292	23.072	23.435	23.521	22.954	23.041	23.17
CaO	4.628	4.197	4.409	4.477	4.669	4.504	4.554	4.703	4.712	4.304	4.392	4.334
FeO	0.218	0.139	0.114	0.221	0.209	0.245	0.166	0.223	0.173	0.229	0.173	0.133
BaO	-	-	-	-	-	-	-	-	-	-	-	-
Na	9.295	9.683	9.591	9.292	9.346	9.196	9.441	9.307	9.15	9.429	9.513	9.626
K	0.467	0.42	0.253	0.573	0.43	0.581	0.413	0.383	0.56	0.479	0.54	0.258
Total	100.587	100.562	100.143	100.229	100.5	100.454	100.387	100.51	100.123	100.176	100.151	99.886
Si	2.769	2.787	2.778	2.775	2.765	2.772	2.778	2.763	2.756	2.784	2.775	2.773
Al	1.216	1.197	1.208	1.208	1.219	1.215	1.204	1.222	1.232	1.2	1.206	1.214
Ca	0.219	0.199	0.209	0.213	0.221	0.214	0.216	0.223	0.224	0.204	0.209	0.206
Fe	0.008	0.005	0.004	0.008	0.008	0.009	0.006	0.008	0.006	0.008	0.006	0.005
Ba	-	-	-	-	-	-	-	-	-	-	-	-
Na	0.797	0.829	0.824	0.799	0.802	0.789	0.81	0.798	0.788	0.811	0.819	0.83
K	0.026	0.024	0.014	0.032	0.024	0.033	0.023	0.022	0.032	0.027	0.031	0.015
Total	5.035	5.041	5.037	5.035	5.039	5.032	5.037	5.036	5.038	5.034	5.046	5.043
Ab	76.44	78.864	78.656	76.522	76.552	76.207	77.2	76.552	75.482	77.784	77.37	78.962
Or	2.527	2.248	1.363	3.106	2.315	3.166	2.221	2.071	3.039	2.597	2.888	1.391
An	21.032	18.888	19.981	20.372	21.133	20.628	20.579	21.377	21.479	19.619	19.742	19.646
Cs	-	-	-	-	-	-	-	-	-	-	-	-

Sample: FP-5-8R1 (continued)

	Plagioclase Mantle											
Analysis:	21 s	21 w	22 se	22 sw	22 ne	22 nw	22 n	22 se	23 e	23 w	24s	24w
SiO_2	61.781	63.143	61.866	62.446	62.392	62.348	62.987	62.009	62.439	62.543	62.407	62.032
Al_2O_3	22.767	23.285	23.475	23.325	23.12	22.472	23.081	23.043	23.051	23.266	23.612	23.658
CaO	4.443	4.473	4.891	4.807	4.344	4.257	4.451	4.681	4.567	4.491	4.687	4.705
FeO	0.274	0.191	0.218	0.184	0.139	0.146	0.159	0.18	0.252	0.169	0.223	0.173
BaO	-	-	-	-	-	-	-	-	-	-	-	-
Na	9.524	9.459	9.132	9.238	9.592	9.385	9.516	9.237	9.481	9.544	9.014	8.918
K	0.237	0.235	0.518	0.399	0.406	0.537	0.5	0.545	0.534	0.429	0.788	0.797
Total	99.026	100.786	100.1	100.399	99.993	99.145	100.694	99.695	100.324	100.442	100.731	100.283
Si	2.774	2.78	2.752	2.766	2.773	2.794	2.781	2.768	2.771	2.769	2.758	2.753
Al	1.205	1.208	1.231	1.217	1.211	1.187	1.201	1.212	1.206	1.214	1.23	1.238
Ca	0.214	0.211	0.233	0.228	0.207	0.204	0.211	0.224	0.217	0.213	0.222	0.224
Fe	0.01	0.007	0.008	0.007	0.005	0.005	0.006	0.007	0.009	0.006	0.008	0.006
Ba	-	-	-	-	-	-	-	-	-	-	-	-
Na	0.829	0.807	0.788	0.793	0.827	0.815	0.815	0.799	0.816	0.819	0.772	0.768
K	0.014	0.013	0.029	0.023	0.023	0.031	0.028	0.031	0.03	0.024	0.044	0.045
Total	5.046	5.026	5.041	5.034	5.046	5.036	5.042	5.041	5.049	5.045	5.034	5.034
Ab	78.48	78.267	75.004	75.992	78.241	77.622	77.34	75.822	76.734	77.541	74.358	74.056
Or	1.285	1.279	2.797	2.158	2.18	2.92	2.671	2.942	2.841	2.295	4.278	4.353
An	20.234	20.454	22.199	21.85	19.579	19.458	19.989	21.236	20.425	20.163	21.364	21.591
Cs	-	-	-	-	-	-	-	-	-	-	-	-

Sample: FP-5-8R1 (continued)

	Plagioclase Mantle											
Analysis:	25s	25w	25n	26e	26n	27s	27e	pb 10n	pb 10s	Pb 10 n	pb 10e	pb 10w
SiO_2	62.427	62.148	62.297	62.072	62.289	61.822	61.726	62.996	62.356	62.8	62.702	62.403
Al_2O_3	23.398	23.583	23.431	23.074	23.426	23.25	23.762	22.905	23.378	22.858	22.894	23.355
CaO	4.578	4.828	4.664	4.615	4.746	4.761	4.817	4.211	4.619	4.059	4.281	4.588
FeO	0.203	0.169	0.23	0.227	0.277	0.189	0.236	0.117	0.182	0.171	0.16	0.211
BaO	-	-	-	-	-	-	-	-	-	-	-	-
Na	9.08	8.889	8.998	9.121	8.913	8.908	8.93	9.348	9.078	9.477	9.564	9.19
K	0.821	0.816	0.826	0.807	0.709	0.726	0.809	0.65	0.683	0.664	0.477	0.723
Total	100.507	100.433	100.446	99.916	100.36	99.656	100.28	100.227	100.296	100.029	100.078	100.47
Si	2.765	2.755	2.762	2.768	2.762	2.761	2.743	2.791	2.766	2.789	2.784	2.765
Al	1.221	1.232	1.224	1.212	1.224	1.224	1.245	1.196	1.222	1.197	1.198	1.22
Ca	0.217	0.229	0.222	0.22	0.225	0.228	0.229	0.2	0.219	0.193	0.204	0.218
Fe	0.008	0.006	0.009	0.008	0.01	0.007	0.009	0.004	0.007	0.006	0.006	0.008
Ba	-	-	-	-	-	-	-	-	-	-	-	-
Na	0.78	0.764	0.773	0.788	0.766	0.771	0.77	0.803	0.781	0.816	0.823	0.789
K	0.046	0.046	0.047	0.046	0.04	0.041	0.046	0.037	0.039	0.038	0.027	0.041
Total	5.037	5.032	5.037	5.042	5.027	5.032	5.042	5.031	5.034	5.039	5.042	5.041
Ab	74.731	73.501	74.248	74.749	74.26	74.134	73.654	77.24	75.15	77.957	78.115	75.321
Or	4.447	4.441	4.486	4.35	3.89	3.973	4.39	3.532	3.72	3.593	2.564	3.899
An	20.822	22.058	21.266	20.902	21.851	21.893	21.957	19.228	21.131	18.45	19.322	20.78
Cs	-	-	-	-	-	-	-	-	-	-	-	-

Sample:	FP-4-7R1										Ba-rich Alkali Feldspar Mantle	
	Ba-poor Alkali Feldspar Core											
Analysis:	Pb12E	Pb12E2	Pb12	Pb11a	Pb11b	Pb10a	Pb10b	Pb9a	Pb9b	Pb9c	Pb8a	Pb8b
SiO_2	63.805	63.884	64.003	64.032	63.924	63.946	64.084	64.07	64.194	64.316	63.907	64.092
Al_2O_3	18.284	18.111	18.398	18.374	18.223	18.331	18.247	18.261	18.561	18.408	18.422	18.78
CaO	0.036	0	0.013	0.063	0.068	0	0	0.008	0.116	0	0.043	0.139
FeO	0.062	0.058	0.112	0.058	0.096	0.119	0.216	0.065	0.066	0.096	0	0.192
BaO	0.076	0.098	0.136	0.124	0.144	0.16	0.042	0.006	0.063	0.059	0.48	0.636
Na	0.654	0.28	0.496	0.99	0.949	0.21	0.292	0.39	1.787	0.474	0.904	1.501
K	16.332	16.814	16.461	15.744	15.699	16.817	16.705	16.667	14.685	16.613	15.831	14.71
Total	99.249	99.245	99.619	99.385	99.103	99.583	99.586	99.467	99.472	99.966	99.587	100.05
Si	2.983	2.991	2.983	2.983	2.987	2.985	2.988	2.989	2.977	2.986	2.98	2.968
Al	1.008	0.999	1.01	1.009	1.004	1.008	1.003	1.004	1.015	1.007	1.012	1.025
Ca	0.002	0	0.001	0.003	0.003	0	0	0	0.006	0	0.002	0.007
Fe	0.002	0.002	0.004	0.002	0.004	0.005	0.008	0.003	0.003	0.004	0	0.007
Ba	0.001	0.002	0.002	0.002	0.003	0.003	0.001	0	0.001	0.001	0.009	0.012
Na	0.059	0.025	0.045	0.089	0.086	0.019	0.026	0.035	0.161	0.043	0.082	0.135
K	0.974	1.004	0.979	0.936	0.936	1.001	0.994	0.992	0.869	0.984	0.942	0.869
Total	5.029	5.023	5.024	5.024	5.023	5.021	5.02	5.023	5.032	5.025	5.027	5.023
Ab	5.719	2.463	4.365	8.676	8.366	1.856	2.583	3.433	15.502	4.155	7.897	13.185
Or	93.975	97.362	95.327	90.8	91.045	97.859	97.341	96.517	83.832	95.741	91.047	85.01
An	0.172	0	0.065	0.303	0.331	0	0	0.038	0.555	0	0.208	0.676
Cs	0.134	0.175	0.243	0.22	0.257	0.285	0.076	0.011	0.111	0.105	0.848	1.129

Sample: FP-4-7R1 (continued)

	Ba-rich Alkali Feldspar Mantle											
Analysis:	Pb8c	Pb8d	Pb8 & Pb7	Pb8 & Pb7a	Pb7 a	Pb7b	Pb7c	Pb7d	Pb7e	Pb6a	Pb6b	Pb6c
SiO_2	63.604	64.366	63.639	65.615	63.744	63.538	63.891	64.266	63.713	64.323	64.033	63.66
Al_2O_3	18.655	18.503	18.294	20.736	18.659	18.93	18.717	19.102	18.821	18.969	18.786	18.687
CaO	0.05	0	0.053	1.249	0.156	0.124	0.012	0.042	0.189	0.115	0.1	0.037
FeO	0.131	0.089	0.004	0.027	0.166	0.154	0.158	0.015	0.119	0.119	0.158	0.127
BaO	0.535	0.254	0.493	0.091	0.545	0.744	0.657	0.701	0.66	0.766	0.568	0.81
Na	0.463	0.963	0.597	10.782	2.587	1.599	1.169	2.748	2.515	2.622	1.861	0.963
K	16.285	15.693	16.098	0.611	13.407	14.593	15.241	13.131	13.243	13.289	14.365	15.489
Total	99.723	99.868	99.178	99.111	99.264	99.682	99.845	100.005	99.26	100.203	99.871	99.773
Si	2.969	2.984	2.982	2.914	2.964	2.956	2.969	2.96	2.961	2.962	2.966	2.967
Al	1.026	1.011	1.01	1.085	1.023	1.038	1.025	1.037	1.031	1.03	1.026	1.027
Ca	0.002	0	0.003	0.059	0.008	0.006	0.001	0.002	0.009	0.006	0.005	0.002
Fe	0.005	0.003	0	0.001	0.006	0.006	0.006	0.001	0.005	0.005	0.006	0.005
Ba	0.01	0.005	0.009	0.002	0.01	0.014	0.012	0.013	0.012	0.014	0.01	0.015
Na	0.042	0.087	0.054	0.928	0.233	0.144	0.105	0.245	0.227	0.234	0.167	0.087
K	0.97	0.928	0.962	0.035	0.795	0.866	0.904	0.772	0.785	0.781	0.849	0.921
Total	5.024	5.018	5.02	5.024	5.039	5.03	5.022	5.03	5.03	5.032	5.029	5.024
Ab	4.093	8.495	5.276	90.663	22.291	14.001	10.311	23.783	21.934	22.632	16.205	8.496
Or	94.71	91.053	93.587	3.38	76.019	84.08	88.46	74.79	75.991	75.485	82.314	89.878
An	0.242	0	0.257	5.802	0.742	0.601	0.058	0.2	0.911	0.547	0.48	0.183
Cs	0.955	0.452	0.88	0.155	0.948	1.317	1.171	1.227	1.163	1.337	1.001	1.443

Sample: FP-4-7R1 (continued)

	Ba-rich Alkali Feldspar Mantle											
Analysis:	Pb5a	Pb5b	Pb5c	Pb5d	Pb4a	Pb4b	Pb4c	Pb3a	Pb3b	Pb3c	Pb2a	Pb2b
SiO_2	63.93	63.898	64.085	64.98	64.521	64.599	63.964	64.902	64.886	65.032	64.515	64.355
Al_2O_3	18.694	18.688	18.746	18.645	18.283	18.469	18.738	19.01	19.069	18.981	18.561	18.781
CaO	0.092	0.069	0.112	0.131	0.018	0	0.015	0.198	0.278	0.334	0.095	0.115
FeO	0.119	0.142	0.142	0.131	0.154	0	0.081	0.093	0.154	0.193	0.104	0.123
BaO	0.453	0.787	0.704	0.218	0	0.035	0	0.544	0.573	0.523	0.569	0.58
Na	1.458	0.951	1.638	2.542	0.718	0.304	0.711	3.927	3.797	4.301	2.383	2.575
K	14.912	15.537	14.644	13.578	16.095	16.781	16.441	11.407	11.42	10.739	13.644	13.335
Total	99.658	100.072	100.071	100.225	99.789	100.188	99.95	100.081	100.177	100.103	99.871	99.864
Si	2.97	2.969	2.968	2.981	2.993	2.99	2.97	2.967	2.965	2.967	2.979	2.97
Al	1.024	1.023	1.023	1.008	0.999	1.007	1.025	1.024	1.027	1.021	1.01	1.021
Ca	0.005	0.003	0.006	0.006	0.001	0	0.001	0.01	0.014	0.016	0.005	0.006
Fe	0.005	0.006	0.006	0.005	0.006	0	0.003	0.004	0.006	0.007	0.004	0.005
Ba	0.008	0.014	0.013	0.004	0	0.001	0	0.01	0.01	0.009	0.01	0.01
Na	0.131	0.086	0.147	0.226	0.065	0.027	0.064	0.348	0.336	0.38	0.213	0.23
K	0.884	0.921	0.865	0.795	0.952	0.991	0.974	0.665	0.666	0.625	0.804	0.785
Total	5.027	5.022	5.028	5.025	5.016	5.016	5.037	5.028	5.024	5.025	5.025	5.027
Ab	12.773	8.362	14.268	21.929	6.342	2.68	6.167	33.703	32.788	36.894	20.668	22.329
Or	85.978	89.905	83.955	77.068	93.57	97.257	93.763	64.413	64.885	60.617	77.877	76.102
An	0.447	0.335	0.538	0.622	0.089	0	0.07	0.94	1.328	1.584	0.457	0.553
Cs	0.802	1.398	1.239	0.381	0	0.063	0	0.944	1	0.906	0.998	1.016

Sample: FP-4-7R1 (continued)

	Ba-rich Alkali Feldspar Mantle			
Analysis:	Pb2c	Pb1a	Pb1b	Pb1d
SiO_2	64.535	64.146	64.46	64.004
Al_2O_3	18.696	18.436	18.604	18.29
CaO	0.216	0	0	0.027
FeO	0.062	0.058	0.077	0.077
BaO	0.657	0.115	0.061	0.061
Na	3.373	0.24	0.487	0.484
K	12.189	16.751	16.47	16.468
Total	99.728	99.746	100.159	99.411
Si	2.972	2.985	2.983	2.987
Al	1.015	1.011	1.015	1.006
Ca	0.011	0	0	0.001
Fe	0.002	0.002	0.003	0.003
Ba	0.012	0.002	0.001	0.001
Na	0.301	0.022	0.044	0.044
K	0.716	0.995	0.972	0.98
Total	5.029	5.017	5.018	5.022
Ab	28.963	2.127	4.293	4.266
Or	68.869	97.667	95.597	95.493
An	1.027	0	0	0.132
Cs	1.141	0.206	0.11	0.11

Sample: FP-6-1P1

	Plagioclase Rim											
Analysis:	1 nw	1 se	1nw	1s	2w	2e	2 w	2 e	2 s	2 n	3 sw	3 n
SiO_2	62.262	62.593	61.673	62.415	62.069	61.006	62.095	61.723	62.362	62.389	62.809	62.488
Al_2O_3	23.668	23.403	23.488	23.311	23.434	24.094	23.298	23.929	23.313	23.349	22.848	23.056
CaO	4.806	4.503	4.71	4.595	4.522	5.173	4.494	5.321	4.435	4.648	4.214	4.607
FeO	0.222	0.231	0.21	0.218	0.327	0.214	0.242	0.225	0.211	0.251	0.256	0.22
BaO	-	-	-	-	-	-	-	-	-	-	-	-
Na	8.974	9.095	8.935	9.055	8.935	8.678	8.959	8.575	9.064	8.969	9.127	9.017
K	0.691	0.791	0.684	0.728	0.874	0.738	0.868	0.738	0.874	0.843	0.961	0.852
Total	100.623	100.616	99.7	100.322	100.161	99.903	99.956	100.511	100.259	100.449	100.215	100.24
Si	2.754	2.768	2.753	2.768	2.76	2.723	2.765	2.737	2.768	2.766	2.788	2.775
Al	1.234	1.22	1.236	1.218	1.228	1.268	1.223	1.25	1.22	1.22	1.195	1.207
Ca	0.228	0.213	0.225	0.218	0.215	0.247	0.214	0.253	0.211	0.221	0.2	0.219
Fe	0.008	0.009	0.008	0.008	0.012	0.008	0.009	0.008	0.008	0.009	0.01	0.008
Ba	-	-	-	-	-	-	-	-	-	-	-	-
Na	0.77	0.78	0.773	0.779	0.77	0.751	0.774	0.737	0.78	0.771	0.786	0.776
K	0.039	0.045	0.039	0.041	0.05	0.042	0.049	0.042	0.05	0.048	0.054	0.048
Total	5.033	5.035	5.034	5.032	5.035	5.039	5.034	5.027	5.037	5.035	5.033	5.033
Ab	74.258	75.144	74.533	75.002	74.406	72.187	74.574	71.452	74.97	74.172	75.504	74.376
Or	3.763	4.297	3.755	3.966	4.786	4.037	4.754	4.045	4.758	4.585	5.232	4.622
An	21.979	20.559	21.711	21.032	20.808	23.776	20.672	24.502	20.273	21.243	19.263	21.002
Cs	-	-	-	-	-	-	-	-	-	-	-	-

Sample: FP-6-1P1 (continued)

	Plagioclase Rim											
Analysis:	3e	3n	3sw	7 s	7 nw	7w	7e	7s	7 se	7 nw	8se	8sw
SiO_2	62.155	61.846	62.069	64.656	63.952	63.454	63.98	64.198	63.602	63.567	62.951	62.58
Al_2O_3	23.284	23.253	23.327	22.225	22.531	22.552	22.554	22.194	22.382	22.445	23.236	23.255
CaO	4.644	4.54	4.472	3.074	3.503	3.491	3.574	3.32	3.441	3.458	4.25	4.583
FeO	0.264	0.315	0.21	0.139	0.105	0.097	0.265	0.128	0.128	0.085	0.23	0.109
BaO	-	-	-	-	-	-	-	-	0	0.003	-	-
Na	9.01	9.058	8.948	10.052	9.816	9.79	9.669	9.853	9.953	9.956	9.066	9.042
K	0.813	0.884	0.894	0.705	0.709	0.709	0.742	0.744	0.661	0.644	0.905	0.824
Total	100.17	99.896	99.92	100.851	100.616	100.093	100.784	100.437	100.167	100.158	100.638	100.393
Si	2.764	2.76	2.765	2.839	2.818	2.812	2.816	2.832	2.817	2.815	2.781	2.773
Al	1.22	1.223	1.225	1.15	1.17	1.178	1.17	1.154	1.168	1.171	1.21	1.214
Ca	0.221	0.217	0.213	0.145	0.165	0.166	0.169	0.157	0.163	0.164	0.201	0.218
Fe	0.01	0.012	0.008	0.005	0.004	0.004	0.01	0.005	0.005	0.003	0.008	0.004
Ba	-	-	-	-	-	-	-	-	0	0	-	-
Na	0.777	0.784	0.773	0.856	0.839	0.841	0.825	0.843	0.855	0.855	0.777	0.777
K	0.046	0.05	0.051	0.039	0.04	0.04	0.042	0.042	0.037	0.036	0.051	0.047
Total	5.038	5.046	5.035	5.034	5.036	5.041	5.032	5.033	5.045	5.044	5.028	5.033
Ab	74.394	74.561	74.518	82.295	80.338	80.337	79.698	80.916	80.987	81.002	75.487	74.623
Or	4.418	4.787	4.9	3.798	3.82	3.83	4.022	4.019	3.54	3.445	4.957	4.477
An	21.188	20.652	20.582	13.907	15.843	15.833	16.28	15.066	15.473	15.549	19.556	20.9
Cs	-	-	-	-	-	-	-	-	0	0.004	-	-

Sample: FP-6-1P1 (continued)

	Plagioclase Rim											
Analysis:	8nw	8A w	8A se	8A n	9n	9s	9se	9 n	9 se	10n	10s	10 n
SiO_2	62.854	61.654	62.459	62.611	62.176	61.411	62.1	61.989	62.439	62.798	62.888	62.376
Al_2O_3	22.932	23.463	22.899	23.687	23.443	24.195	23.312	23.309	23.48	23.467	23.299	23.302
CaO	4.335	4.586	4.205	4.851	4.72	5.371	4.575	4.692	4.663	4.43	4.539	4.421
FeO	0.233	0.229	0.166	0.128	0.35	0.245	0.245	0.232	0.193	0.272	0.202	0.198
BaO	-	0.018	0	0	-	-	-	0.022	0.018	-	-	0.052
Na	9.181	9.173	9.339	8.865	8.93	8.686	8.974	9.118	9.137	8.985	9.031	9.047
K	0.878	0.789	0.875	0.823	0.708	0.676	0.747	0.601	0.638	0.896	0.917	0.801
Total	100.413	99.912	99.943	100.965	100.327	100.584	99.953	99.963	100.568	100.848	100.876	100.197
Si	2.785	2.751	2.781	2.759	2.759	2.723	2.765	2.761	2.763	2.77	2.774	2.77
Al	1.198	1.234	1.202	1.23	1.226	1.265	1.223	1.223	1.224	1.22	1.211	1.22
Ca	0.206	0.219	0.201	0.229	0.224	0.255	0.218	0.224	0.221	0.209	0.215	0.21
Fe	0.009	0.009	0.006	0.005	0.013	0.009	0.009	0.009	0.007	0.01	0.007	0.007
Ba	-	0	0	0	-	-	-	0	0	-	-	0.001
Na	0.789	0.794	0.806	0.757	0.768	0.747	0.775	0.787	0.784	0.769	0.772	0.779
K	0.05	0.045	0.05	0.046	0.04	0.038	0.042	0.034	0.036	0.05	0.052	0.045
Total	5.037	5.052	5.046	5.026	5.03	5.037	5.032	5.038	5.035	5.028	5.031	5.032
Ab	75.536	75.005	76.311	73.34	74.392	71.793	74.824	75.287	75.281	74.735	74.374	75.218
Or	4.753	4.247	4.703	4.482	3.879	3.677	4.099	3.267	3.461	4.902	4.968	4.383
An	19.711	20.719	18.986	22.178	21.729	24.53	21.077	21.41	21.228	20.363	20.657	20.312
Cs	-	0.029	0	0	-	-	-	0.037	0.029	-	-	0.088

Sample: FP-6-1P1 (continued)

	Plagioclase Rim											
Analysis:	10 s	11 ne	11 sw	11ne	11sw	11w	13w	13w	13ne	13 w	13 ne	14 se
SiO_2	62.105	62.186	62.606	62.469	62.618	62.293	62.176	62.144	62.197	62.134	62.646	62.483
Al_2O_3	23.457	23.209	23.358	23.36	23.35	23.4	23.683	23.356	23.783	23.313	23.165	23.473
CaO	4.632	4.527	4.758	4.56	4.291	4.475	4.701	4.673	4.664	4.655	4.659	4.78
FeO	0.218	0.218	0.234	0.265	0.276	0.261	0.183	0.206	0.222	0.232	0.196	0.254
BaO	0.017	-	-	-	-	-	-	-	-	-	-	-
Na	9.016	9.095	9.086	9.073	9.105	9.11	9.096	9.034	9.02	8.866	9.031	8.987
K	0.84	0.729	0.684	0.751	0.795	0.766	0.708	0.761	0.716	0.769	0.721	0.763
Total	100.285	99.964	100.726	100.478	100.435	100.305	100.547	100.174	100.602	99.969	100.418	100.74
Si	2.759	2.768	2.766	2.767	2.773	2.764	2.753	2.762	2.752	2.765	2.775	2.762
Al	1.228	1.218	1.216	1.219	1.218	1.224	1.236	1.223	1.24	1.223	1.209	1.223
Ca	0.22	0.216	0.225	0.216	0.204	0.213	0.223	0.223	0.221	0.222	0.221	0.226
Fe	0.008	0.008	0.009	0.01	0.01	0.01	0.007	0.008	0.008	0.009	0.007	0.009
Ba	0	-	-	-	-	-	-	-	-	-	-	-
Na	0.776	0.785	0.778	0.779	0.782	0.784	0.781	0.778	0.774	0.765	0.776	0.77
K	0.048	0.041	0.039	0.042	0.045	0.043	0.04	0.043	0.04	0.044	0.041	0.043
Total	5.039	5.036	5.033	5.033	5.032	5.038	5.04	5.037	5.035	5.028	5.029	5.033
Ab	74.315	75.315	74.688	75.063	75.88	75.372	74.805	74.553	74.74	74.23	74.761	74.085
Or	4.558	3.971	3.697	4.089	4.36	4.171	3.83	4.134	3.904	4.234	3.927	4.137
An	21.098	20.714	21.615	20.848	19.76	20.457	21.365	21.313	21.356	21.536	21.312	21.778
Cs	0.028	-	-	-	-	-	-	-	-	-	-	-

Sample: FP-6-1P1 (continued)

	Plagioclase Rim			Plagioclase Core								
Analysis:	14 n	14s	14n	4nnw	4sw	4e	4 n	4 sw	5 w	5 wb	5 s	5 w
SiO_2	62.028	62.798	61.876	64.245	63.652	63.333	64.231	63.885	61.209	61.399	61.031	61.505
Al_2O_3	23.42	23.534	23.59	22.509	22.954	23.138	22.483	22.955	23.786	23.949	23.696	23.908
CaO	4.724	4.451	4.6	3.138	3.641	4.07	3.309	3.744	5.303	5.452	5.289	5.348
FeO	0.227	0.179	0.303	0.16	0.214	0.187	0.103	0.146	0.202	0.251	0.278	0.207
BaO	-	-	-	-	-	-	0	0	-	-	-	-
Na	8.966	9.036	8.958	10.298	10.221	9.597	10.272	10.043	8.951	8.795	8.955	8.829
K	0.761	0.746	0.757	0.307	0.269	0.453	0.204	0.309	0.362	0.454	0.348	0.339
Total	100.126	100.744	100.084	100.657	100.951	100.778	100.602	101.082	99.813	100.3	99.597	100.136
Si	2.759	2.77	2.753	2.825	2.797	2.789	2.824	2.802	2.732	2.729	2.731	2.734
Al	1.228	1.224	1.237	1.166	1.189	1.201	1.165	1.186	1.251	1.254	1.25	1.253
Ca	0.225	0.21	0.219	0.148	0.171	0.192	0.156	0.176	0.254	0.26	0.254	0.255
Fe	0.008	0.007	0.011	0.006	0.008	0.007	0.004	0.005	0.008	0.009	0.01	0.008
Ba	-	-	-	-	-	-	0	0	-	-	-	-
Na	0.773	0.773	0.773	0.878	0.871	0.819	0.876	0.854	0.775	0.758	0.777	0.761
K	0.043	0.042	0.043	0.017	0.015	0.025	0.011	0.017	0.021	0.026	0.02	0.019
Total	5.036	5.026	5.036	5.04	5.051	5.033	5.036	5.04	5.041	5.036	5.042	5.03
Ab	74.241	75.384	74.664	84.176	82.358	79.025	83.957	81.547	73.854	72.648	73.966	73.529
Or	4.145	4.096	4.153	1.652	1.428	2.455	1.099	1.653	1.967	2.467	1.892	1.86
An	21.614	20.52	21.184	14.172	16.214	18.52	14.944	16.8	24.179	24.885	24.142	24.612
Cs	-	-	-	-	-	-	0	0	-	-	-	-

Sample: FP-6-1P1 (continued)

	Plagioclase Core											
Analysis:	5 e	5 eb	5 sw	5 ne	5ne	5nw	5s	6s	6n	6ne	6sw	6 ne
SiO_2	61.024	60.988	61.302	61.315	61.27	61.584	61.877	62.84	62.536	62.382	62.901	61.264
Al_2O_3	24.365	24.64	23.974	24.189	24.238	24.39	23.862	23.073	23.472	23.051	22.976	23.975
CaO	5.755	5.929	5.316	5.544	5.538	5.576	4.963	4.084	4.6	4.313	4.093	5.443
FeO	0.252	0.247	0.205	0.175	0.183	0.156	0.175	0.191	0.175	0.117	0.121	0.211
BaO	-	-	0.059	0.037	-	-	-	-	-	-	-	0.026
Na	8.705	8.603	8.993	8.942	8.794	8.719	9.135	9.695	9.322	9.415	9.616	8.991
K	0.298	0.292	0.385	0.31	0.368	0.339	0.384	0.443	0.442	0.46	0.421	0.301
Total	100.399	100.699	100.234	100.512	100.391	100.764	100.396	100.326	100.547	99.738	100.128	100.211
Si	2.71	2.701	2.727	2.72	2.72	2.721	2.742	2.782	2.765	2.778	2.788	2.725
Al	1.275	1.286	1.257	1.265	1.268	1.27	1.246	1.204	1.223	1.21	1.2	1.257
Ca	0.274	0.281	0.253	0.263	0.263	0.264	0.236	0.194	0.218	0.206	0.194	0.259
Fe	0.009	0.009	0.008	0.006	0.007	0.006	0.006	0.007	0.006	0.004	0.004	0.008
Ba	-	-	0.001	0.001	-	-	-	-	-	-	-	0
Na	0.75	0.739	0.776	0.769	0.757	0.747	0.785	0.832	0.799	0.813	0.826	0.775
K	0.017	0.016	0.022	0.018	0.021	0.019	0.022	0.025	0.025	0.026	0.024	0.017
Total	5.035	5.032	5.044	5.042	5.036	5.027	5.037	5.044	5.036	5.037	5.036	5.041
Ab	72.054	71.269	73.737	73.193	72.7	72.521	75.308	79.184	76.697	77.802	79.11	73.682
Or	1.623	1.59	2.079	1.671	2.003	1.853	2.085	2.382	2.392	2.501	2.28	1.624
An	26.322	27.141	24.086	25.075	25.297	25.627	22.608	18.434	20.912	19.697	18.61	24.651
Cs	-	-	0.097	0.061	-	-	-	-	-	-	-	0.044

Sample: FP-6-1P1 (continued)

	Plagioclase Core						
Analysis:	6 nw	12e	12w	12se	12n	12 w	12 e
SiO_2	60.365	61.822	61.869	61.172	62.772	61.952	62.375
Al_2O_3	24.605	23.853	23.409	23.744	23.842	23.751	23.715
CaO	6.025	4.993	4.921	5.349	4.632	4.998	5.185
FeO	0.204	0.183	0.3	0.191	0.14	0.182	0.24
BaO	0.041	-	-	-	-	-	-
Na	8.623	8.963	9.165	9.007	9.331	9.121	9.001
K	0.292	0.403	0.457	0.386	0.249	0.407	0.465
Total	100.155	100.217	100.121	99.849	100.966	100.411	100.981
Si	2.692	2.744	2.752	2.731	2.76	2.746	2.75
Al	1.293	1.248	1.227	1.249	1.235	1.241	1.232
Ca	0.288	0.237	0.235	0.256	0.218	0.237	0.245
Fe	0.008	0.007	0.011	0.007	0.005	0.007	0.009
Ba	0.001	-	-	-	-	-	-
Na	0.745	0.771	0.791	0.78	0.795	0.784	0.769
K	0.017	0.023	0.026	0.022	0.014	0.023	0.026
Total	5.044	5.03	5.042	5.045	5.027	5.038	5.031
Ab	70.956	74.774	75.216	73.727	77.41	75.065	73.948
Or	1.579	2.21	2.467	2.077	1.357	2.206	2.514
An	27.398	23.016	22.316	24.197	21.233	22.729	23.538
Cs	0.067	-	-	-	-	-	-

APPENDIX 3

Trace element LA-ICP-MS analyses

Sample	FP-4-1R1												
Analysis No.	28	29	30	31	32	33	34	35	36	37	38	39	40
Mg	23.3	15.6	32.2	98.8	77.7	66.3	57.0	53.1	37.8	31.1	26.2	42.7	41.0
Si (%)	28.41	30.46	28.94	28.55	31.21	32.02	29.97	28.86	27.16	27.12	28.80	27.26	27.74
Ca (%)	3.16	3.09	3.26	2.90	3.15	3.32	3.17	3.19	3.04	3.00	3.33	3.11	3.26
Ti	58.1	57.2	62.6	32.1	61.3	79.8	77.1	87.5	70.8	65.9	68.8	71.2	63.8
Fe	1306	1454	1763	1442	1824	1889	1952	1870	1767	1578	1739	1624	1834
Zn	3.42	4.28	4.97	5.00	5.95	5.53	4.82	4.58	5.23	4.68	4.77	5.05	3.84
Ga	26.0	34.1	26.8	32.6	30.5	40.2	35.4	38.0	34.3	32.9	33.5	30.4	33.4
Rb	0.67	1.36	1.31	1.94	1.00	1.40	1.94	1.90	1.23	0.80	1.49	1.03	2.61
^{86}Sr	389	415	430	407	398	502	508	508	460	433	428	408	474
^{88}Sr	397	415	437	398	393	519	502	509	469	431	448	414	483
Y	0.24	0.21	0.08	0.37	0.35	0.25	0.39	0.28	0.33	0.22	0.29	0.30	0.29
Zr	-	-	-	-	-	-	0.22	-	-	-	-	-	-
Nb	-	-	-	-	-	-	-	-	-	-	-	-	-
^{137}Ba	35	40	91	41	162	373	365	455	325	309	278	245	289
^{138}Ba	34	43	93	41	168	397	359	446	323	315	277	237	286
La	7.9	17.6	7.0	11.3	21.5	25.5	25.9	27.2	24.1	24.0	25.6	25.2	21.8
Ce	11	20	9	16	29	34	31	33	28	29	29	30	26
Nd	2.48	3.19	1.65	3.52	4.96	4.92	5.54	5.71	4.86	5.09	5.89	5.79	4.78
Sm	-	-	-	0.33	0.46	0.38	0.38	0.43	0.39	-	0.59	0.43	0.17
Eu	2.50	2.53	2.15	2.54	2.15	3.14	3.47	3.05	3.11	2.94	2.62	2.82	3.14
Gd	-	0.30	-	0.12	-	0.40	0.10	0.36	0.34	0.14	-	0.28	0.34
Tb	-	-	-	-	-	-	-	-	-	-	-	-	-
Yb	-	-	-	-	-	-	-	-	-	-	-	-	-
Pb	13.19	12.85	13.95	13.20	15.97	16.95	15.60	14.02	14.60	14.33	14.35	12.35	14.17

Sample	FP-4-1R1							FP-4-7R2				
Analysis No.	41	42	43	44	45	46	47	48	49	50	51	52
Mg	29.8	15.1	29.0	63.6	36.3	24.1	17.8	13.9	32.8	31.8	26.8	29.8
Si (%)	28.37	28.36	30.00	29.26	29.51	27.74	29.46	26.52	28.20	27.82	31.04	29.04
Ca (%)	3.31	3.21	3.07	3.08	3.28	3.19	3.19	2.98	3.03	2.80	3.32	3.44
Ti	76.2	76.7	53.5	60.3	81.3	70.0	21.8	50.9	62.8	53.6	72.2	74.7
Fe	1848	1564	1686	1819	1849	1636	1563	1316	1610	1659	1859	1834
Zn	4.01	4.79	5.35	4.33	5.15	5.20	4.76	3.76	4.13	5.55	4.75	5.20
Ga	34.1	29.6	32.7	32.1	35.5	34.0	32.2	27.4	27.5	29.9	33.0	33.8
Rb	2.36	0.67	1.21	2.20	0.80	-	1.23	0.59	0.89	0.95	0.14	1.56
^{86}Sr	494	464	425	440	478	482	443	316	357	341	480	445
^{88}Sr	508	460	404	444	467	479	448	318	352	331	486	474
Y	0.24	0.15	0.46	0.23	0.19	0.13	0.30	0.10	0.18	0.16	0.18	0.31
Zr	-	-	-	-	-	-	-	-	-	-	-	-
Nb	-	-	-	-	-	-	-	-	-	-	-	-
^{137}Ba	310	263	211	214	328	264	100	117	173	142	280	305
^{138}Ba	302	269	207	217	321	256	106	115	171	141	261	302
La	25.6	24.1	19.6	22.0	26.2	23.4	7.2	16.1	21.4	16.4	23.9	25.6
Ce	29	28	24	27	32	27	10	18	23	19	30	30
Nd	5.66	5.04	3.82	4.62	5.91	4.39	2.83	3.58	4.40	3.16	5.33	6.27
Sm	0.43	0.40	0.39	0.46	0.48	-	0.17	-	-	-	-	0.45
Eu	3.01	2.94	2.69	2.65	2.96	3.22	2.59	1.90	2.41	2.19	2.95	2.91
Gd	0.14	-	-	-	-	-	0.60	-	0.14	-	-	0.07
Tb	-	-	-	-	-	-	-	-	-	-	-	-
Yb	-	-	-	-	-	-	-	-	-	-	-	-
Pb	15.19	14.46	14.56	14.52	15.40	13.21	15.13	12.71	13.14	15.04	14.78	13.72

Sample	FP-4-7R2								FP-3-1R1			
Analysis No.	53	54	55	56	57	58	59	60	1	2	3	4
Mg	32.1	44.5	17.2	14.4	20.5	16.4	37.8	34.1	56.7	42.8	49.8	69.0
Si (%)	30.60	27.57	26.49	25.18	29.44	26.73	28.22	28.20	29.87	28.74	30.45	34.25
Ca (%)	3.20	3.36	3.22	3.10	3.21	3.24	3.06	3.25	3.03	2.97	3.38	3.41
Ti	64.4	70.7	56.6	53.6	58.1	60.5	62.7	76.6	56.2	52.5	94.3	127.2
Fe	1624	1813	1559	1235	1446	1531	1793	1765	1880	1729	1939	2342
Zn	4.57	5.62	3.66	4.32	5.15	4.39	4.42	5.30	4.29	3.26	4.08	6.88
Ga	32.5	33.9	25.5	26.0	29.8	28.5	31.7	32.6	29.4	28.7	37.9	42.5
Rb	0.79	0.63	0.54	-	1.25	1.90	1.69	1.48	2.97	2.51	2.89	2.42
^{86}Sr	481	470	370	339	368	374	412	448	361	387	506	503
^{88}Sr	482	476	367	345	376	374	400	448	351	385	504	513
Y	0.51	0.28	0.31	0.10	0.24	0.28	0.25	0.24	0.24	0.32	0.36	0.34
Zr	-	-	-	-	-	-	-	-	-	-	-	-
Nb	-	-	-	-	-	-	-	-	-	-	-	-
^{137}Ba	302	308	114	113	166	152	154	299	136	150	341	407
^{138}Ba	293	297	125	110	167	153	155	293	125	137	334	417
La	24.9	27.4	23.5	20.5	21.5	19.6	20.3	25.0	18.4	17.2	27.6	27.6
Ce	29	31	28	23	25	23	23	29	21	19	31	35
Nd	5.55	5.99	5.15	4.00	4.56	4.77	4.34	5.11	3.50	3.46	6.40	6.26
Sm	0.43	0.86	-	0.59	-	0.45	0.40	0.43	0.44	0.16	0.45	0.48
Eu	2.84	2.96	2.42	1.87	2.24	2.31	2.26	2.80	2.29	2.51	3.13	3.11
Gd	0.68	-	-	-	-	-	-	0.08	-	-	0.34	0.38
Tb	-	-	-	-	-	-	-	-	-	-	-	-
Yb	-	-	-	-	-	-	-	-	-	-	-	-
Pb	14.67	13.58	15.35	13.61	14.04	13.95	14.70	14.89	15.20	13.88	15.33	17.09

Sample	FP-3-1R1												
Analysis No.	5	6	7	8	9	10	11	12	13	14	15	16	17
Mg	75.8	20.1	40.7	110.0	9.8	37.9	17.1	20.5	34.9	1.8	15.2	11.9	8.9
Si (%)	29.23	28.63	27.36	31.36	30.06	27.96	29.36	27.74	29.73	30.50	28.68	30.58	29.13
Ca (%)	3.31	2.45	3.16	3.32	2.40	3.02	3.06	3.25	3.19	2.29	3.41	2.45	2.41
Ti	70.8	24.0	76.8	73.1	19.1	72.0	76.1	325.0	79.1	21.7	72.3	33.2	30.4
Fe	1937	1049	1642	1719	1117	1708	1762	1531	1775	1156	1403	1172	1252
Zn	5.25	2.19	3.88	5.95	3.63	5.15	4.63	6.12	5.02	2.74	5.86	4.95	3.57
Ga	36.0	24.9	29.9	36.3	29.7	32.0	30.6	33.3	34.9	32.7	30.3	26.6	28.7
Rb	1.65	2.70	3.22	2.68	0.59	2.18	0.70	2.51	0.83	2.14	-	0.86	0.46
^{86}Sr	507	198	430	449	222	471	468	476	533	184	391	206	263
^{88}Sr	502	194	440	455	206	459	491	473	517	201	394	208	267
Y	0.41	0.02	0.31	0.39	0.06	0.09	0.29	0.73	0.12	-	0.12	-	0.07
Zr	-	0.21	-	-	-	-	-	3.01	-	-	-	-	-
Nb	-	-	-	-	-	-	-	2.66	-	-	-	-	-
^{137}Ba	346	19	281	296	30	319	297	278	300	30	159	29	56
^{138}Ba	343	18	277	310	28	318	288	292	318	30	155	28	60
La	25.5	4.2	24.0	25.7	2.8	26.3	24.0	28.3	25.6	3.5	24.4	4.9	8.0
Ce	30	2	26	29	2	28	25	29	28	3	25	4	6
Nd	6.05	-	5.30	6.04	-	5.46	5.20	6.97	5.47	-	4.78	0.38	0.64
Sm	0.48	-	-	0.57	-	0.38	0.45	0.52	0.18	-	0.27	-	-
Eu	2.78	0.32	2.73	3.33	0.27	3.01	3.05	2.89	3.01	0.43	2.12	0.51	1.28
Gd	0.40	-	0.34	-	-	-	0.32	0.47	-	-	-	-	-
Tb	-	-	-	-	-	-	-	-	-	-	-	-	-
Yb	-	-	-	-	-	-	-	-	-	-	-	-	-
Pb	15.67	13.27	12.77	13.81	16.43	13.78	15.12	15.99	14.59	18.46	16.89	14.70	14.28

Sample	FP-3-1R1				FP-5-8R1							
Analysis No.	18	19	20	21	1	2	3	4	5	6	7	8
Mg	-	0.4	12.5	13.7	11.5	6.1	-	17.2	27.0	5.6	25.7	9.7
Si (%)	15.17	7.33	30.71	30.39	31.80	27.93	24.03	27.22	29.88	27.24	28.68	27.86
Ca (%)	0.05	0.03	3.14	3.24	3.18	3.09	2.69	3.30	3.21	3.18	3.15	2.67
Ti	28.7	8.4	73.0	72.6	73.5	62.7	54.3	69.9	62.8	62.4	53.5	41.0
Fe	517	163	1205	1503	1583	1425	698	1673	1826	1410	1550	1085
Zn	0.74	0.03	4.00	5.02	4.34	5.43	2.70	4.38	3.48	4.12	3.00	2.40
Ga	38.9	13.7	30.8	37.1	33.3	32.5	25.5	30.2	35.6	29.7	34.4	30.8
Rb	122.43	95.79	0.77	0.65	2.27	0.42	0.42	0.88	1.26	0.82	0.72	0.09
^{86}Sr	115	46	319	411	443	434	291	394	487	377	459	281
^{88}Sr	123	43	337	407	447	451	286	401	487	370	456	277
Y	-	-	0.06	0.09	0.22	0.18	-	0.26	0.30	0.24	0.29	0.01
Zr	-	-	-	-	-	-	-	-	-	-	-	-
Nb	-	-	-	-	-	-	-	-	-	-	-	-
^{137}Ba	1200	309	93	201	269	272	73	248	365	120	170	93
^{138}Ba	1234	325	90	206	267	268	70	253	357	118	171	94
La	1.2	0.3	21.8	23.6	24.6	24.8	15.9	28.2	24.7	20.7	22.3	9.6
Ce	1	0	22	25	29	27	16	32	28	25	26	12
Nd	0.14	-	3.38	4.77	5.36	4.90	2.87	6.34	5.24	4.90	5.06	1.90
Sm	-	-	-	-	0.39	0.60	-	0.40	0.45	0.38	0.15	-
Eu	0.80	0.16	1.71	2.38	2.52	2.58	1.29	2.58	3.08	2.31	2.89	0.92
Gd	-	-	-	-	-	-	-	0.29	-	0.33	-	0.24
Tb	-	-	-	-	-	-	-	-	-	-	-	-
Yb	-	-	-	-	-	-	-	-	-	-	-	-
Pb	13.46	9.66	19.42	16.73	13.76	14.76	12.83	11.46	13.53	13.79	14.14	13.96

Sample	FP-5-8R1												
Analysis No.	9	10	11	12	13	14	15	16	17	18	19	20	21
Mg	26.2	20.1	37.7	35.0	34.6	28.8	9.8	31.9	9.4	21.9	32.0	12.9	19.5
Si (%)	30.68	31.52	26.58	29.03	28.23	29.57	27.83	30.16	28.39	27.14	27.06	25.30	26.11
Ca (%)	3.07	3.24	3.28	3.38	3.29	3.26	3.08	3.27	3.21	3.24	3.36	3.11	3.16
Ti	82.6	48.6	62.3	78.2	83.3	83.6	51.2	77.8	67.1	84.7	80.6	73.5	72.9
Fe	1429	1720	1782	1818	1774	1952	1169	1947	1532	1611	1763	1599	1487
Zn	4.06	4.19	3.76	4.13	3.45	4.66	2.08	3.51	4.55	4.28	4.76	4.64	4.48
Ga	36.0	30.8	34.7	35.3	33.1	33.9	28.6	36.0	30.1	33.7	33.9	35.0	31.4
Rb	0.69	0.93	1.18	1.70	0.58	1.14	-	1.31	0.46	0.71	1.25	0.68	0.99
^{86}Sr	380	393	500	475	493	554	370	521	412	524	496	485	433
^{88}Sr	385	366	503	470	501	556	370	521	420	521	527	501	452
Y	0.23	0.21	0.31	0.26	0.33	0.32	0.11	0.23	0.21	0.29	0.38	0.33	0.13
Zr	-	-	-	-	-	0.12	-	-	-	-	-	-	-
Nb	-	-	-	-	-	-	-	-	-	-	-	-	-
^{137}Ba	250	123	346	294	329	346	176	347	247	380	362	357	304
^{138}Ba	229	121	343	287	336	338	173	363	257	372	371	354	280
La	26.6	16.1	27.4	25.5	26.4	27.2	23.1	26.1	24.5	25.6	26.0	25.6	26.4
Ce	31	21	30	31	33	31	27	32	28	30	31	30	29
Nd	5.46	3.91	6.00	7.23	6.21	5.94	4.83	6.21	4.50	5.68	5.89	6.15	5.55
Sm	0.37	0.40	0.46	0.20	0.48	0.60	0.20	0.40	-	0.49	0.63	0.59	0.13
Eu	2.36	1.95	3.31	2.80	2.74	2.99	2.05	2.99	2.61	2.99	3.00	3.04	2.86
Gd	0.24	0.10	0.31	-	0.28	0.23	-	0.28	0.39	-	0.35	-	0.32
Tb	0.02	-	-	-	0.05	-	-	-	-	-	-	-	-
Yb	-	-	-	-	-	-	-	-	-	-	-	-	-
Pb	13.63	14.23	14.28	13.70	11.65	14.18	11.92	11.84	11.06	13.90	13.92	12.37	13.09

Sample	FP-5-8R1						FP-6-1P1					
Analysis No.	22	23	24	25	26	27	1	2	3	4	5	6
Mg	24.7	22.0	55.2	43.1	33.6	81.0	171.9	93.1	54.1	14.2	25.3	8.9
Si (%)	31.45	28.30	30.07	28.51	26.95	27.96	33.91	33.42	29.74	28.19	27.98	29.17
Ca (%)	3.27	3.24	3.36	3.35	3.35	3.42	3.33	3.46	3.25	2.56	3.88	3.05
Ti	78.7	80.3	81.3	66.7	74.9	80.9	86.5	98.4	70.2	24.2	128.2	36.4
Fe	1789	1739	2012	1837	1672	1954	2131	2242	1965	1071	1772	1309
Zn	4.59	5.09	6.24	3.50	4.37	3.77	7.62	7.19	4.78	4.44	4.70	4.30
Ga	33.1	34.4	40.1	35.2	34.6	35.7	40.9	39.9	34.7	26.9	38.6	27.1
Rb	1.43	0.97	2.82	2.57	1.47	2.05	2.67	2.32	2.31	0.70	0.02	1.09
^{86}Sr	387	493	497	508	473	511	547	556	480	254	631	306
^{88}Sr	380	496	490	469	473	503	541	558	481	261	665	313
Y	0.22	0.26	0.44	1.76	0.33	0.71	0.30	0.34	0.31	-	-	0.05
Zr	-	-	-	-	-	-	-	-	0.09	-	-	-
Nb	-	-	-	-	-	-	-	-	-	-	-	-
^{137}Ba	251	405	322	315	312	323	400	426	305	33	453	57
^{138}Ba	245	402	325	317	295	330	412	435	310	36	463	59
La	25.8	26.3	25.1	24.6	24.6	27.4	25.4	27.2	23.5	4.7	23.8	9.7
Ce	33	31	32	29	30	33	33	35	30	3	25	10
Nd	5.17	5.97	6.64	6.23	6.61	7.00	6.17	6.10	5.12	0.20	5.33	1.96
Sm	0.12	0.48	0.06	0.53	0.27	0.51	0.36	0.39	0.50	-	-	-
Eu	2.24	2.84	2.83	3.00	2.85	2.88	2.95	3.14	3.07	0.74	2.77	1.23
Gd	0.31	0.46	0.33	0.43	0.38	0.24	-	0.32	0.45	-	-	-
Tb	-	-	-	0.03	-	0.03	0.04	-	-	-	-	-
Yb	-	-	-	-	-	-	-	-	-	-	-	-
Pb	13.72	13.60	13.38	14.50	13.23	13.10	17.93	17.16	15.80	14.69	11.90	14.71

Sample	FP-6-1P1							
Analysis No.	7	8	9	10	11	12	13	14
Mg	10.9	28.3	31.4	34.4	40.7	14.5	24.4	41.7
Si (%)	27.68	29.80	29.35	29.25	28.52	26.64	27.92	30.93
Ca (%)	2.47	3.14	3.49	3.24	3.17	3.55	3.33	3.32
Ti	20.9	56.6	85.5	76.9	66.7	93.4	81.1	78.2
Fe	1098	1815	1896	1805	1916	1455	1633	1965
Zn	3.06	4.69	5.47	5.30	5.09	3.55	6.08	5.20
Ga	23.6	35.4	34.6	37.9	34.4	29.9	30.6	35.6
Rb	2.14	1.98	0.66	2.38	1.40	0.63	2.25	0.91
^{86}Sr	181	553	555	541	543	549	458	551
^{88}Sr	188	576	586	561	573	546	466	543
Y	-	0.19	0.31	0.34	0.26	0.19	0.23	0.50
Zr	-	-	-	-	-	-	-	-
Nb	-	-	-	-	-	-	-	-
^{137}Ba	20	377	306	415	377	275	256	354
^{138}Ba	18	382	318	399	364	270	257	347
La	4.0	24.1	28.8	28.4	24.5	24.4	27.4	30.4
Ce	2	25	33	30	26	25	30	30
Nd	0.18	4.87	6.36	6.19	5.65	5.08	6.42	5.45
Sm	-	0.60	0.55	0.36	0.21	0.25	0.61	0.54
Eu	0.22	3.30	3.07	3.22	3.19	2.62	2.62	3.43
Gd	-	0.44	0.46	0.30	0.37	-	-	-
Tb	-	-	-	-	-	-	-	0.06
Yb	-	-	-	-	-	-	-	-
Pb	14.33	15.66	15.41	15.63	16.13	13.72	15.56	14.82

APPENDIX 4

Pb isotope LA-MC-ICP-MS analyses

Sample No.	$^{208}Pb/^{206}Pb$	2se	$^{207}Pb/^{206}Pb$	2se
FP-4-1R1				
1	2.063	0.004	0.843	0.002
2	2.071	0.004	0.846	0.002
3	2.069	0.004	0.847	0.002
4	2.074	0.004	0.848	0.001
5	2.086	0.003	0.853	0.001
6	2.090	0.003	0.853	0.001
7	2.071	0.003	0.849	0.001
8	2.083	0.003	0.852	0.001
9	2.077	0.003	0.852	0.002
10	2.084	0.004	0.853	0.002
11	2.072	0.004	0.850	0.002
12	2.070	0.004	0.851	0.002
FP-4-7R2				
1	2.075	0.004	0.849	0.002
2	2.070	0.004	0.849	0.002
3	2.068	0.004	0.848	0.002
4	2.077	0.004	0.852	0.002
5	2.057	0.005	0.842	0.002
6	2.078	0.002	0.850	0.001
7	2.079	0.002	0.852	0.001
8	2.072	0.002	0.849	0.001
9	2.082	0.002	0.851	0.001
10	2.084	0.002	0.852	0.001
11	2.077	0.003	0.850	0.001
12	2.082	0.002	0.852	0.001
FP-3-1R1				
1	2.074	0.003	0.849	0.002
2	2.074	0.003	0.849	0.002
3	2.077	0.003	0.850	0.002
4	2.078	0.004	0.852	0.002
5	2.080	0.001	0.851	0.001
6	2.077	0.002	0.850	0.001
7	2.078	0.002	0.851	0.001
8	2.078	0.002	0.851	0.001
9	2.075	0.003	0.849	0.002
10	2.075	0.003	0.848	0.001
11	2.075	0.003	0.849	0.001
12	2.078	0.003	0.850	0.002

Sample No.	$^{208}Pb/^{206}Pb$	2se	$^{207}Pb/^{206}Pb$	2se
FP-5-8R1				
1	2.063	0.005	0.845	0.002
2	2.064	0.004	0.845	0.002
3	2.068	0.004	0.847	0.002
4	2.070	0.005	0.848	0.002
5	2.072	0.004	0.851	0.001
6	2.069	0.003	0.850	0.001
7	2.069	0.003	0.850	0.001
8	2.087	0.003	0.855	0.001
9	2.072	0.005	0.849	0.002
10	2.068	0.005	0.849	0.002
11	2.082	0.005	0.852	0.002
12	2.070	0.004	0.849	0.001
FP-4-7R1				
1	2.081	0.003	0.852	0.001
2	2.089	0.003	0.855	0.001
3	2.084	0.004	0.852	0.001
4	2.084	0.004	0.852	0.001
5	2.082	0.004	0.853	0.001
6	2.078	0.004	0.852	0.001
7	2.082	0.004	0.853	0.001
8	2.071	0.003	0.850	0.001
9	2.063	0.004	0.846	0.001
10	2.068	0.004	0.846	0.001
11	2.083	0.003	0.851	0.001
12	2.090	0.004	0.851	0.001